Sensing structure design

Application note

XENSIV™ magnetic current sensors

About this document

This application note provides sensing structure implementation guidelines for external current rail sensor of the XENSIV™ product family.

Scope and purpose

The purpose of this application note is to enable system developers to design a sensing structure for XENSIV™ current sensors in busbar based and PCB based applications.

Intended audience

This application note is written for XENSIV™ current sensors users who are dealing with the implementation of the product in the system.

Table of contents

1 Introduction

1.1 Sensing principle

In the figure below the sensor die is shown together with a sensing structure example realized on a conductor. The sensor features two Hall based sensing elements, or probes, enabling a differential sensing principle. The Hall probes are sensitive to the component of the magnetic field orthogonal to the conductor. The magnetic field lines are generated so that the orthogonal component of the magnetic field has opposite directions on the two sensing elements.

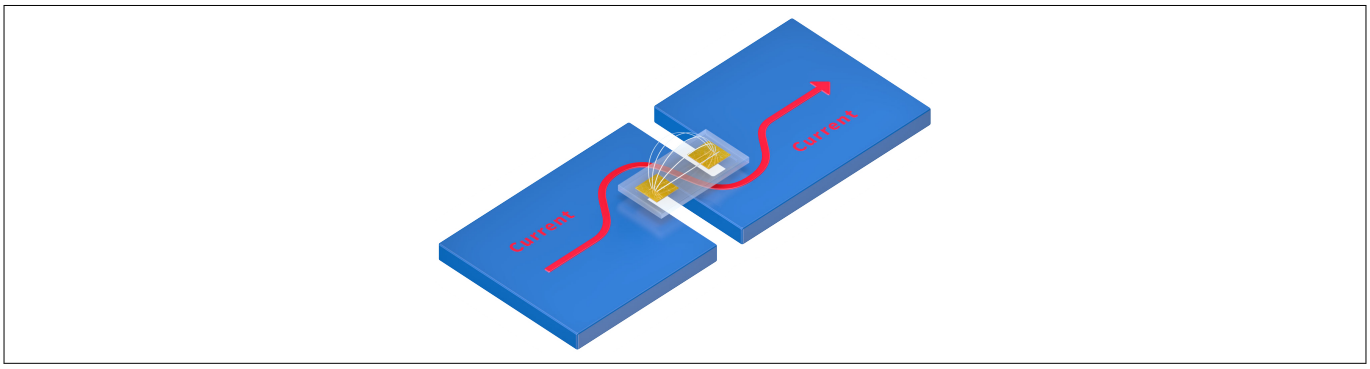

Figure 1 Magnetic field on sensing elements with core-less differential current sensor

B_{DIFF} is the average differential magnetic field at the Hall probes location, respectively B_{H1} and B_{H2}:

$$B_{DIFF} = \frac{B_{H1} - B_{H2}}{2} \quad (1)$$

1.2 Sensitivity and transfer factor

The sensor features an analog output, which is used to provide the information of the measured current. The analog measurement result is available as the differential output voltage V_O.

Being S_X the sensitivity in [mV/mT] and V_{OQ} the quiescent voltage of the sensor in [V], in all output modes except fully-differential, the differential output voltage V_O can be expressed as:

$$V_O = V(AOUT) - V(VREF) = S_X \times B_{DIFF} \quad (2)$$

In fully-differential mode, the differential output voltage V_O can be expressed as:

$$V_O = V(AOUT) - V(VREF) = 2 \times S_X \times B_{DIFF} \quad (3)$$

The sensitivity S, whose dimension is [V/A], is defined as:

$$S = S_X \times TF \quad (4)$$

where S_X is the sensitivity in [mV/mT] linked to the measurement range programmed in the EEPROM and TF is the current rail transfer factor in [T/A] associated to the sensing structure, defined as B_{DIFF} [T] divided by I [A]. The configurable values for S_X (S_X=S_1,...,S_6) are reported in the product datasheet [1].

The current rail transfer factor TF indicates the magnetic coupling between sensor and sensing structure. This value is usually expressed as its nominal value for a DC current, when the sensor is in the nominal position with respect to the current rail.

1 Introduction

It will be directly influenced by:

- Displacement of sensor in the 3 directions of space, due to e.g. soldering tolerances, mechanical vibrations or material expansion/contraction over temperature and lifetime;
- Manufacturing tolerances of busbars and PCB traces;
- Skin effect and eddy current effect in the conductor, when an AC current flows through it;
- Presence of magnetic parts in the system, or of heatsinks/conductor nearby the sensor; eddy currents can be induced in any conductor, also on an aluminum heatsink, and they can hence influence the frequency response of the current measurement system.

Further details about calibration are reported in the User manual [2].

2 Sensing structures

2.1 Sensing structure shapes

The conductor underneath the sensor is responsible for the shape of the magnetic field and therefore it influences the magnetic circuit. Optimizing the sensing structure shape on the conductor at the sensing position is necessary in order to obtain optimal current sensor performance. Depending on the system requirements assigned to current sensing, different supports for the current conduction can be used:

- Internal layers of a PCB;
- External busbar conductors.

Moreover, different sensing structure shapes can be utilized:

- Lateral insertion, S-bend slit shape;
- Lateral insertion, Straight slit shape;
- Vertical insertion.

The different sensing structure shapes can be implemented on either PCB based or busbar based solutions, with the exception of vertical insertion, which is only suitable for busbars. Typical examples of sensing structures are shown in the figures below. In the next chapters sensing structure examples are analyzed in detail.

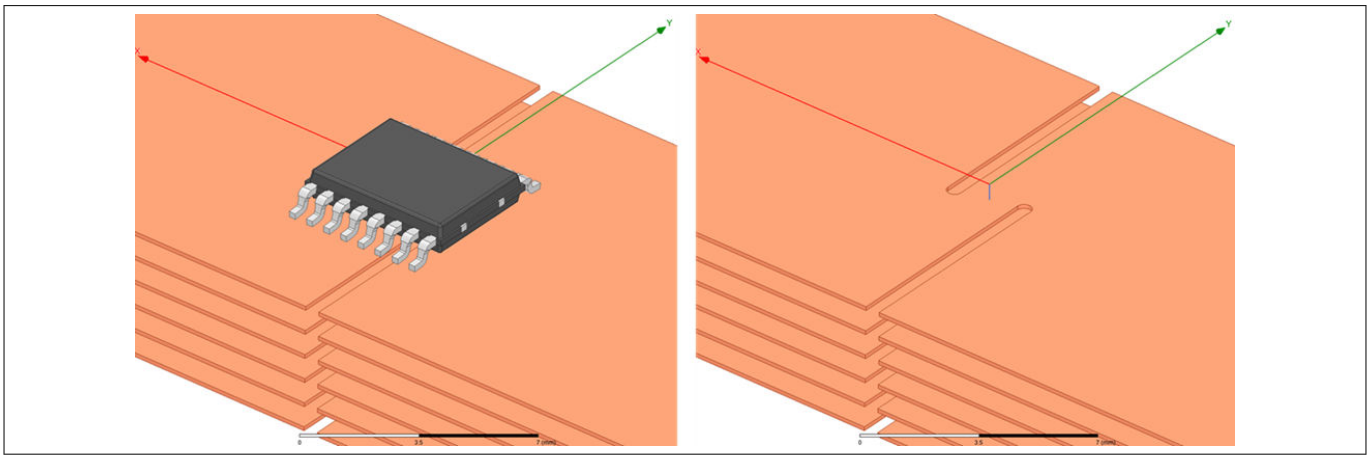

Figure 2 **PG-TDSO-16 package, PCB support, 6 layers, lateral insertion, S-bend slit sensing structure**

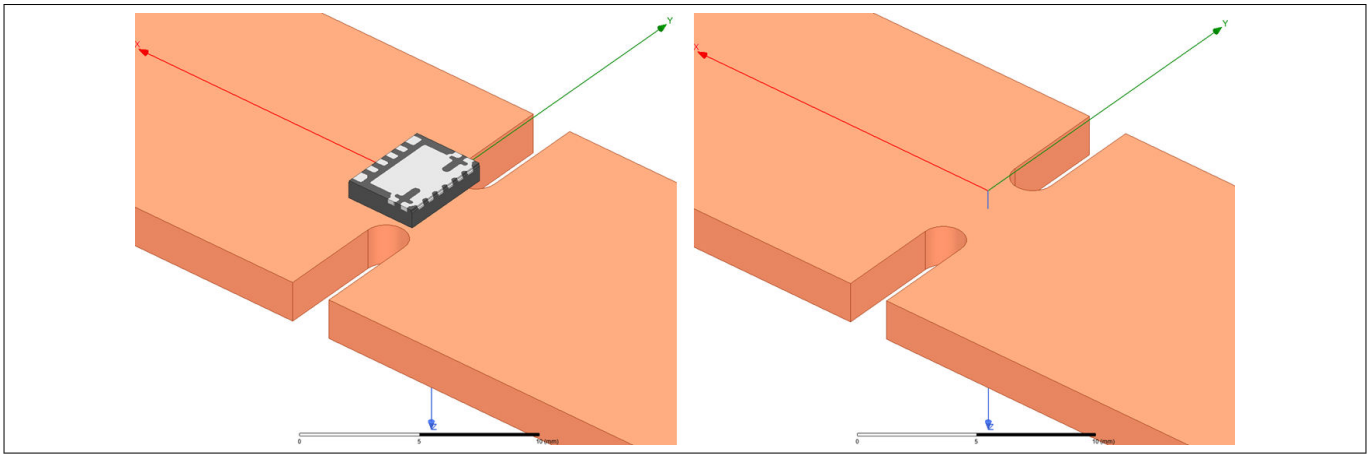

Figure 3 **PG-VSON-6 package, busbar support, lateral insertion, Straight slit shaped sensing structure**

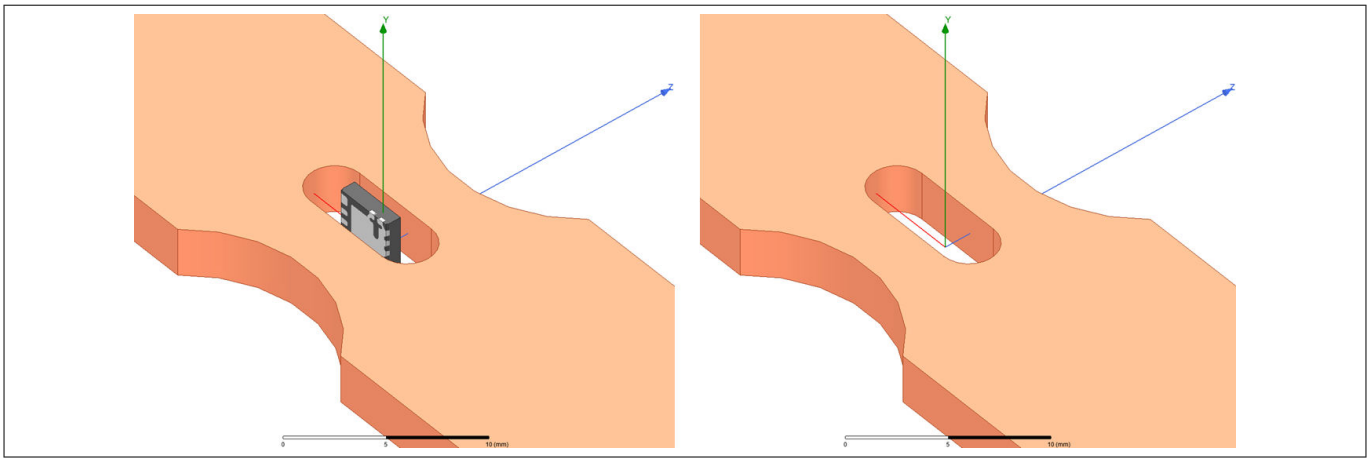

Figure 4 PG-VSON-6 package, busbar support, vertical insertion

2.2 Sensing structure optimization

In order to evaluate the performance of each sensing structure and to optimize it Electro-Magnetic FEM solvers can be used.

The choice of a sensing structure is driven by the need to meet requirements at system level. The main performance factors are shown in the figure below.

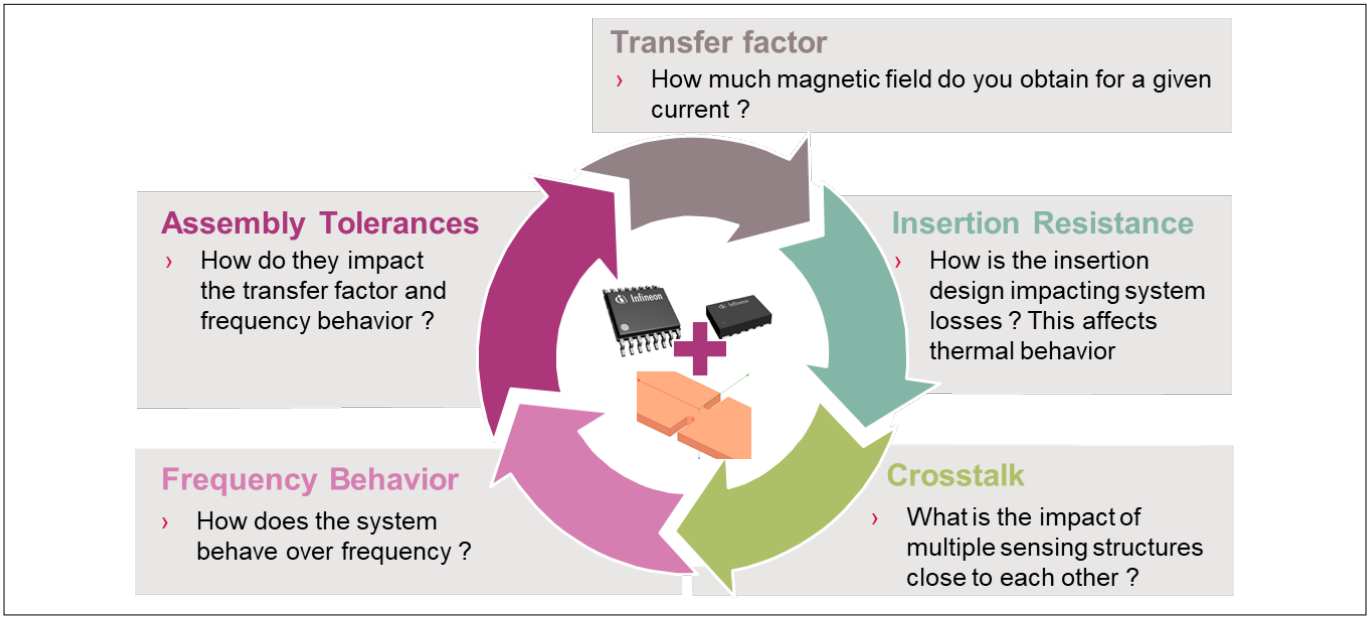

Figure 5 Key performance factors of a sensing structure for external current rail applications

These factors are not independent from each other. As an example, a tentative to lower the insertion resistance will lead to an increase of the cross section of the conductor at sensing location. This will decrease the current density and hence the transfer factor and potentially worsen the frequency behavior, since the current will have more room to be squeezed toward the edges of the conductor at higher frequencies. Suggestions regarding how to steer the optimization of the sensing structure toward one or the other performance factor are given in the next chapters.

The main limiting factor for the full scale range is the power dissipation on the sensing structure. The maximum full scale current that a sensing structure can handle will depend on the cooling capabilities and efficiency requirements of the final system.

3 Busbar support

3.1 Lateral insertion on busbar support

Typically, busbars are used to carry the current in systems with current ratings above 500A. It is possible to realize a sensing structure on a busbar by realizing slits at the sensing location, in order to increase the current density and hence the magnetic field on the sensing elements. The preferred sensor package is the PG-VSON-6 because it is leadless and compact, allowing easy mechanical integration and overmolding procedure. The sensor is typically soldered on a PCB and an isolation layer is provided to fulfill voltage isolation requirements, as shown in the picture below.

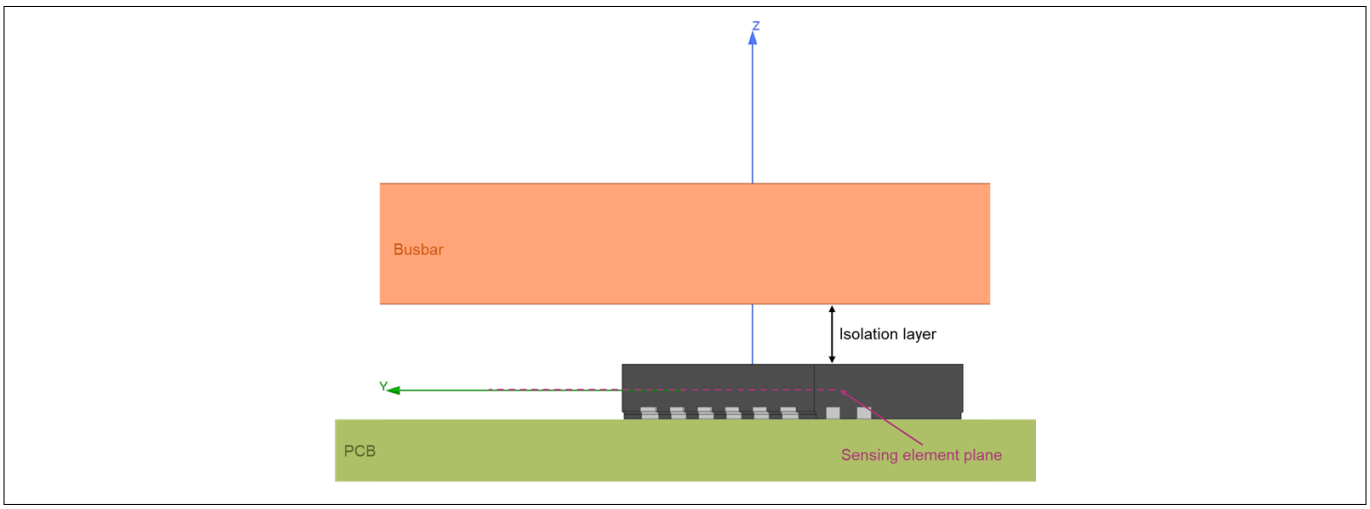

Figure 6 Lateral insertion on busbar support, sensor in the middle

Another possibility is to solder the sensor on a carrier PCB, which is then secured to the busbar, and use the PCB to achieve the voltage isolation, as shown in the figure below.

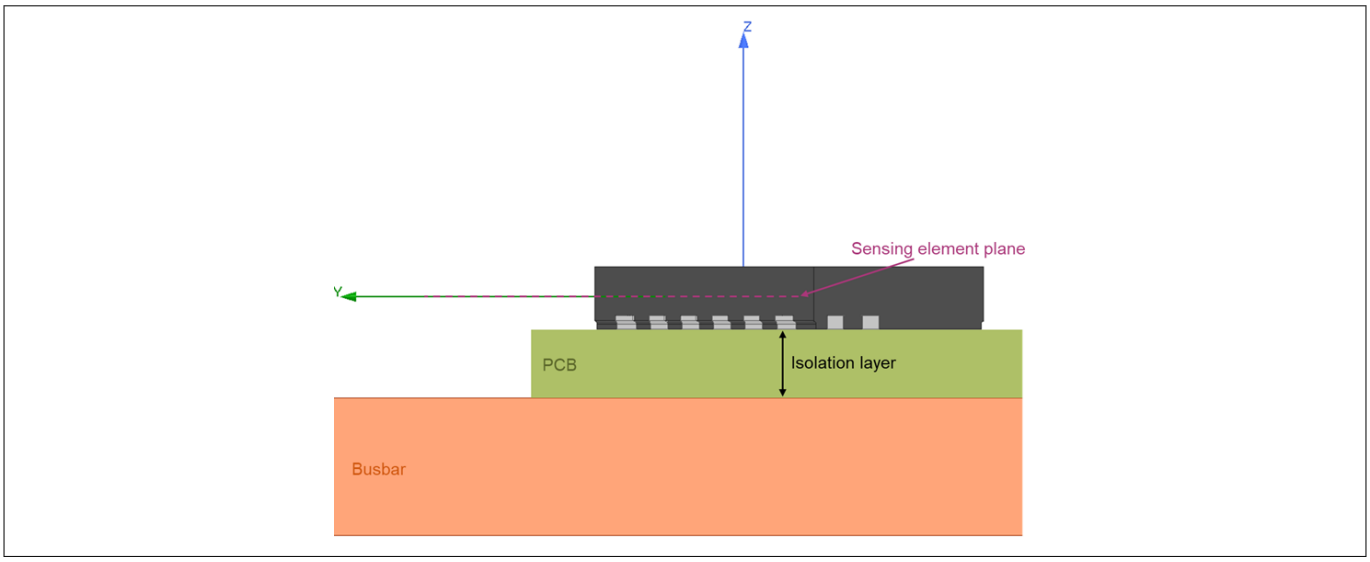

Figure 7 Lateral insertion on busbar support, PCB in the middle

Regarding the sensing structure shape to be realized on the busbar at sensing element location, two shapes can be considered: Straight shaped and S-bend shaped.

3.1.1 Straight shaped sensing structure

3.1.1.1 Introduction

The Straight slit shape is the simplest of the sensing structure shapes in case of lateral insertion. It will be used as an example to demonstrate the effect of all geometrical parameters on the aforementioned performance factors: transfer factor, insertion resistance, frequency behavior, misalignment and crosstalk. The considerations done for this sensing structure can be extended to the case of an S-bend sensing structure.

The Straight slit sensing structure is optimal for systems in which the most important requirement is obtaining low power losses due to the insertion. It is in fact possible to obtain lower insertion resistance with respect to the S-bend case thanks to the fact that the current doesn't have to follow a "S shaped" path at sensor location, but rather flows always in the "Straight" direction. The drawback is higher sensitivity to crosstalk; detailed explanation is given in Chapter 3.1.2. The busbar geometry is depicted in the following figures.

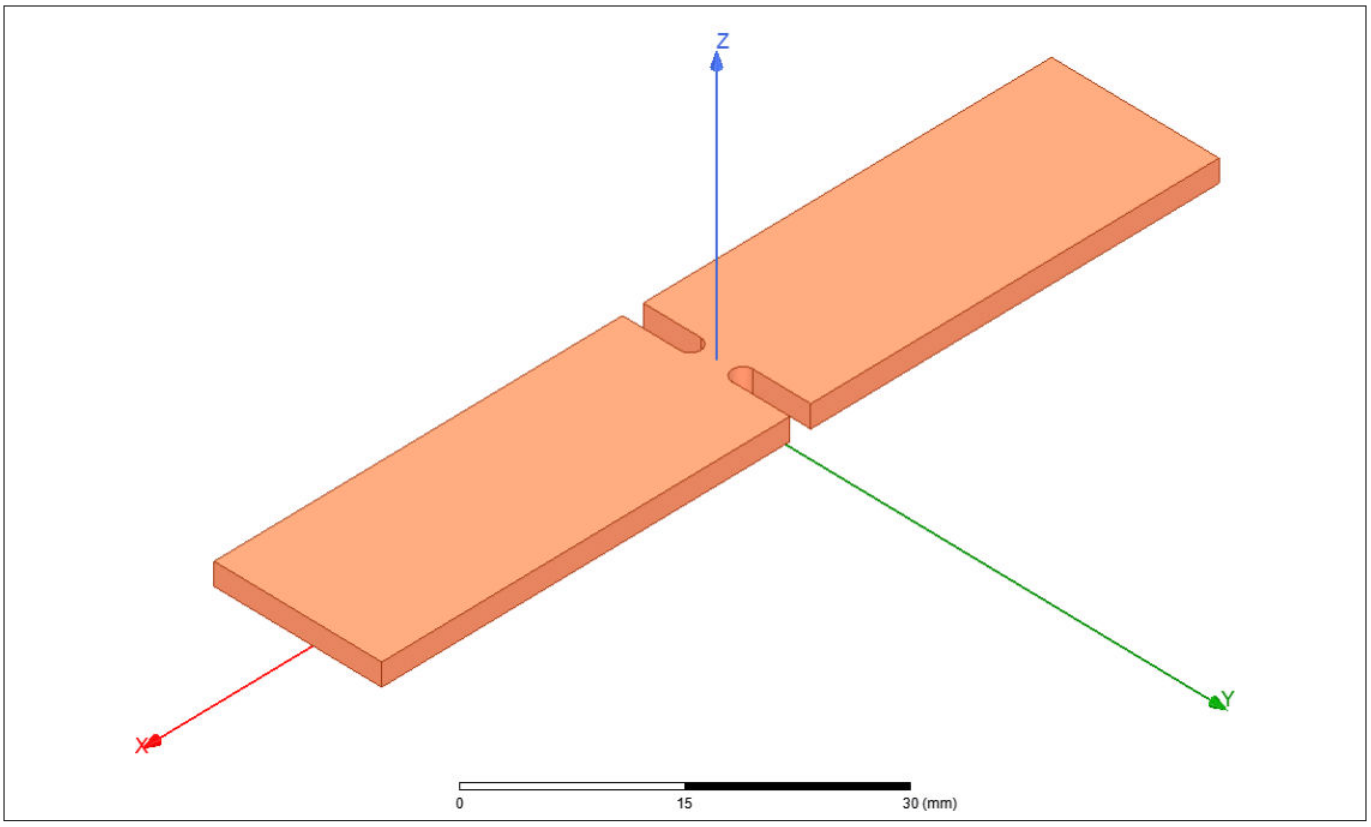

Figure 8 PG-VSON-6 package, busbar support, Straight slit shaped sensing structure

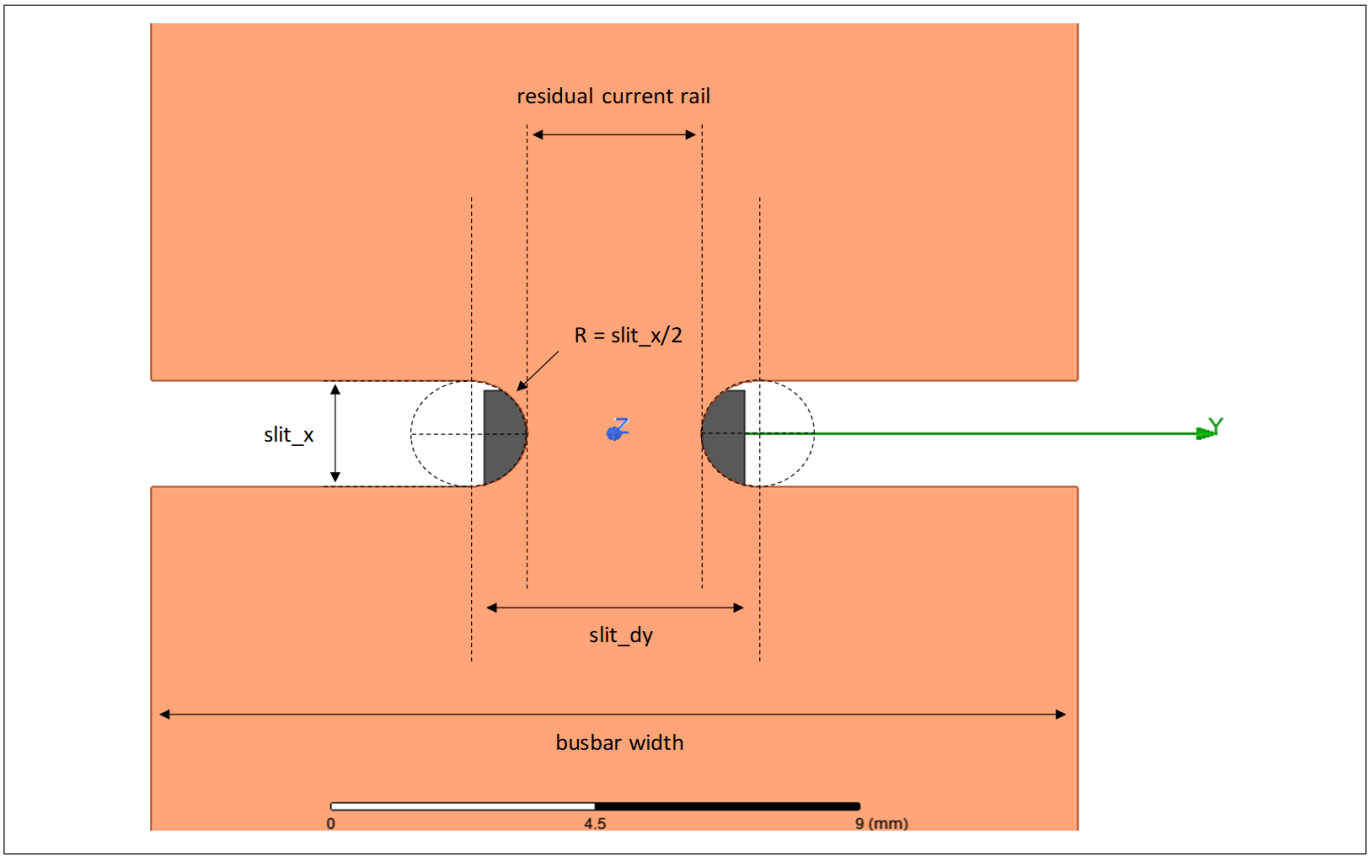

Figure 9 **PG-VSON-6 package, busbar support, Straight slit shaped sensing structure, top view**

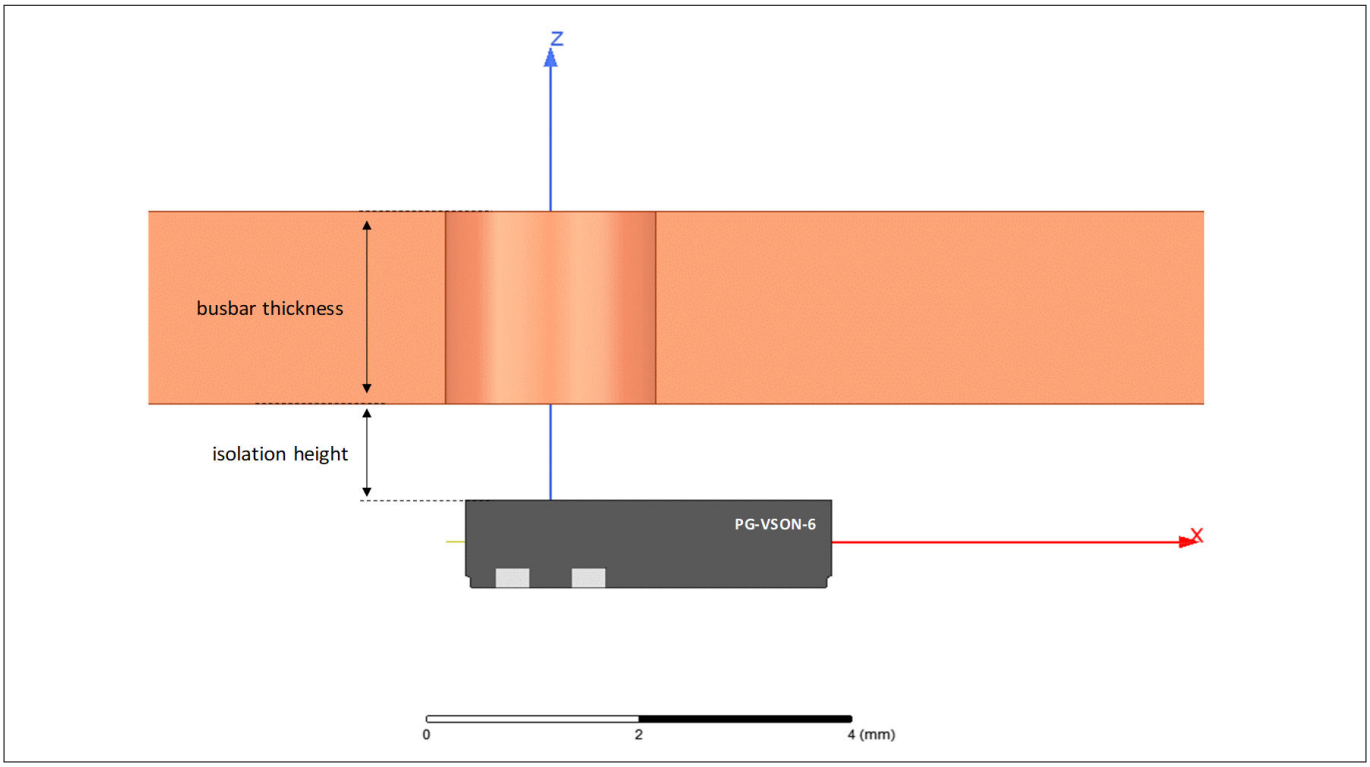

Figure 10 **PG-VSON-6 package, busbar support, Straight slit shaped sensing structure, side view**

3.1.1.2 Current rail transfer factor and insertion resistance

In first instance, the choice of the geometry will be the result of a trade-off between target transfer factor, which is directly linked to the target current full scale, and insertion resistance, which gives an indication of the additional power losses in the system due to the modifications done to the conductor. The result of FEM simulations regarding current rail transfer factor and insertion resistance is shown. The isolation height has been set to 0.5 mm. Different residual current rail and slit_x values have been swept in order to show what is the impact on the current rail transfer factor and on the insertion resistance. The analysis is done for different busbar thicknesses.

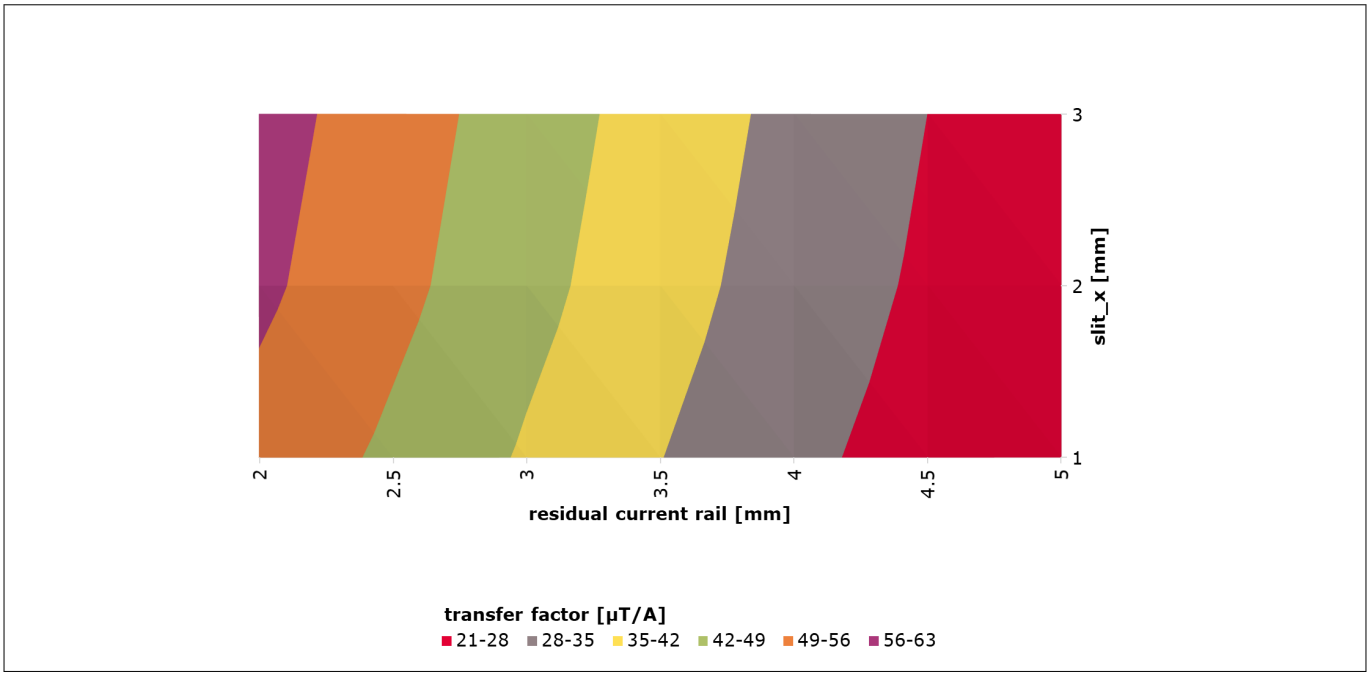

Figure 11 **Current rail transfer factor for a 1 mm thick busbar, 16 mm wide. Isolation height set to 0.5 mm. Sweep of residual current rail and slit_x values**

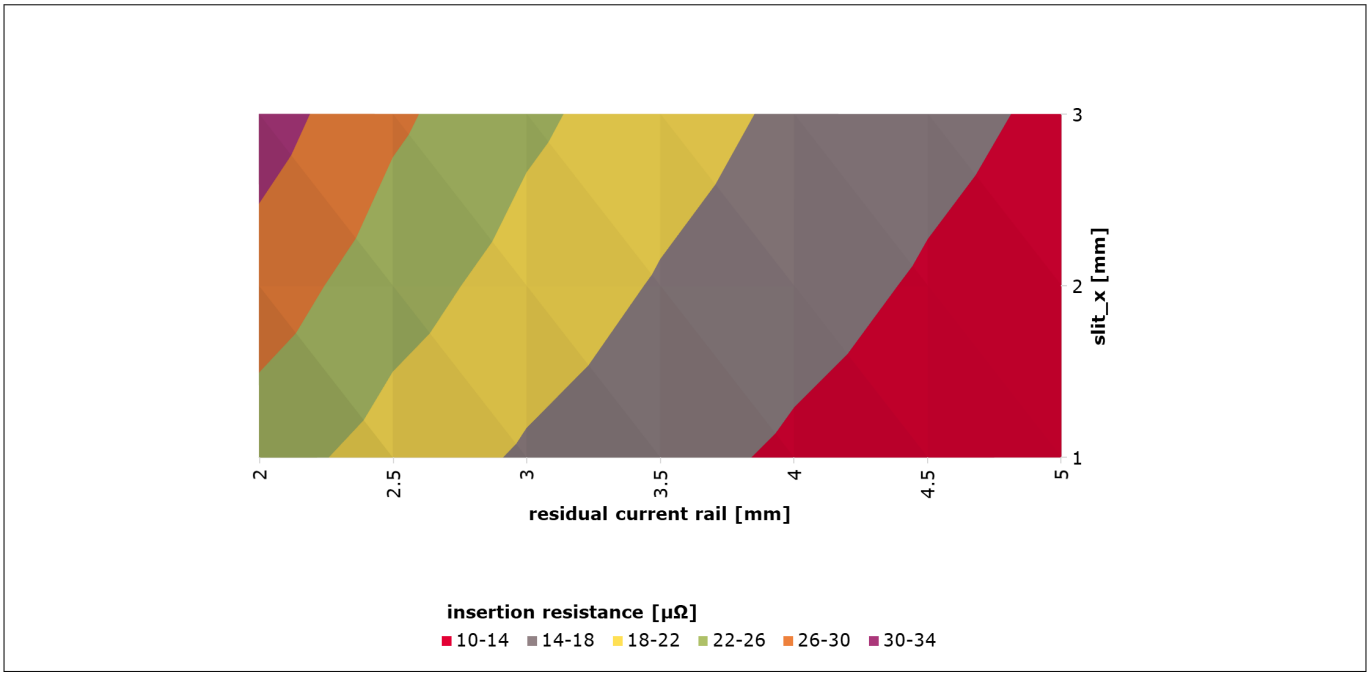

Figure 12 **Insertion resistance for a 1 mm thick busbar, 16 mm wide. Isolation height set to 0.5 mm. Sweep of residual current rail and slit_x values**

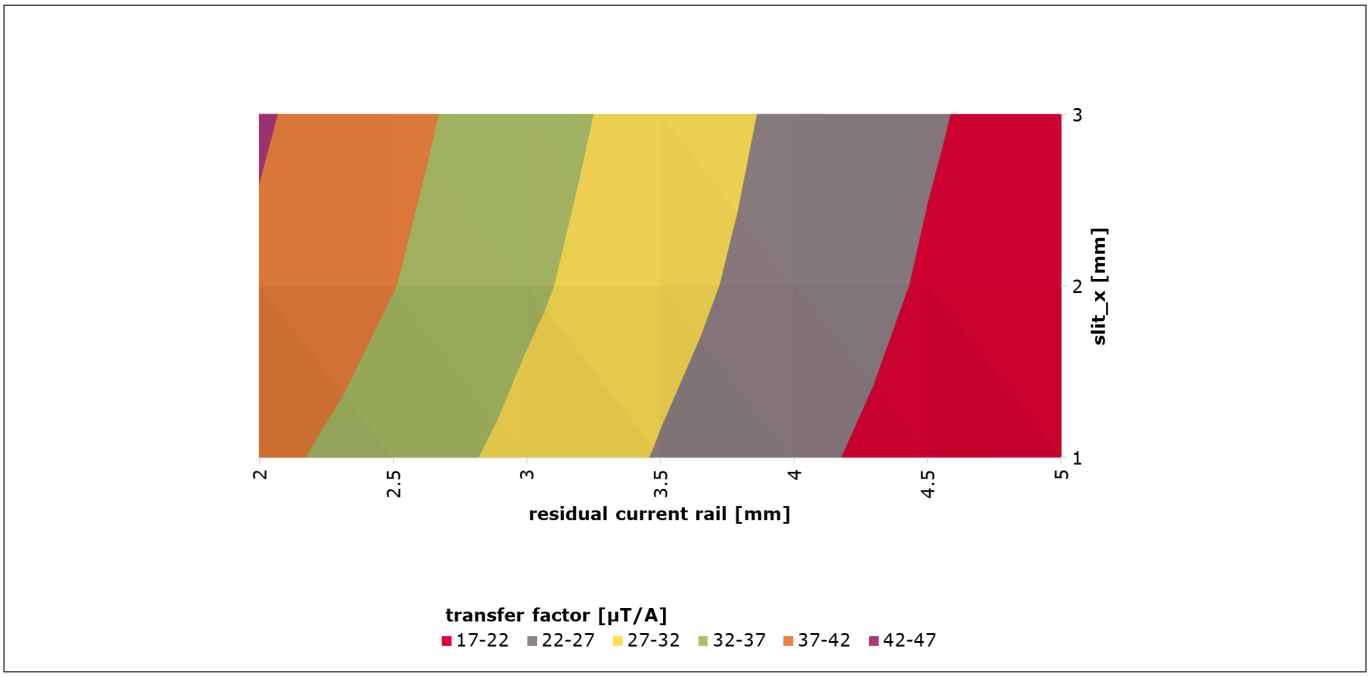

Figure 13 **Current rail transfer factor for a 2 mm thick busbar, 16 mm wide. Isolation height set to 0.5 mm. Sweep of residual current rail and slit_x values**

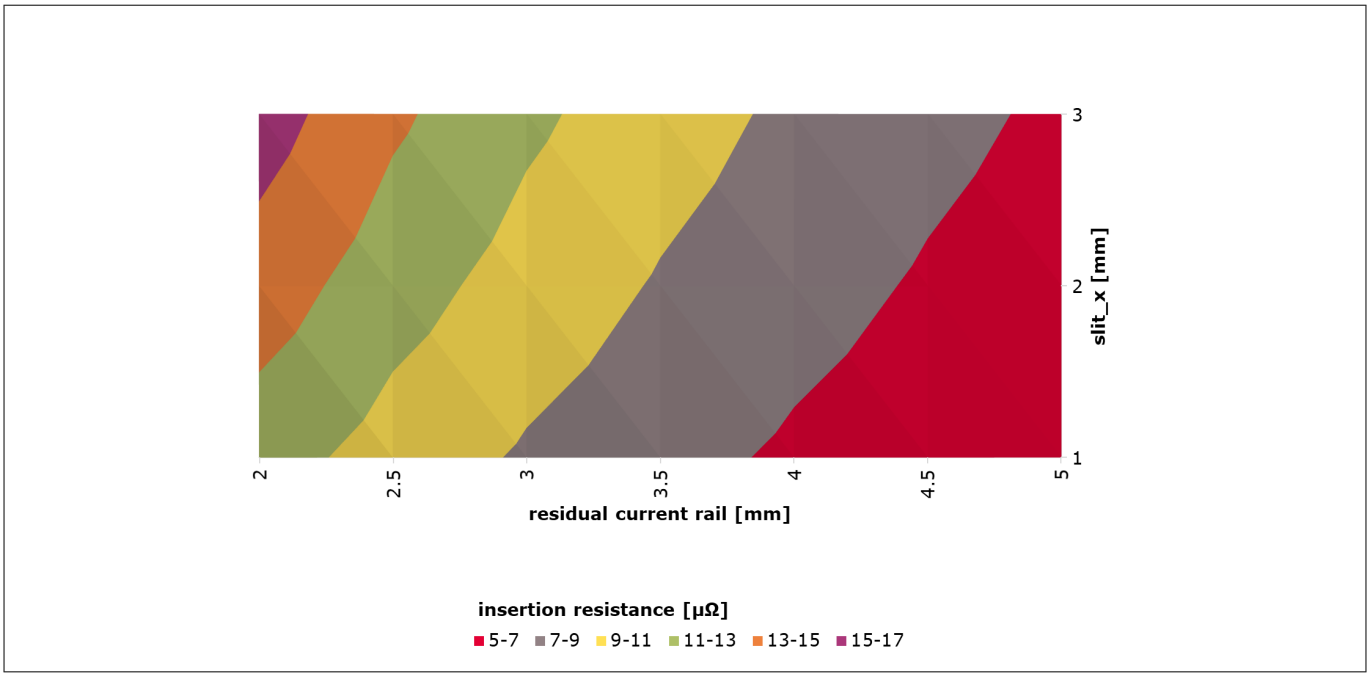

Figure 14 **Insertion resistance for a 2 mm thick busbar, 16 mm wide. Isolation height set to 0.5 mm. Sweep of residual current rail and slit_x values**

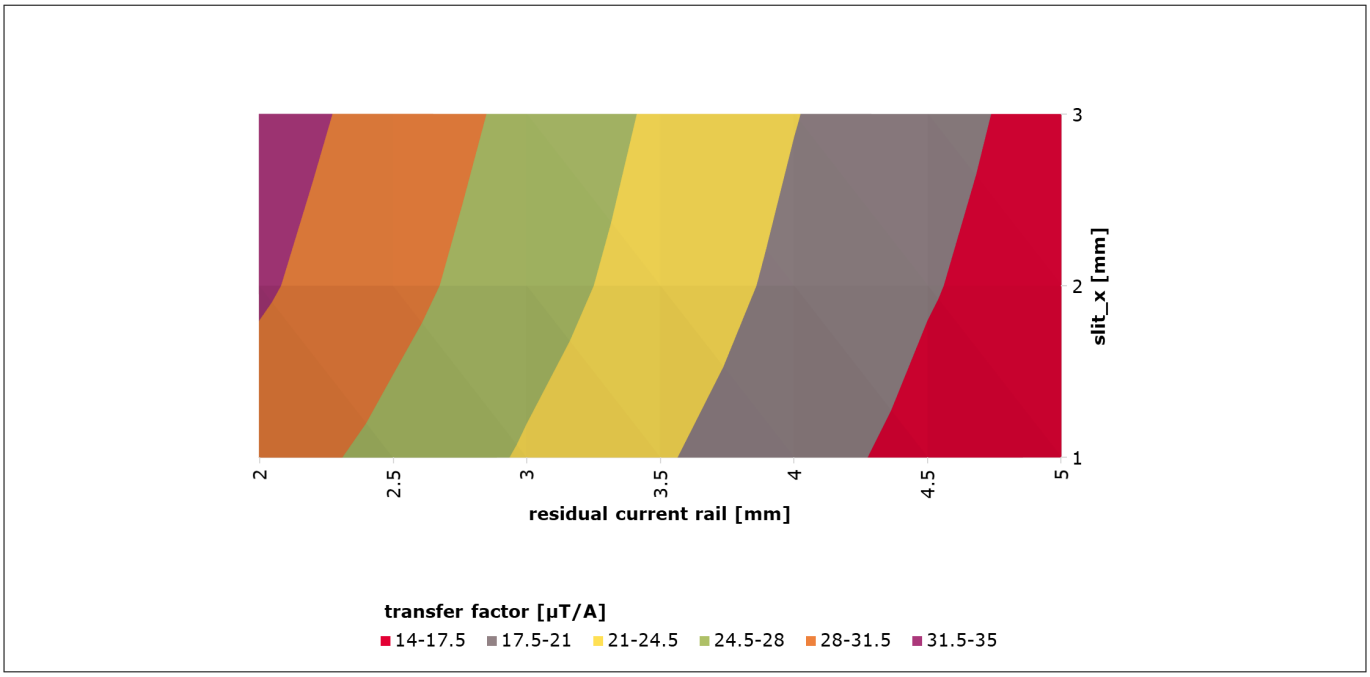

Figure 15 **Current rail transfer factor for a 3 mm thick busbar, 16 mm wide. Isolation height set to 0.5 mm. Sweep of residual current rail and slit_x values**

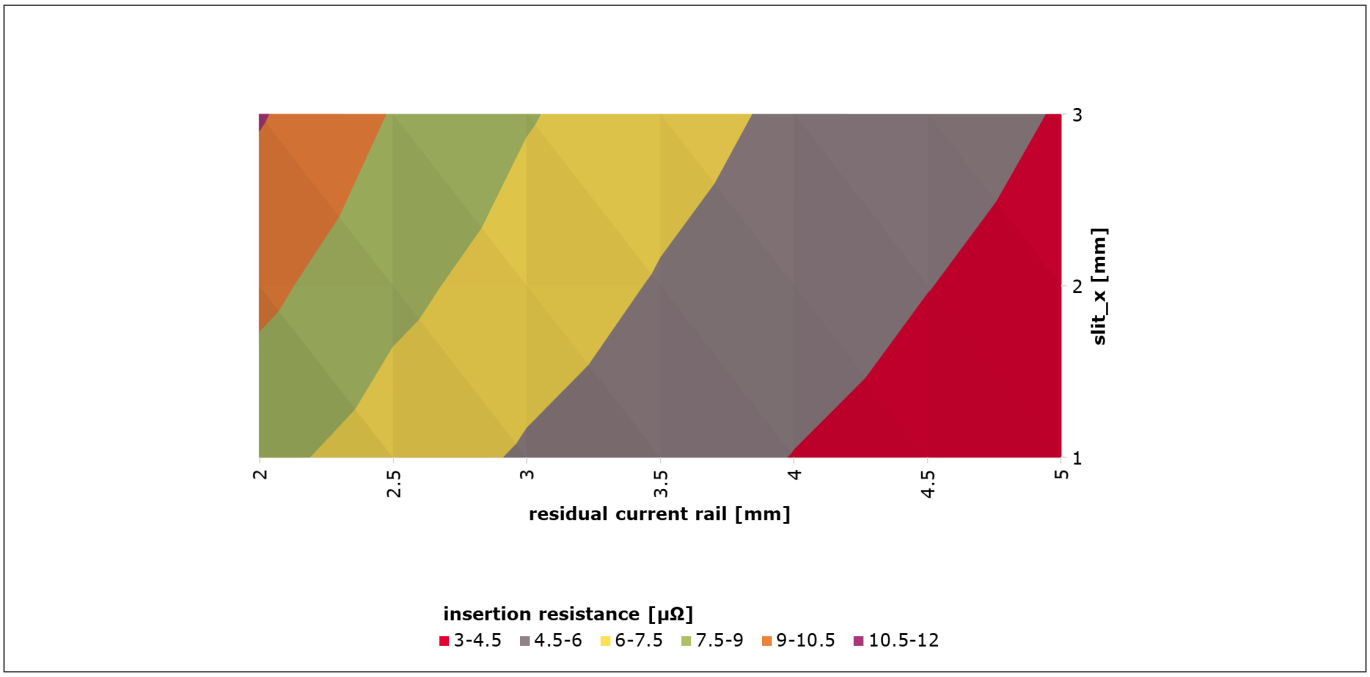

Figure 16 **Insertion resistance for a 3 mm thick busbar, 16 mm wide. Isolation height set to 0.5 mm. Sweep of residual current rail and slit_x values**

A bigger busbar thickness is clearly beneficial for the insertion resistance reduction since it creates a bigger cross section for the current flow, but it leads to lower transfer factors because of the lower current density. In the same way, a wider residual current rail is beneficial for the insertion resistance reduction but leads to lower transfer factors.

Regarding the slit_x parameter, which indicates how wide the slit in the busbar is, it's usually better to keep it as small as possible, within the limits of the manufacturing rules. In fact, a wider slit increases the insertion resistance without bringing a significant increase in the transfer factor, as it can be seen from the previously shown simulation data. However, small slit_x and residual current rail values result in increased sensitivity to misalignment errors.

3.1.1.3 Bandwidth

Given the typical bandwidth of the current sensor, reported in the product datasheet [1], the bandwidth of the complete current measurement solution will be significantly influenced by the geometry of the sensing structure. The reason for this behavior is the change of the current density within the section of the conductor over frequency. Due to skin effect, the current is pushed toward the surface of the conductor, and induced eddy currents create an opposing field to the one generated by the current in the conductor that changes in amplitude depending on the frequency. The figures below show how the current density is altered in the busbar over frequency. The impact on the frequency response will heavily depend on the geometry of the sensing structure. The typical magnitude [dB], phase shift [deg] and gain error [%] for different busbar thicknesses, residual current rail lengths and slit_x values are shown.

A smaller busbar thickness helps in terms of bandwidth; the impact of both skin effect and eddy current effect is limited since a smaller thickness of the conductor forces the current to be confined in a smaller, restricted area at the sensing location. For the same reason, a smaller residual current rail and a bigger slit_x are beneficial in terms of bandwidth.

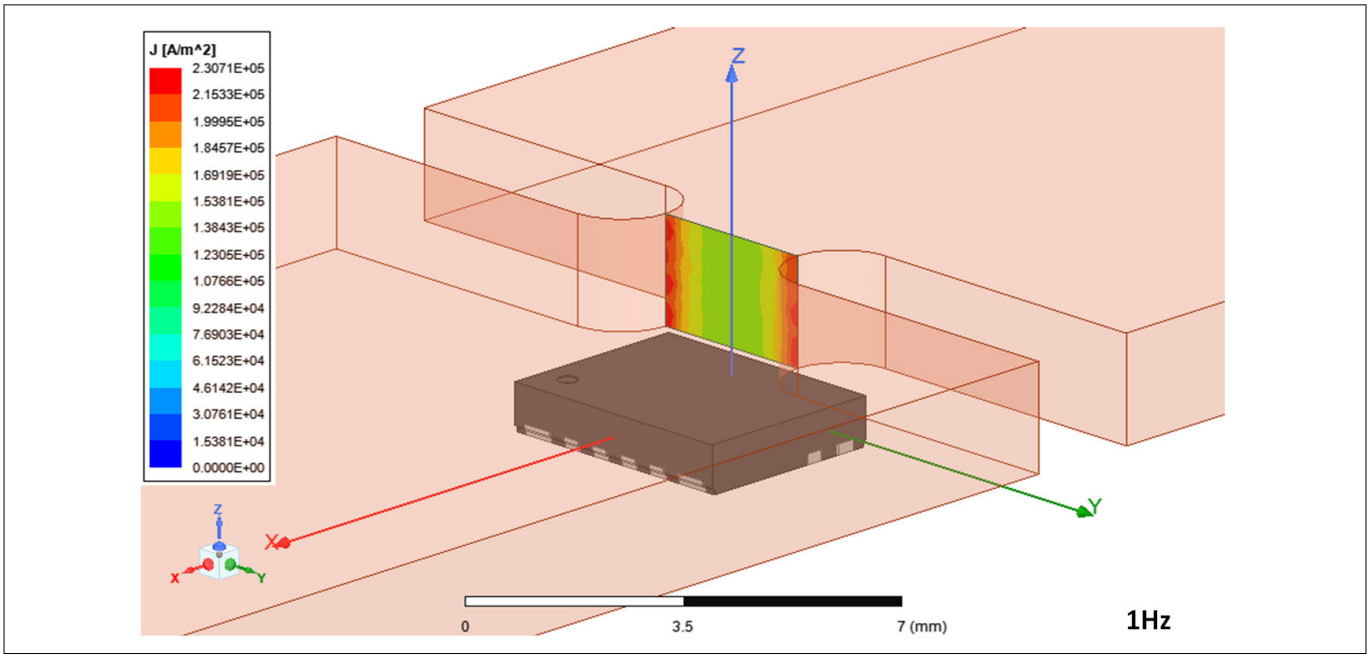

Figure 17 **Current density distribution in the section of a 16 mm wide busbar. Residual current rail = 3 mm. Slit_x = 2 mm. Isolation height set to 0.5 mm. Peak input current = 1 A, 1 Hz**

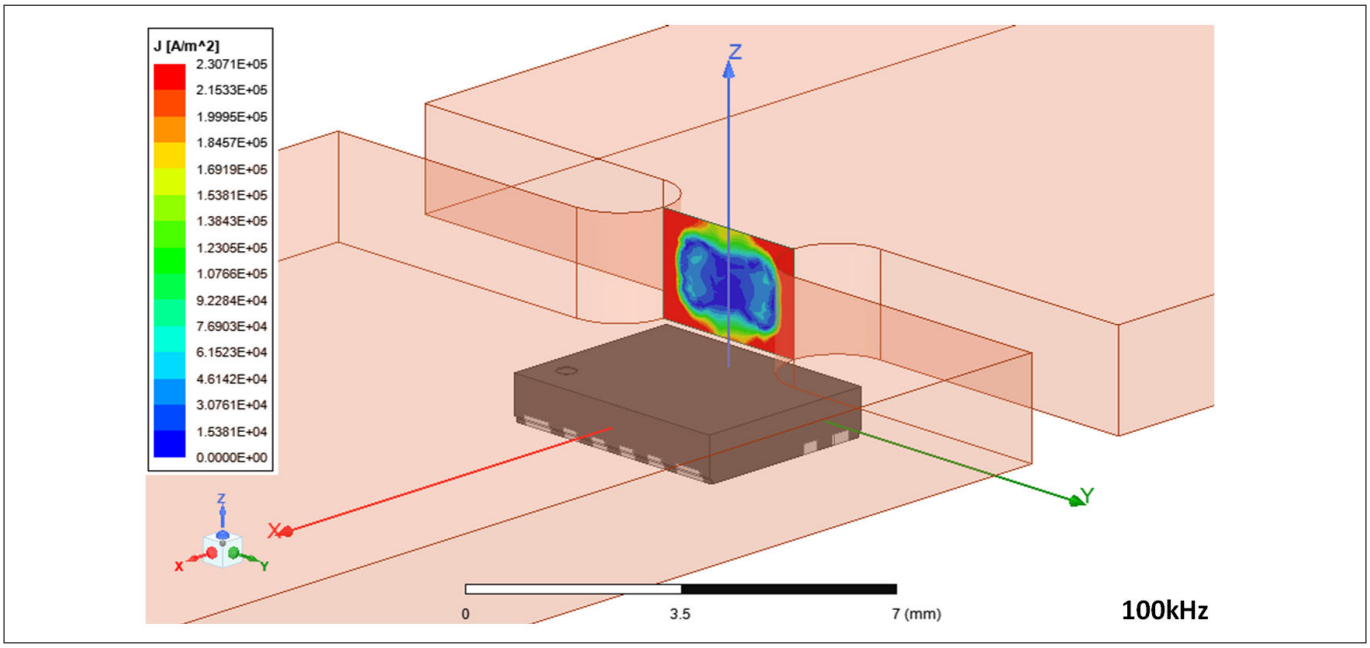

Figure 18 **Current density distribution in the section of a 16 mm wide busbar. Residual current rail = 3 mm. Slit_x = 2 mm. Isolation height set to 0.5 mm. Peak input current = 1 A, 100 kHz**

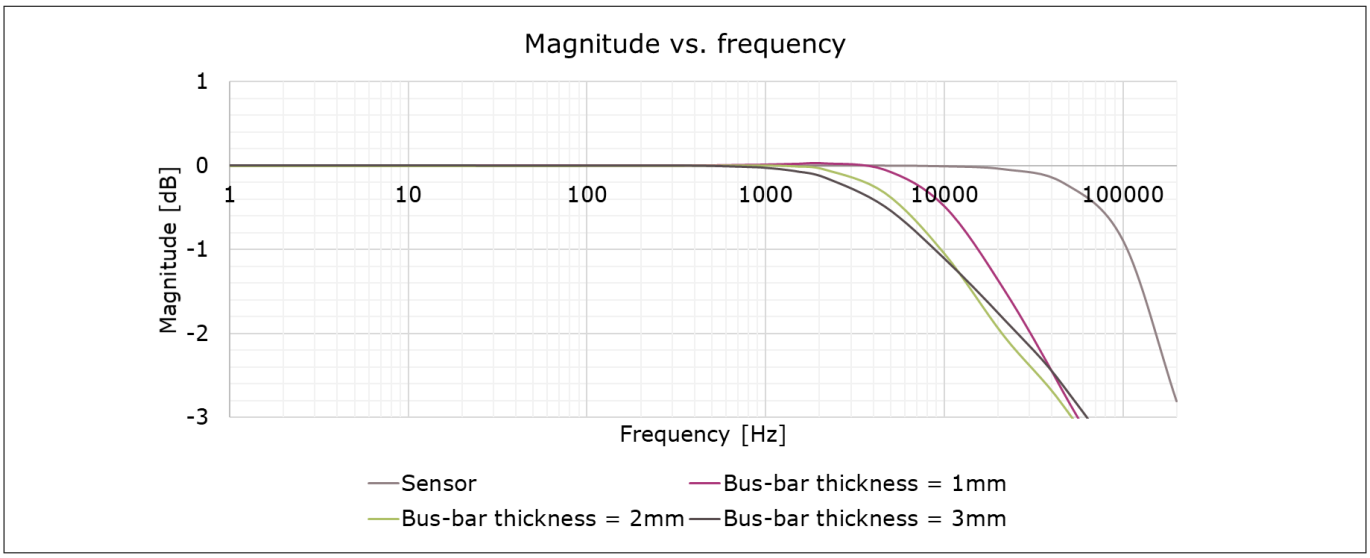

Figure 19 **Magnitude over frequency for a 16 mm wide busbar. Residual current rail = 3 mm. Slit_x = 2 mm. Isolation height set to 0.5 mm. Sweep of busbar thickness value**

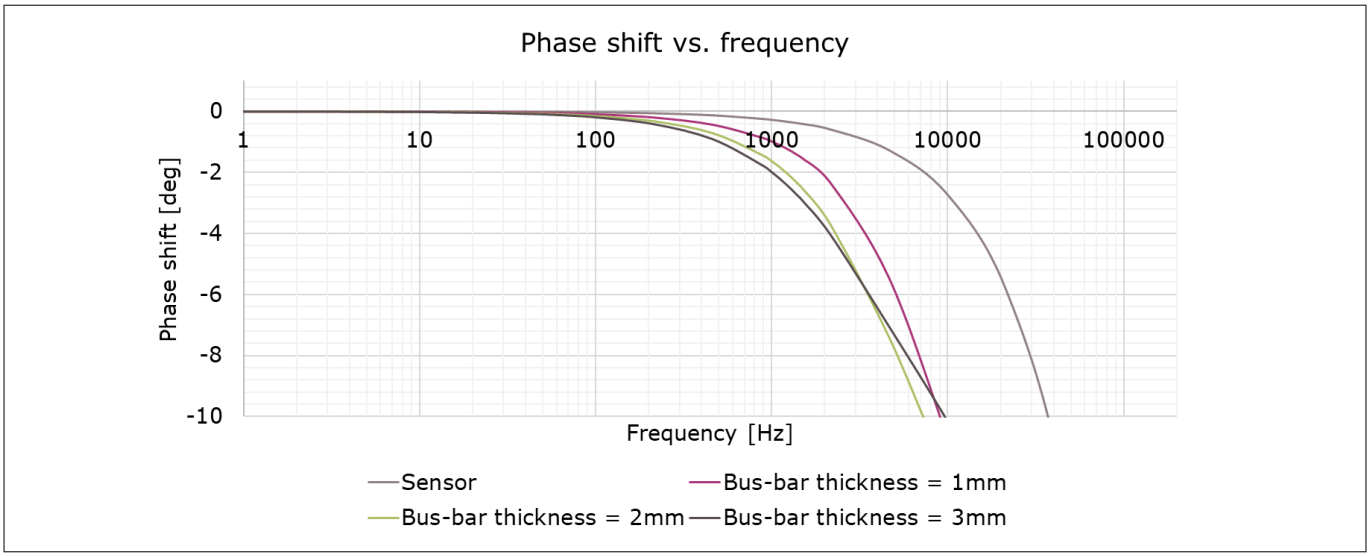

Figure 20 **Phase shift over frequency for a 16 mm wide busbar. Residual current rail = 3 mm. Slit_x = 2 mm. Isolation height set to 0.5 mm. Sweep of busbar thickness value**

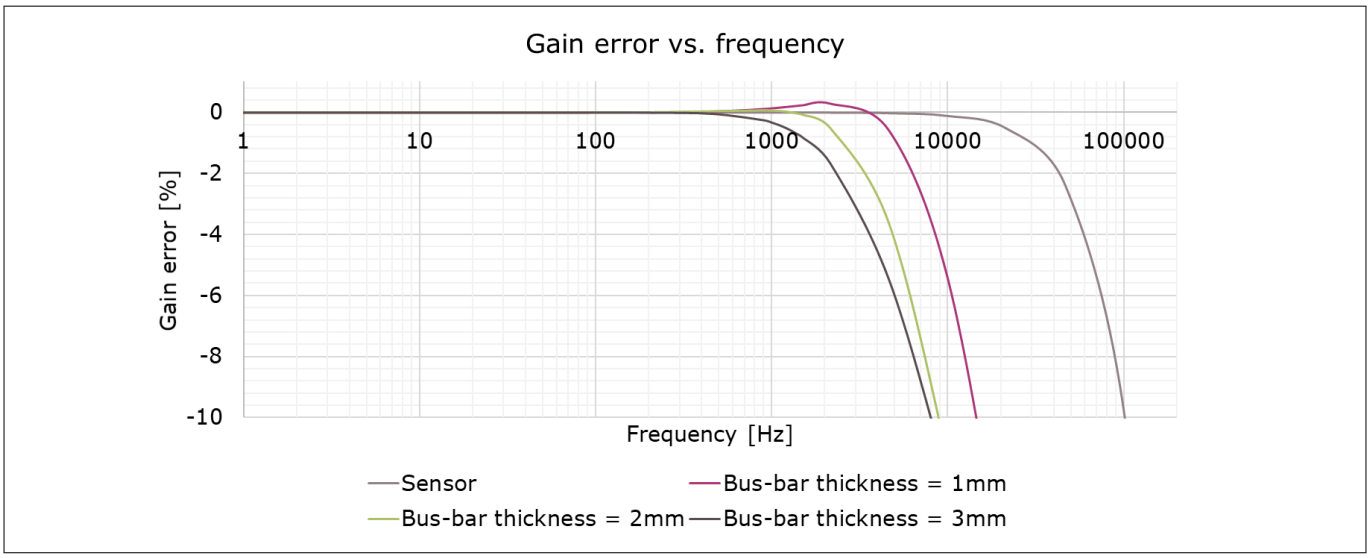

Figure 21 **Gain error over frequency for a 16 mm wide busbar. Residual current rail = 3 mm. Slit_x = 2 mm. Isolation height set to 0.5 mm. Sweep of busbar thickness value**

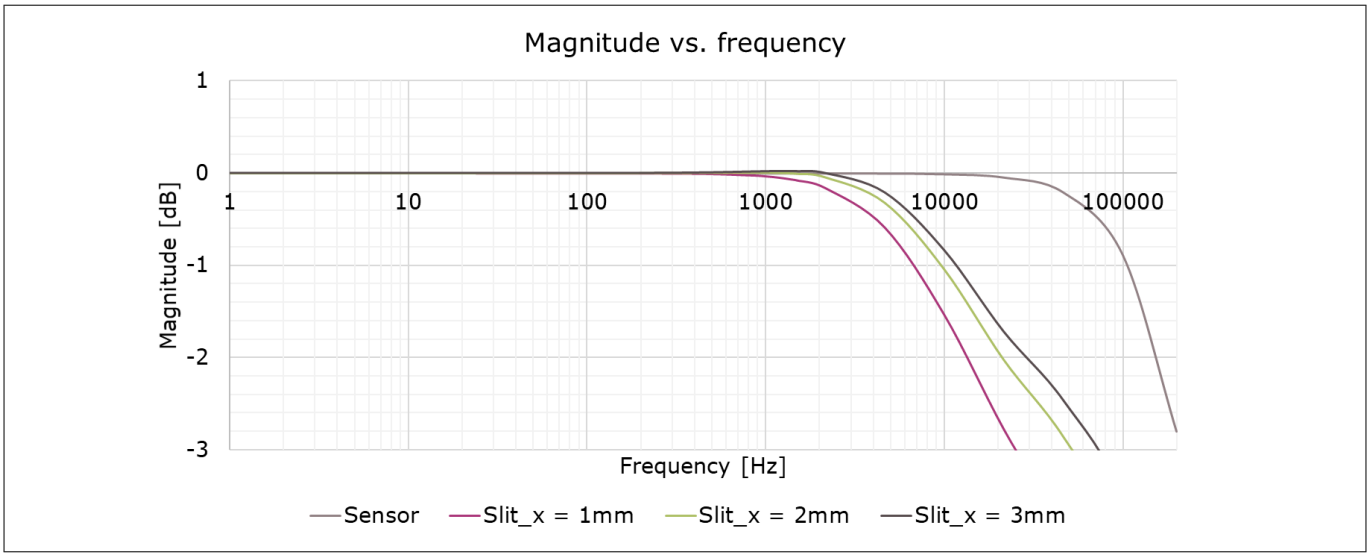

Figure 22 **Magnitude over frequency for a 2 mm thick busbar, 16 mm wide. Residual current rail = 3 mm. Isolation height set to 0.5 mm. Sweep of slit_x value**

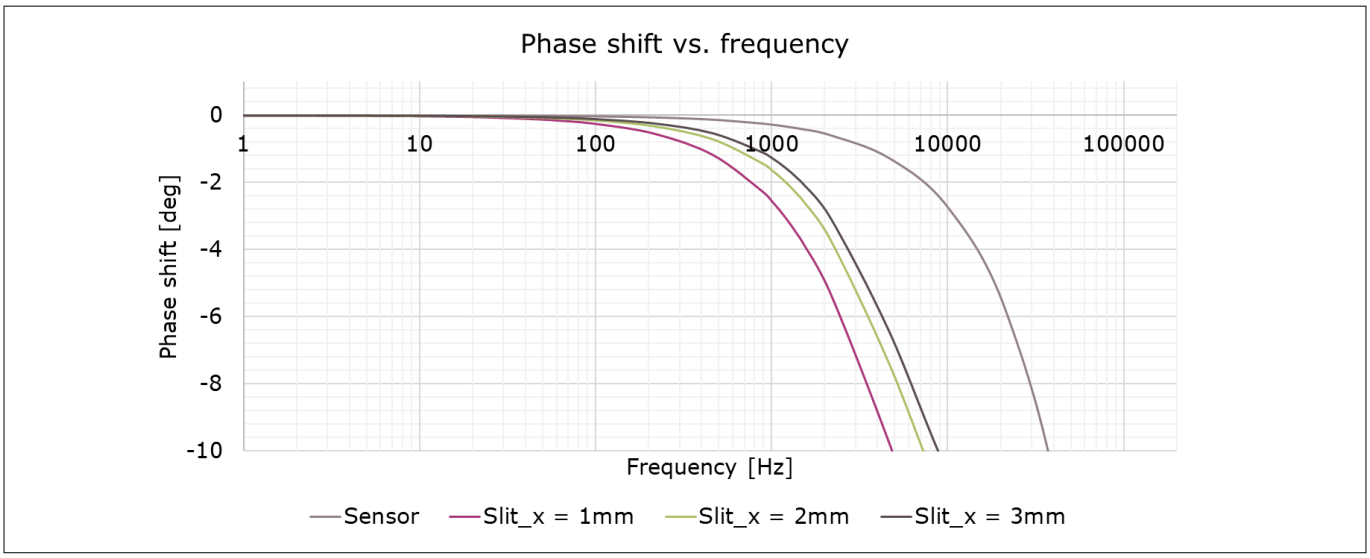

Figure 23 **Phase shift over frequency for a 2 mm thick busbar, 16 mm wide. Residual current rail = 3 mm. Isolation height set to 0.5 mm. Sweep of slit_x value**

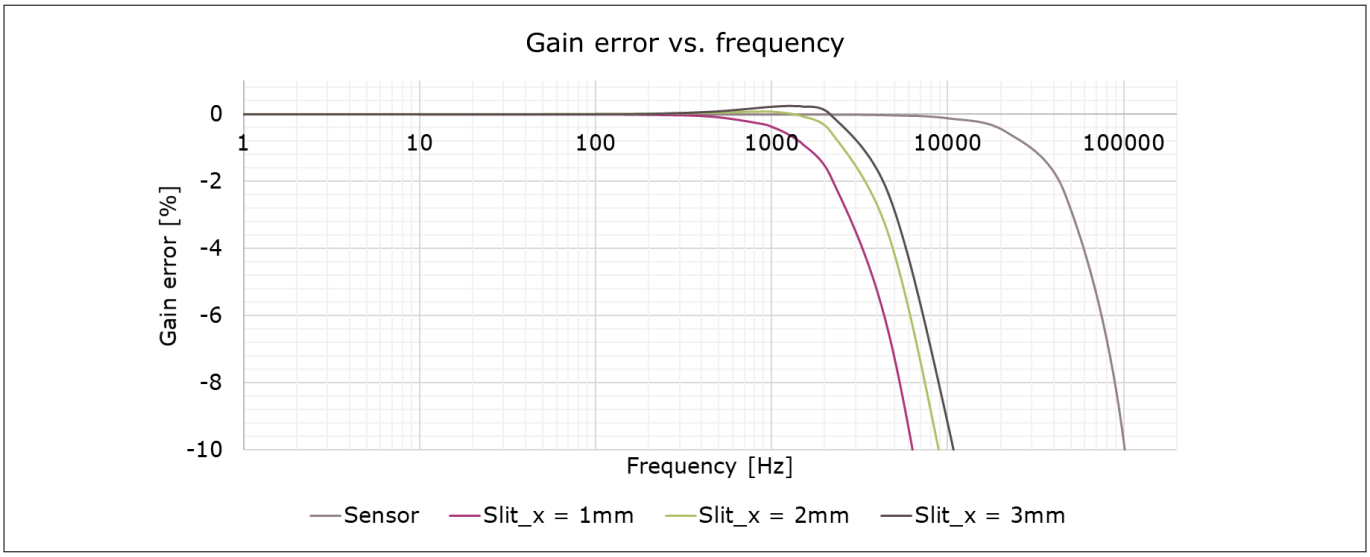

Figure 24 **Gain error over frequency for a 2 mm thick busbar, 16 mm wide. Residual current rail = 3 mm. Isolation height set to 0.5 mm. Sweep of slit_x value**

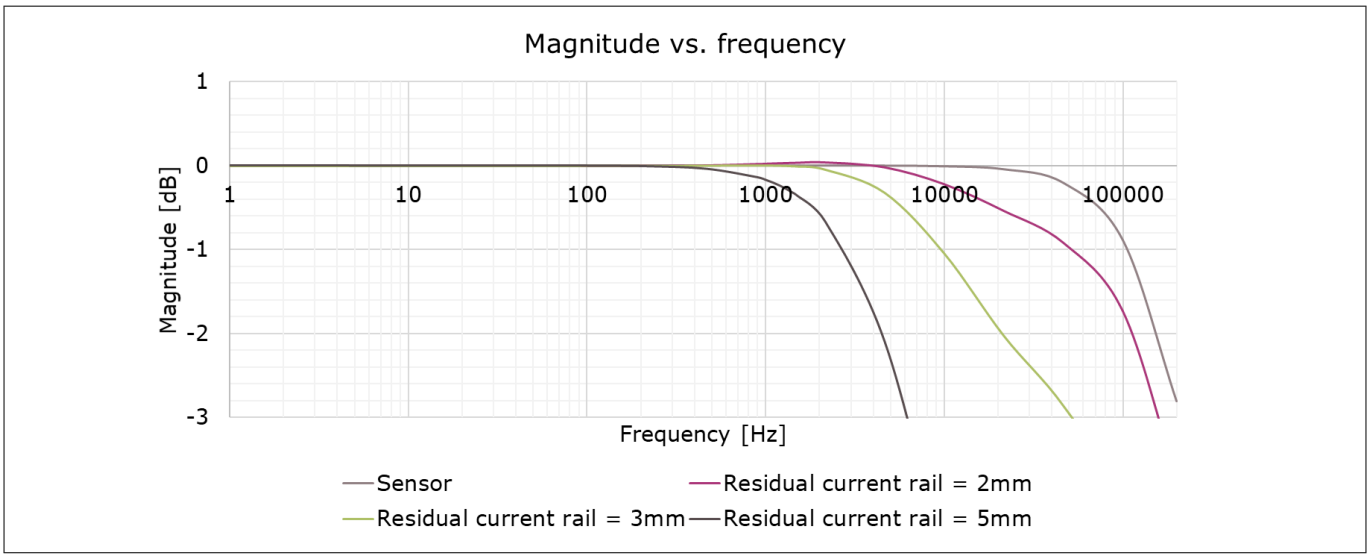

Figure 25 **Magnitude over frequency for a 2 mm thick busbar, 16 mm wide. Slit_x = 2 mm. Isolation height set to 0.5 mm. Sweep of residual current rail value**

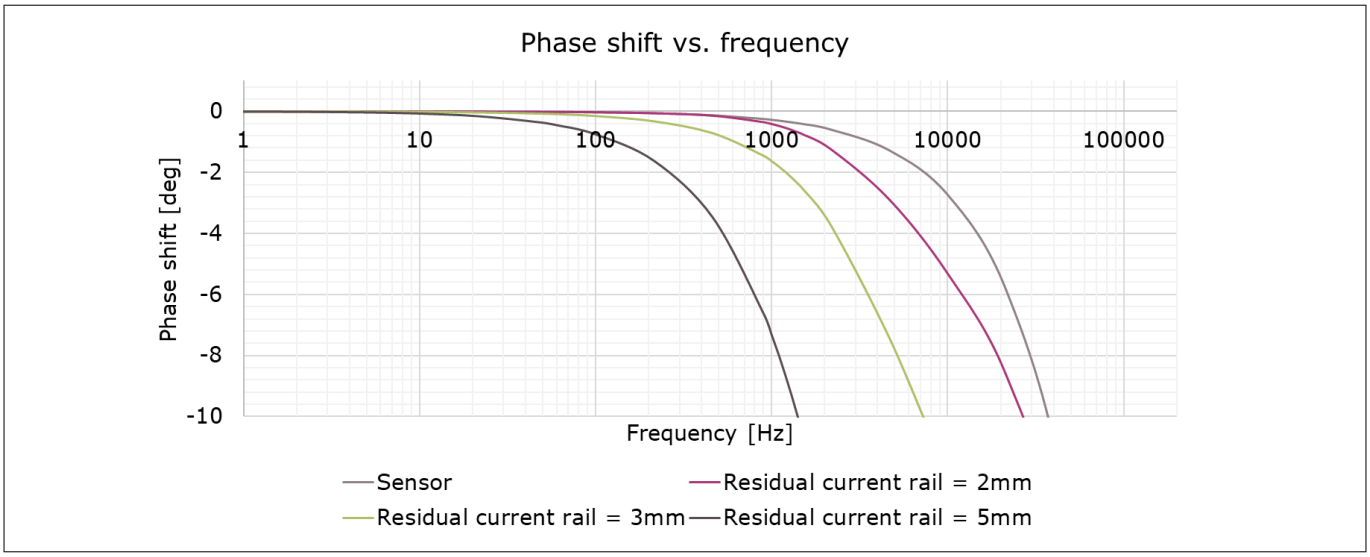

Figure 26 **Phase shift over frequency for a 2 mm thick busbar, 16 mm wide. Slit_x = 2 mm. Isolation height set to 0.5 mm. Sweep of residual current rail value**

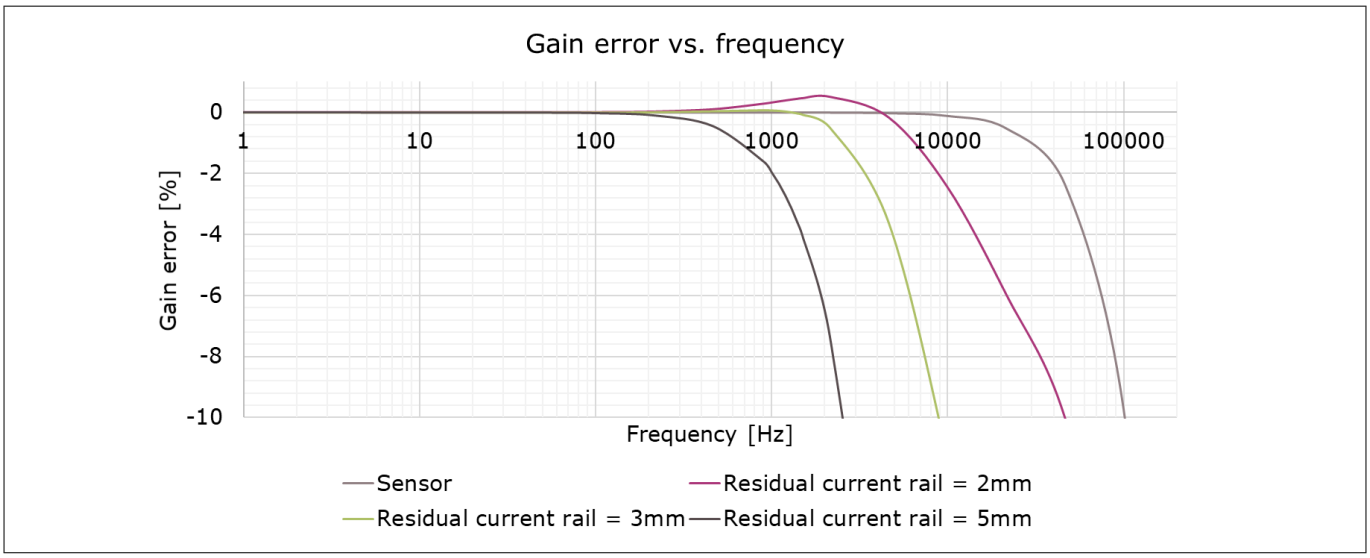

Figure 27 **Gain error over frequency for a 2 mm thick busbar, 16 mm wide. Slit_x = 2 mm. Isolation height set to 0.5 mm. Sweep of residual current rail value**

3.1.1.4 Misalignment effect

If the sensor is not aligned with the current rail in its nominal position due to manufacturing tolerances, the transfer factor will differ from the nominal one. We refer to this error component as "transfer factor error". This error component will contribute to the total initial sensitivity error, and it is possible to compensate it within the calibration range specified in the product datasheet [1]. However, if the sensor gets displaced during system operation due to mechanical vibrations or thermal expansion effects, the transfer factor will experience a drift. Quantifying this error component is important in order to verify that the in-system end of line calibration is feasible and that the transfer factor doesn't drift outside specifications during operation.

In the figures below, the results of transfer factor simulations in which the sensor is displaced in the three directions of space are shown, in case of different slit_x and residual current rail values. The busbar design has been chosen among the lateral insertion Straight slit designs proposed in the previous chapters.

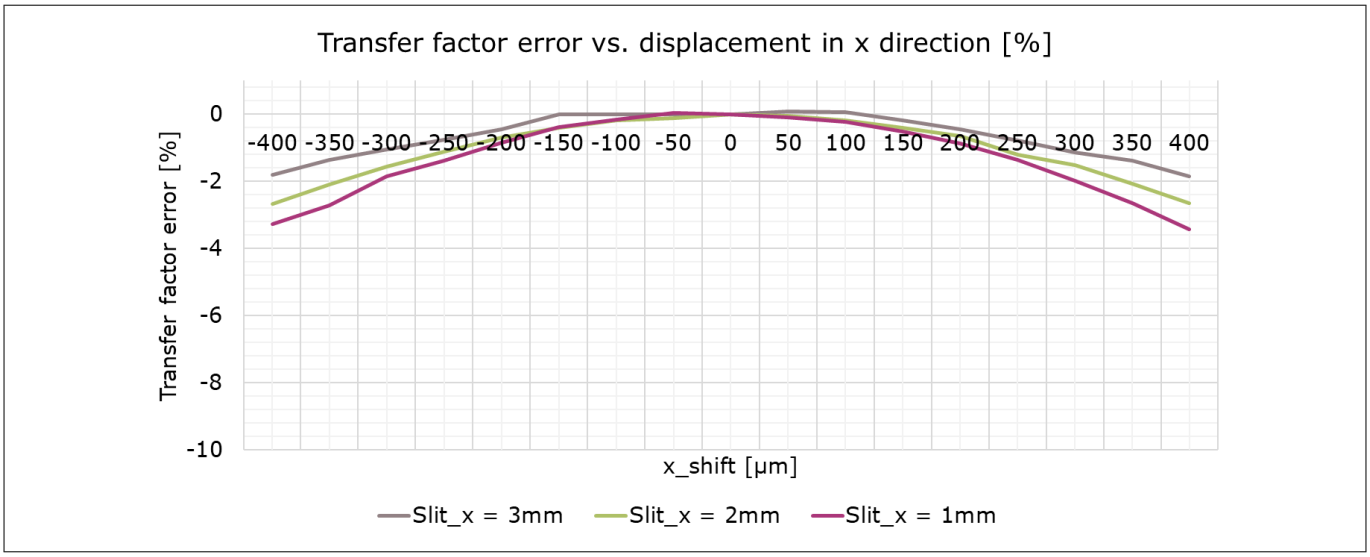

Figure 28 **Displacement in X direction. Current rail transfer factor error for a 2 mm thick busbar, 16 mm wide. Residual current rail = 3 mm. Isolation height set to 0.5 mm. Sweep of slit_x value**

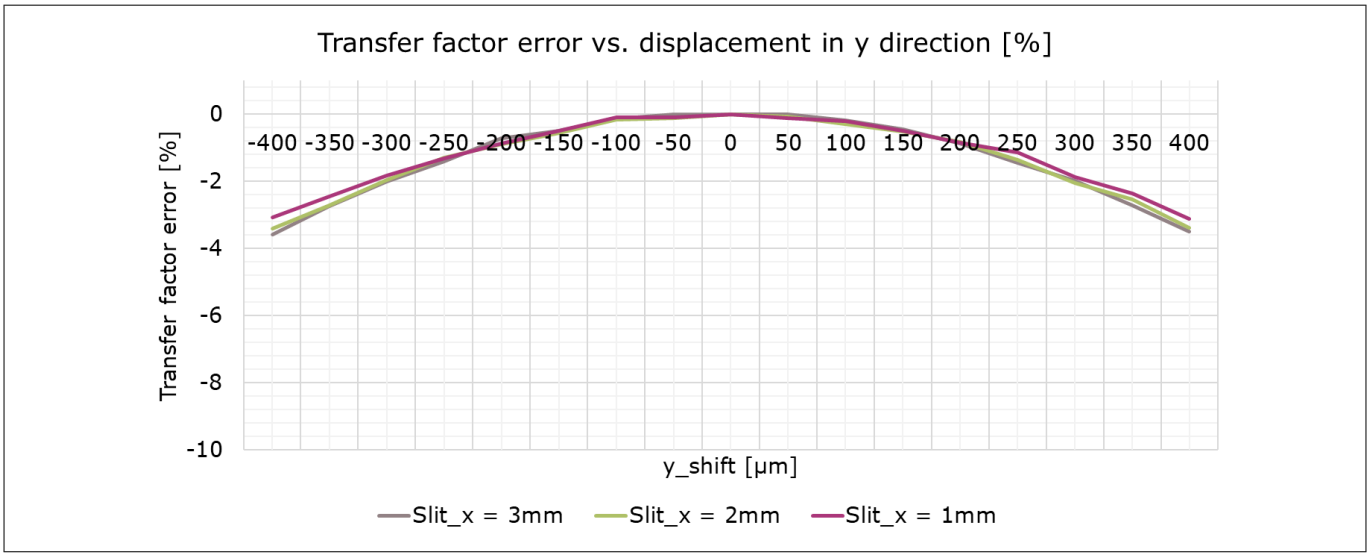

Figure 29 **Displacement in Y direction. Current rail transfer factor error for a 2 mm thick busbar, 16 mm wide. Residual current rail = 3 mm. Isolation height set to 0.5 mm. Sweep of slit_x value**

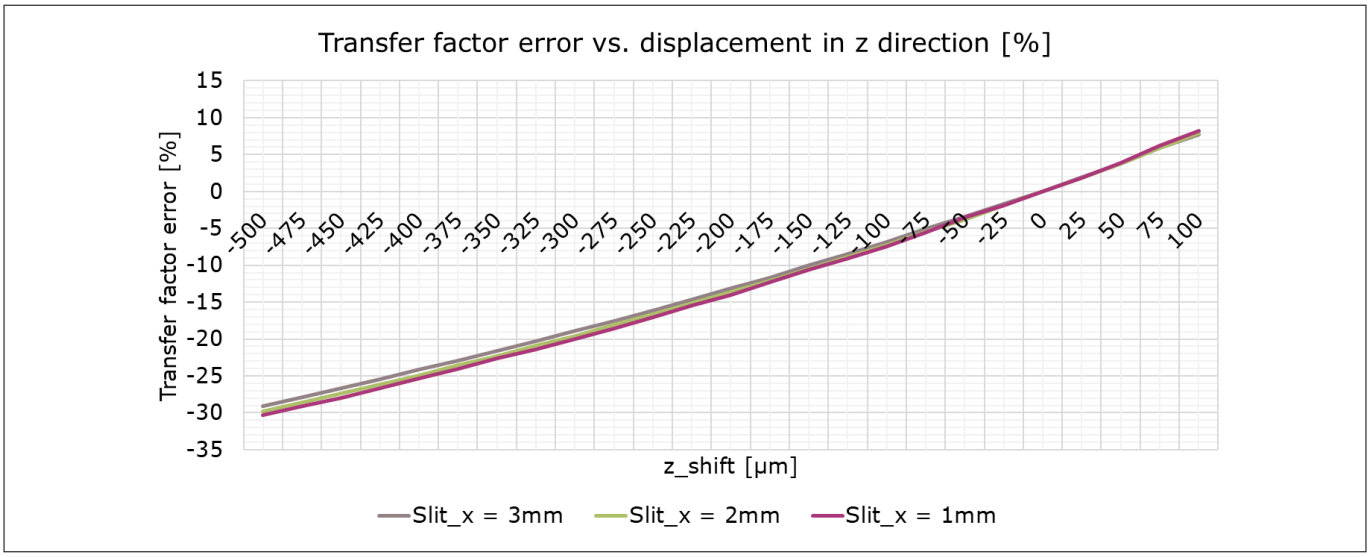

Figure 30 **Displacement in Z direction. Current rail transfer factor error for a 2 mm thick busbar, 16 mm wide. Residual current rail = 3 mm. Isolation height set to 0.5 mm. Sweep of slit_x value**

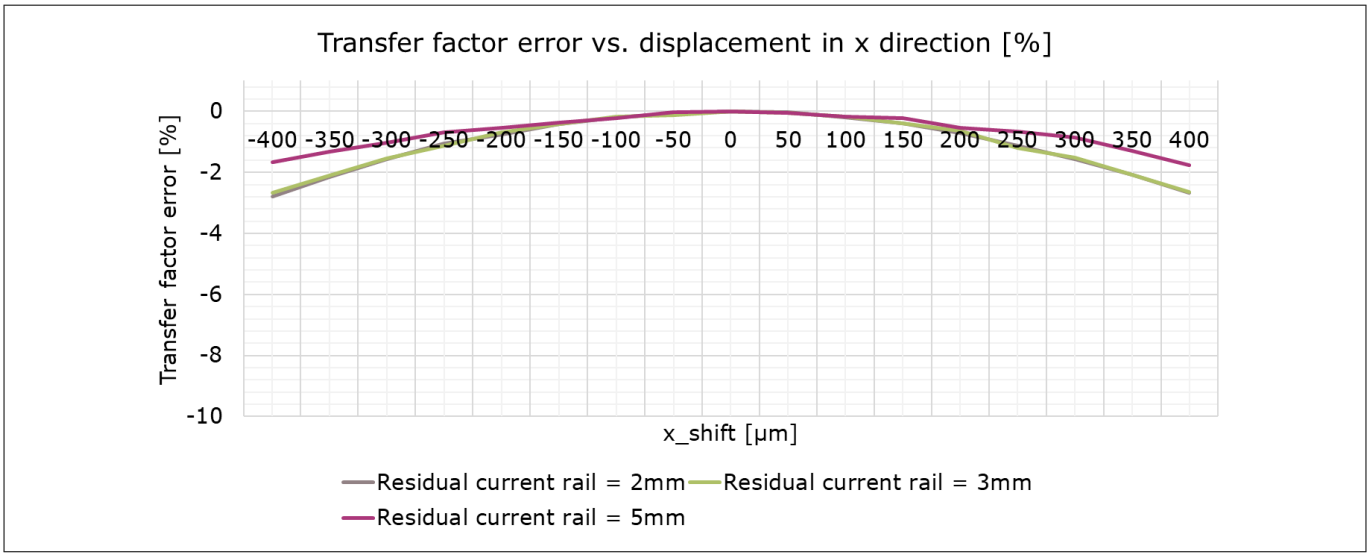

Figure 31 **Displacement in X direction. Current rail transfer factor error for a 2 mm thick busbar, 16 mm wide. Slit_x = 2 mm. Isolation height set to 0.5 mm. Sweep of residual current rail value**

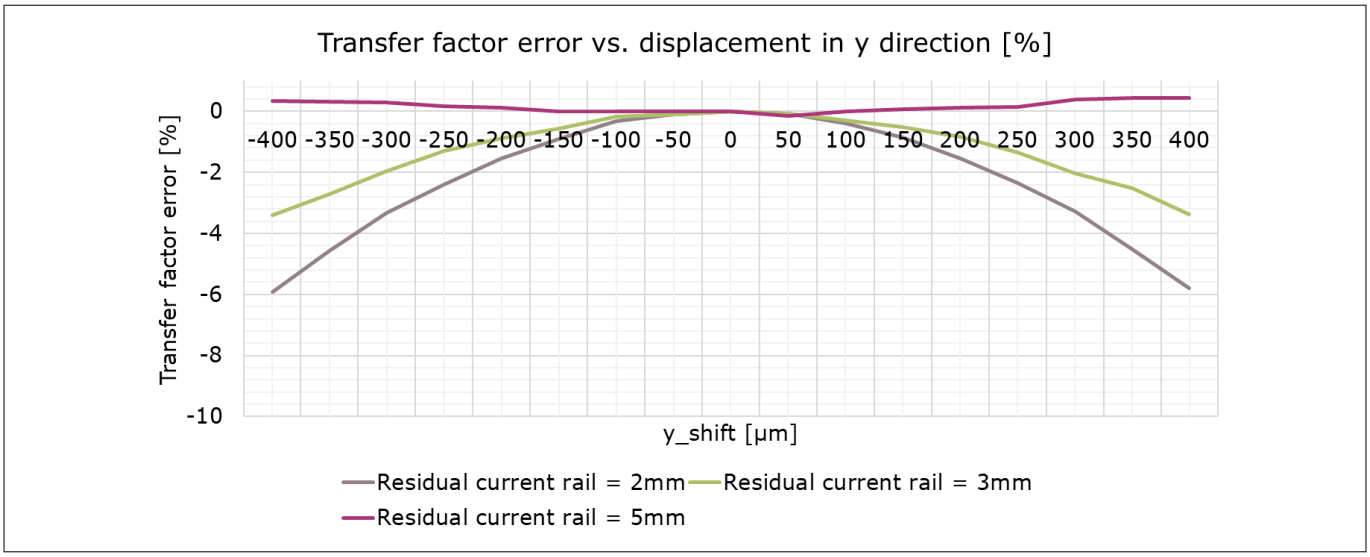

Figure 32 **Displacement in Y direction. Current rail transfer factor error for a 2 mm thick busbar, 16 mm wide. Slit_x = 2 mm. Isolation height set to 0.5 mm. Sweep of residual current rail value**

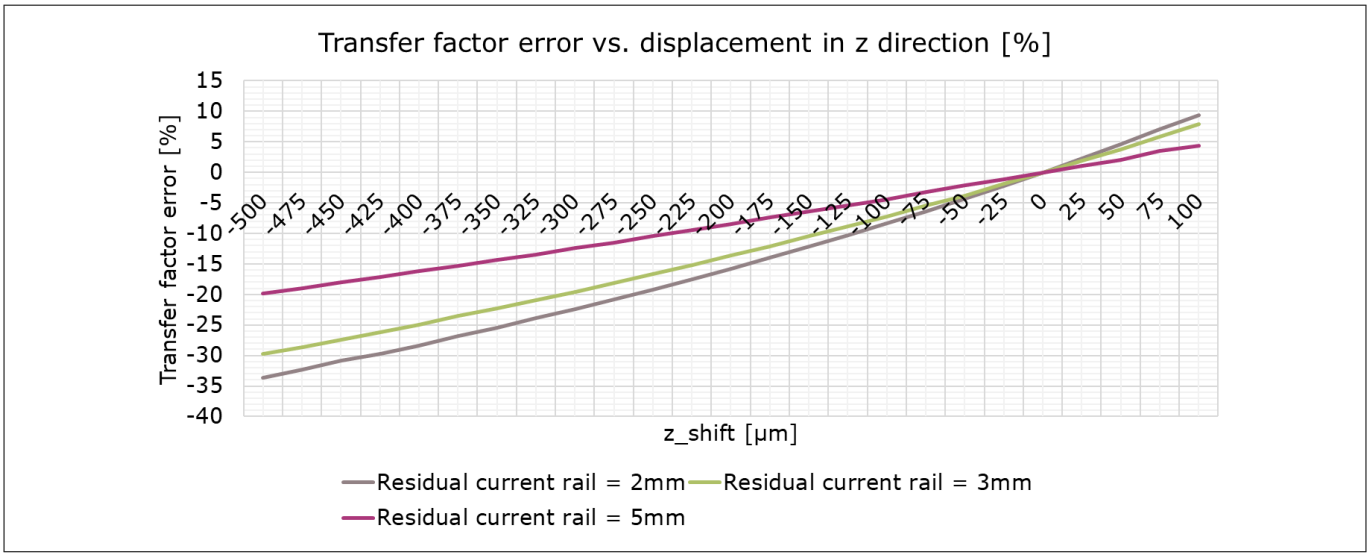

Figure 33 **Displacement in Z direction. Current rail transfer factor error for a 2 mm thick busbar, 16 mm wide. Slit_x = 2 mm. Isolation height set to 0.5 mm. Sweep of residual current rail value**

In case misalignment has a critical impact, a wider slit_x value can help with obtaining less sensitivity to misalignments in X direction. A wider residual current rail can in turn reduce the sensitivity to misalignments in Y direction. However, both measures will lead to a reduction of the nominal transfer factor, as shown in the previous paragraphs.

Misalignments have a minor impact on the frequency response as well. This impact is limited and usually neglectable if the sensing structure is symmetric with respect to the sensing elements location. Magnitude and phase shift are affected; in the figures below the misalignment impact on the frequency response on the busbar is shown, for a worst-case misalignment of ± 0.4 mm in X and Y directions, -0.4 mm to +0.1 mm for Z direction.

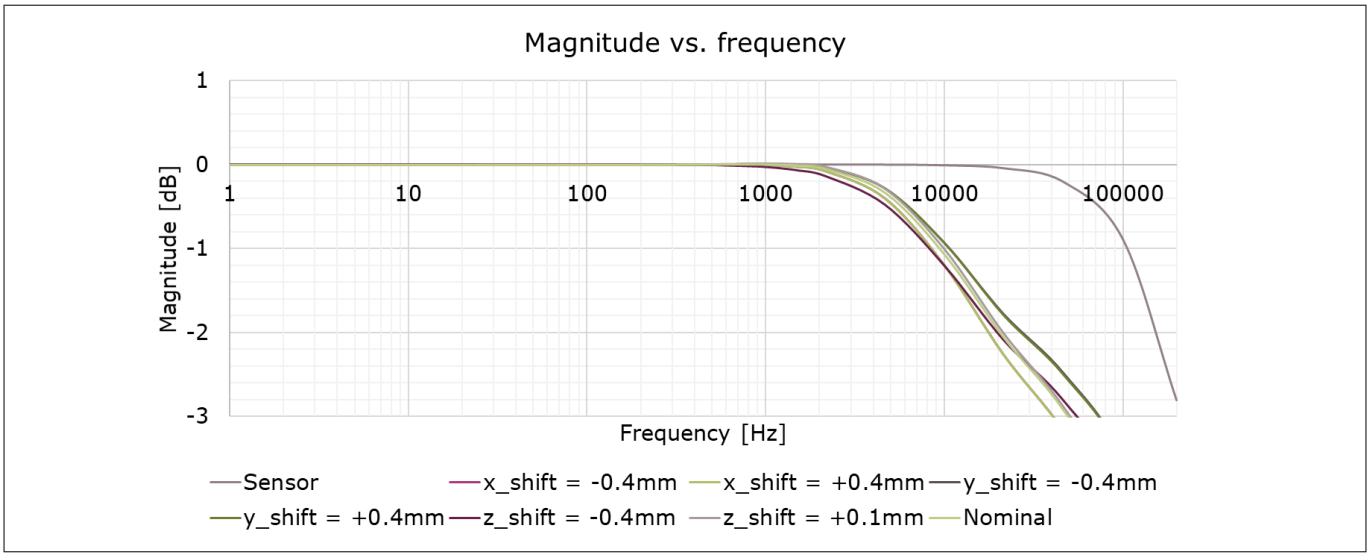

Figure 34 **Magnitude over frequency for a 2 mm thick busbar, 16 mm wide. Slit_x = 2 mm. Isolation height set to 0.5 mm. Residual current rail = 3 mm. Sweep of x_shift, y_shift and z_shift values**

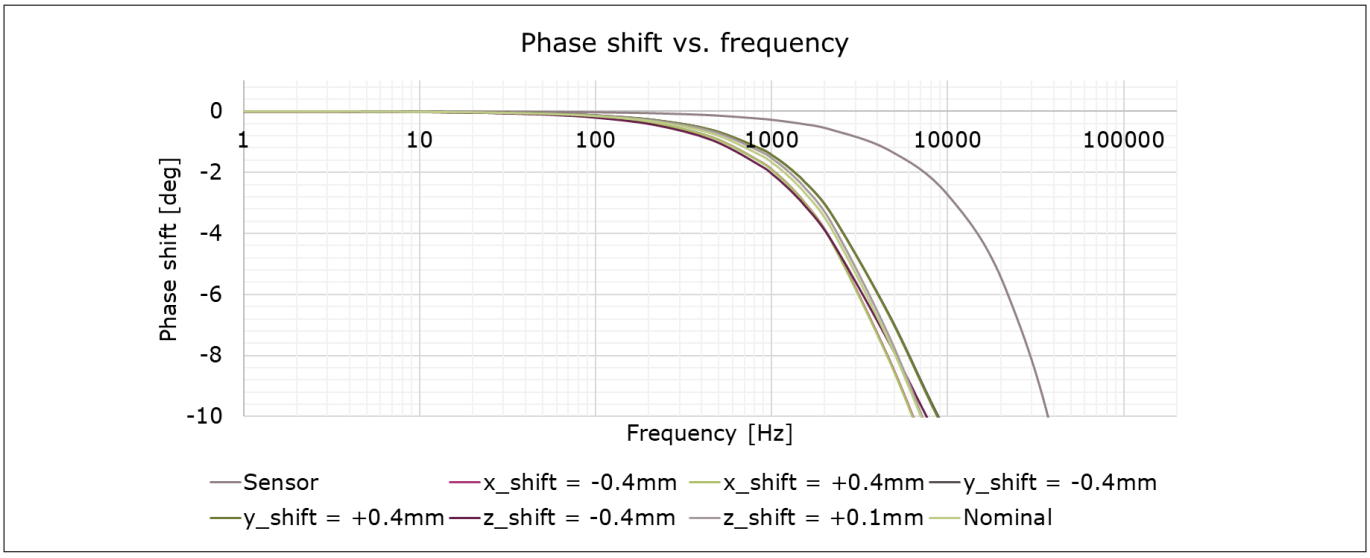

Figure 35 **Phase shift over frequency for a 2 mm thick busbar, 16 mm wide. Slit_x = 2 mm. Isolation height set to 0.5 mm. Residual current rail = 3 mm. Sweep of x_shift, y_shift and z_shift values**

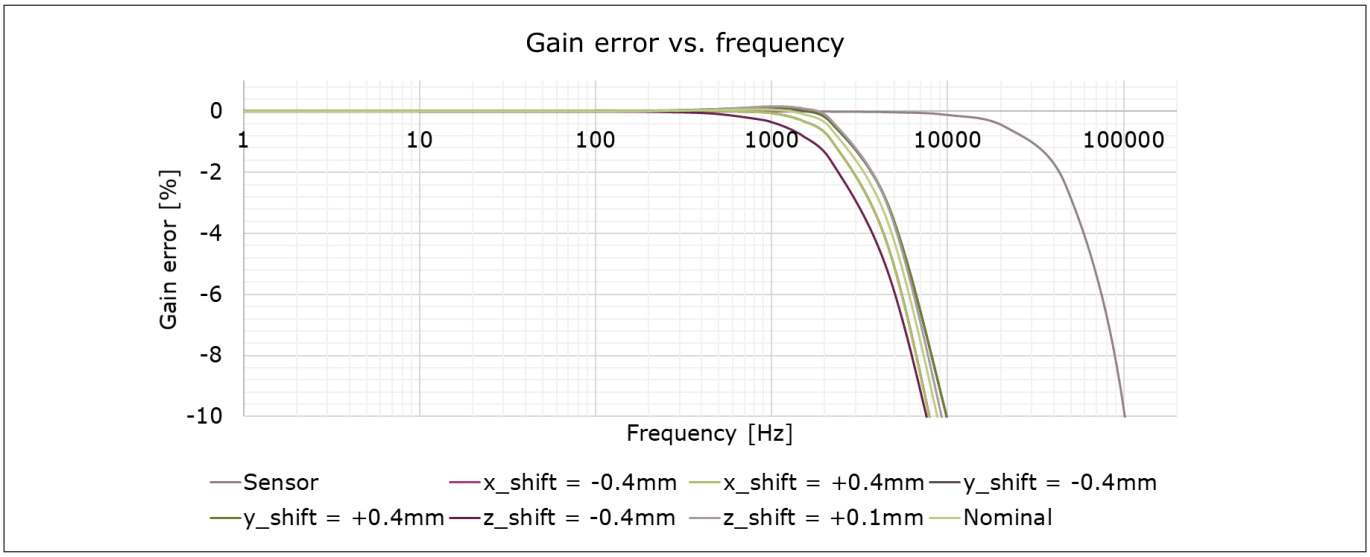

Figure 36 **Gain error over frequency for a 2 mm thick busbar, 16 mm wide. Slit_x = 2 mm. Isolation height set to 0.5 mm. Residual current rail = 3 mm. Sweep of x_shift, y_shift and z_shift values**

3.1.1.5 Crosstalk

In case of multi-phase systems, the magnetic field generated by the current flowing in nearby phases can influence the current measurement. The percentage of signal that is measured on a phase and that flows in the nearby phase is here denominated as crosstalk factor.

The figure below shows an example of three phase system constituted of three of the busbars presented in the previous paragraphs. The middle-to-middle spacing in Y direction is 26 mm; this corresponds to the distance between the sensing structure centers belonging to adjacent phases. That results in a crosstalk factor of 1.1 % between adjacent phases, 0.29 % between right and left phases. In case the phases are very close to each other, like in the outer to middle case, the crosstalk factor is 1.1 %. This value can be reduced through a different sensor orientation and it is important to mention that the crosstalk factor is stable over temperature and lifetime; it can be characterized and the resulting error can be compensated. Further details about crosstalk compensation are available in the User manual [2].

In the next paragraph it is shown how to reduce the crosstalk factor at the expense of either transfer factor or insertion resistance.

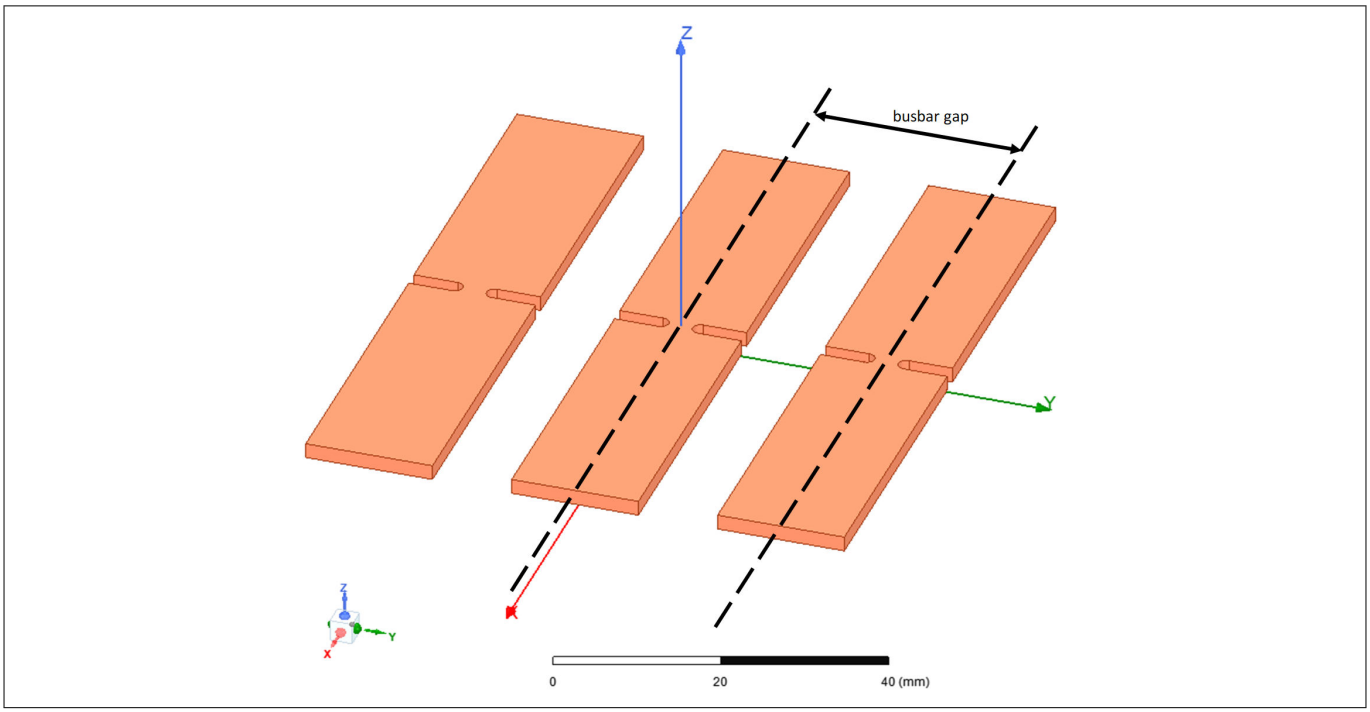

Figure 37 Three phases system made by three 2 mm thick busbar, 16 mm wide. Slit_x = 2 mm. Isolation height set to 0.5 mm. Residual current rail = 3 mm. Busbar gap = 26 mm

3.1.2 S-bend shaped sensing structure

The sensing structure can be realized using the so called "S-bend" shape. Instead of following a "Straight" path, the current is forced to flow in a "S" shape path. In order to better exploit the field lines, the sensor is rotated as well. In the figures below the typical S-bend shapes are shown.

The rotation of the sensor brings another positive effect: rotating the sensors so that the sensing elements of different sensors don't lie on the same line reduces significantly the crosstalk factors between adjacent sensors in multi-phase systems. With the increment of the rotation angle from 0° to 90°, the difference between the distances of each sensing element and the adjacent busbar reduces, going from 2.26 mm (sensing element pitch) in case of Straight shape to 0 mm in case of 90° S-bend. That means that while in the 90° S-bend case the current in the adjacent busbar will generate the same field components on the two sensing elements, in the Straight case it will generate slightly different components, due to the 2.26 mm distance difference; hence a differential field component will appear. In the 45° S-bend case, the crosstalk factors will have a value in between.

However, the mismatch of the sensing elements will generate a differential component in the 90° S-bend case as well. This is neglectable as demonstrated by the stray field suppression factor, which is reported in the product datasheet [1]. Further details about crosstalk compensation are available in the User manual [2].

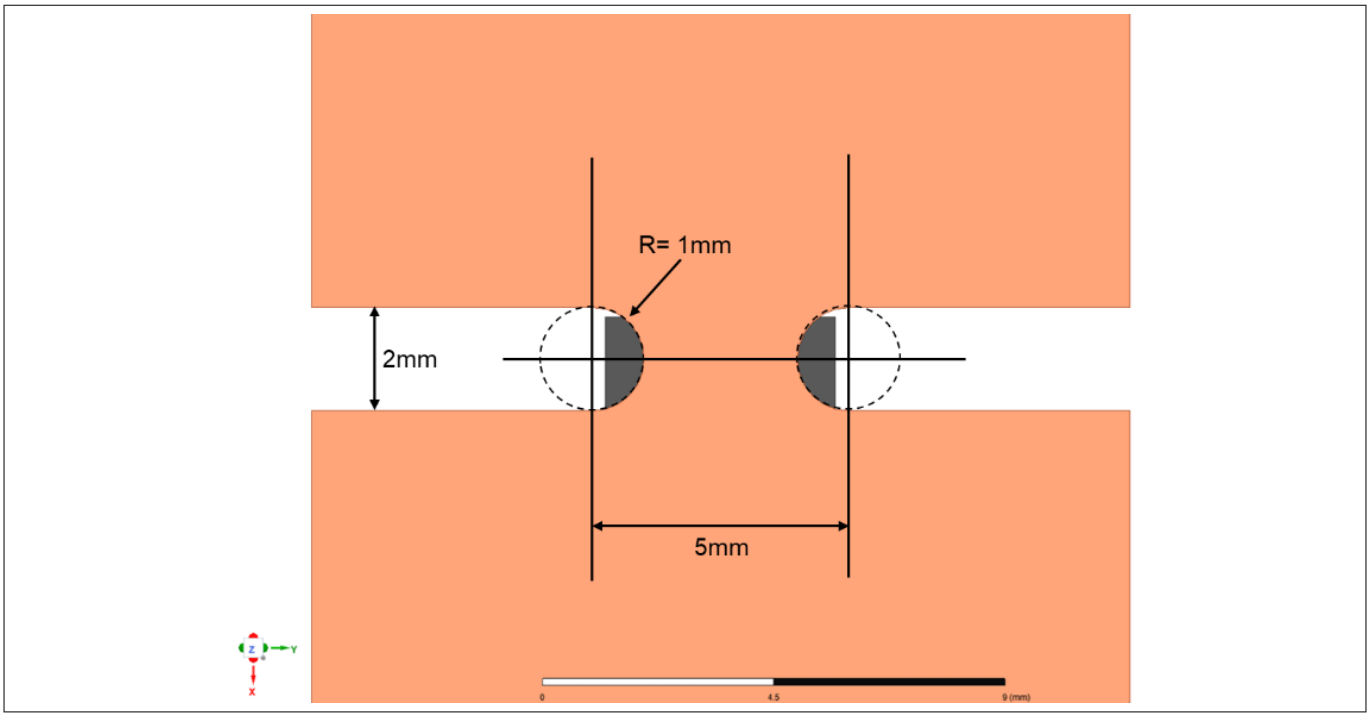

Figure 38 Straight sensing structure shape

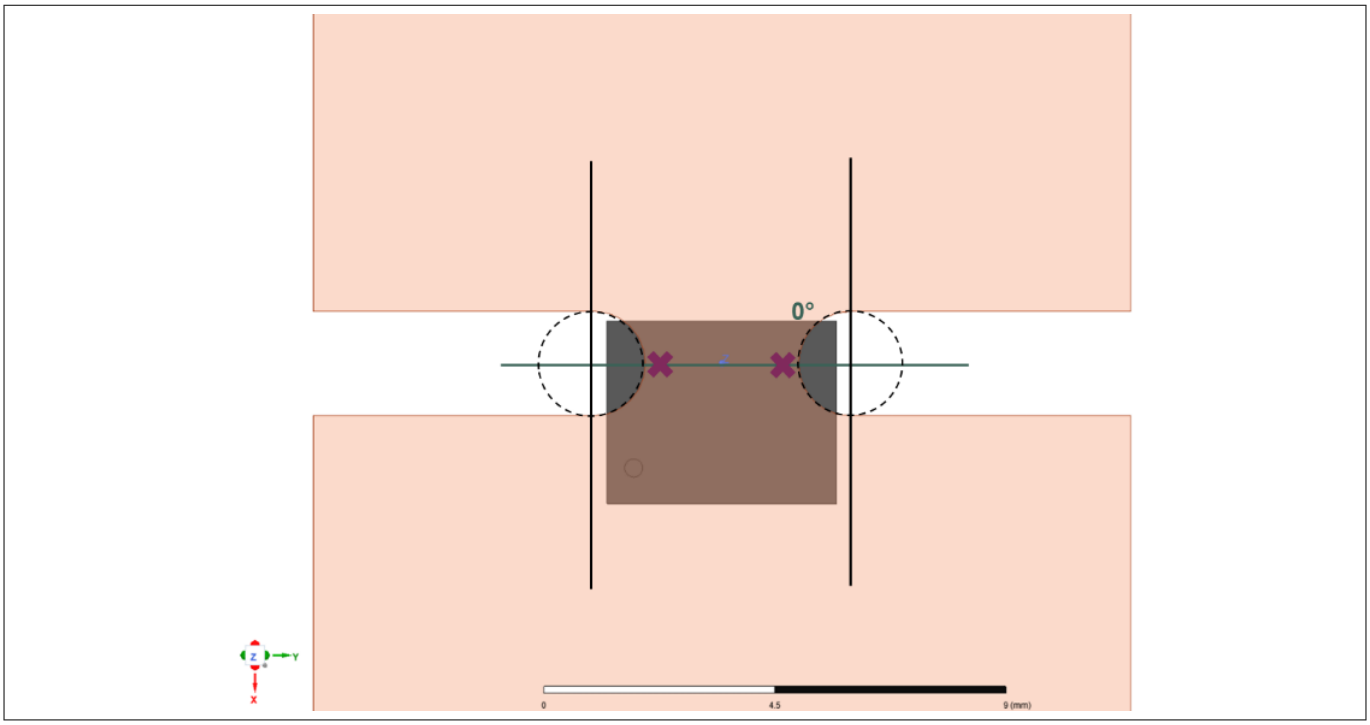

Figure 39 Straight sensing structure shape

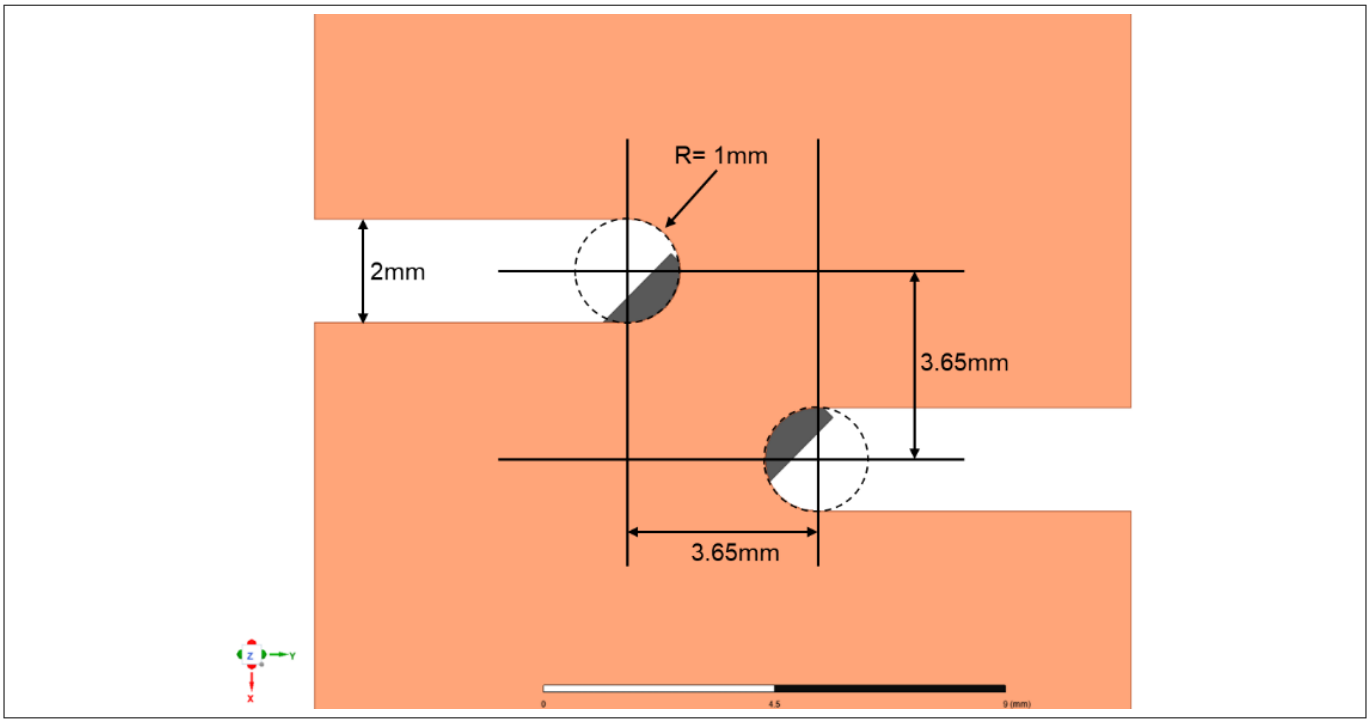

Figure 40 **45° S-bend sensing structure shape**

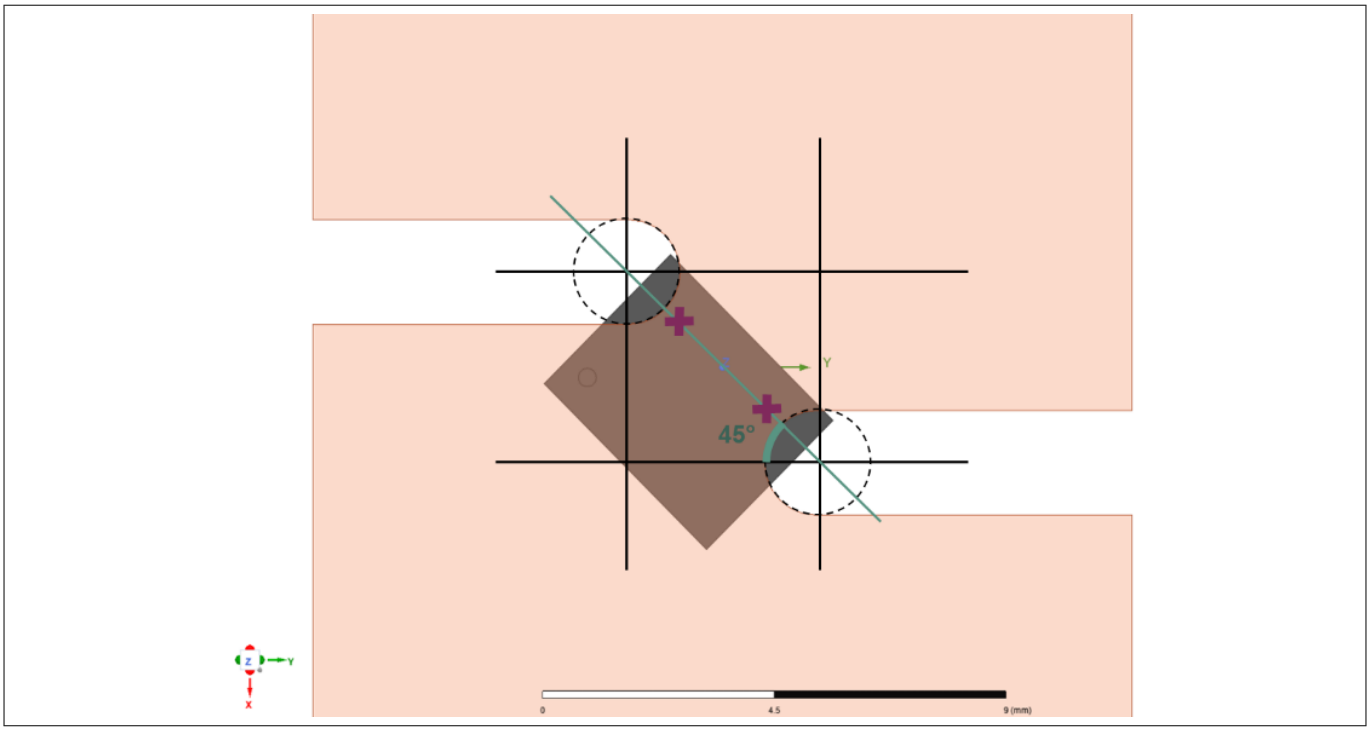

Figure 41 **45° S-bend sensing structure shape**

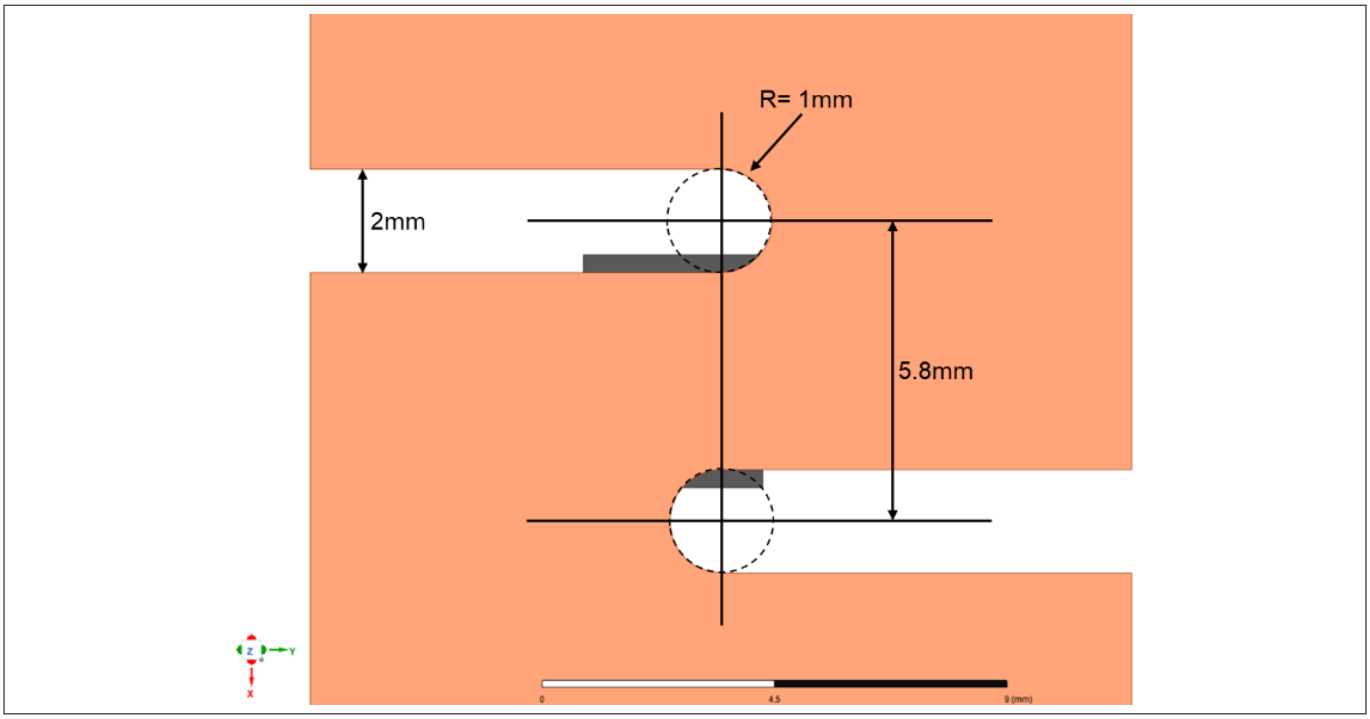

Figure 42 90° S-bend sensing structure shape

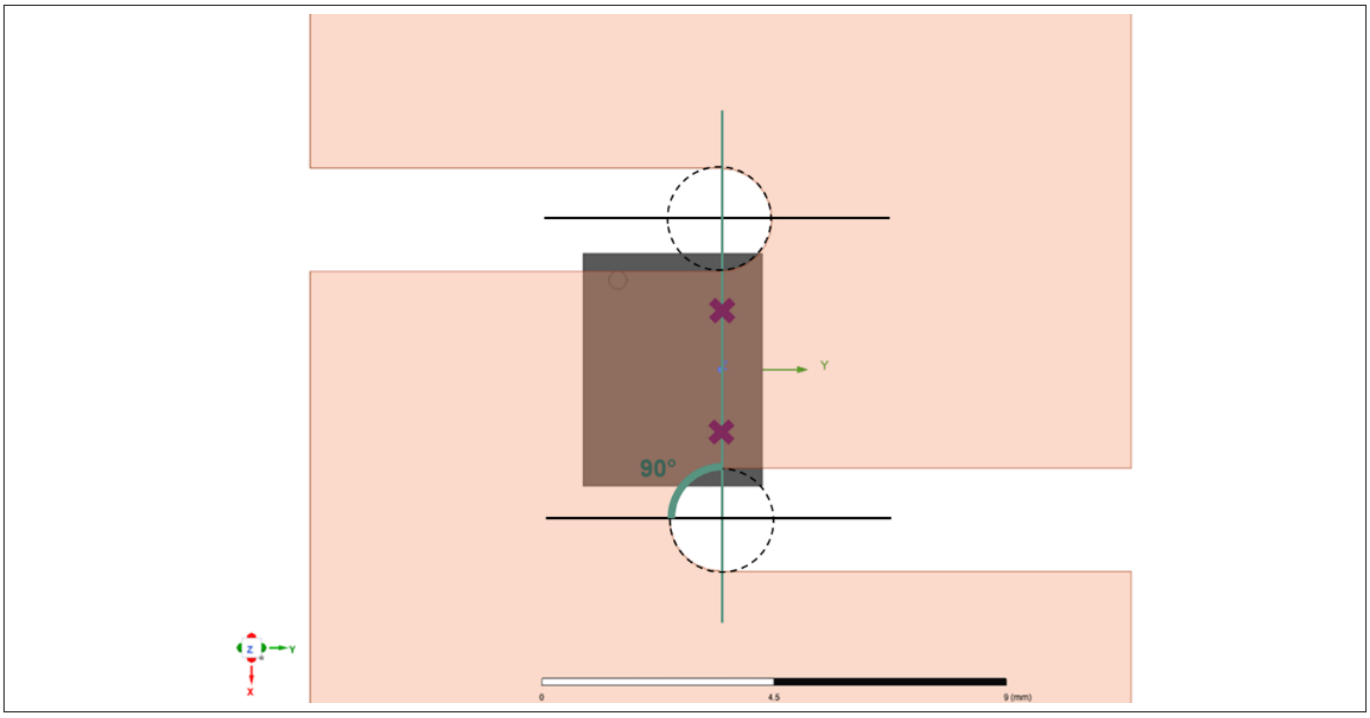

Figure 43 90° S-bend sensing structure shape

The simulation results confirm the significant reduction of the crosstalk factor, at the expense of the insertion resistance. For the same transfer factor, the resistance nearly doubles switching from Straight to 90° S-bend sensing structure. The three sensing structures have been analyzed through FEM simulation. In all cases, the busbar thickness is 2 mm and the busbar width is 16 mm. The isolation height is set to 0.5 mm. The slit dimension and position has been tuned in order to achieve the same current rail transfer factor, that is 33 µT/A in all cases. In the figures below the simulation results for insertion resistance and crosstalk factor calculation are shown.

The frequency response behavior in the three cases is also reported. As for insertion resistance, there's a worsening of the performance in case of frequency response switching from Straight to 90° S-bend shape, but less significant.

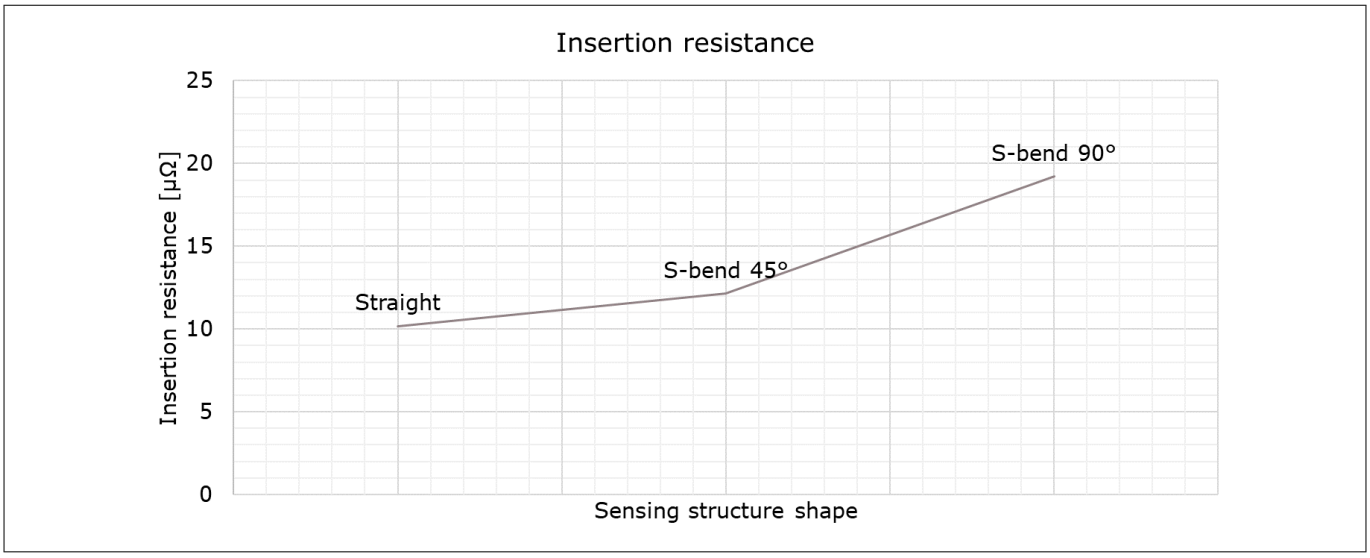

Figure 44 Insertion resistance for Straight, 45° S-bend and 90° S-bend sensing structures

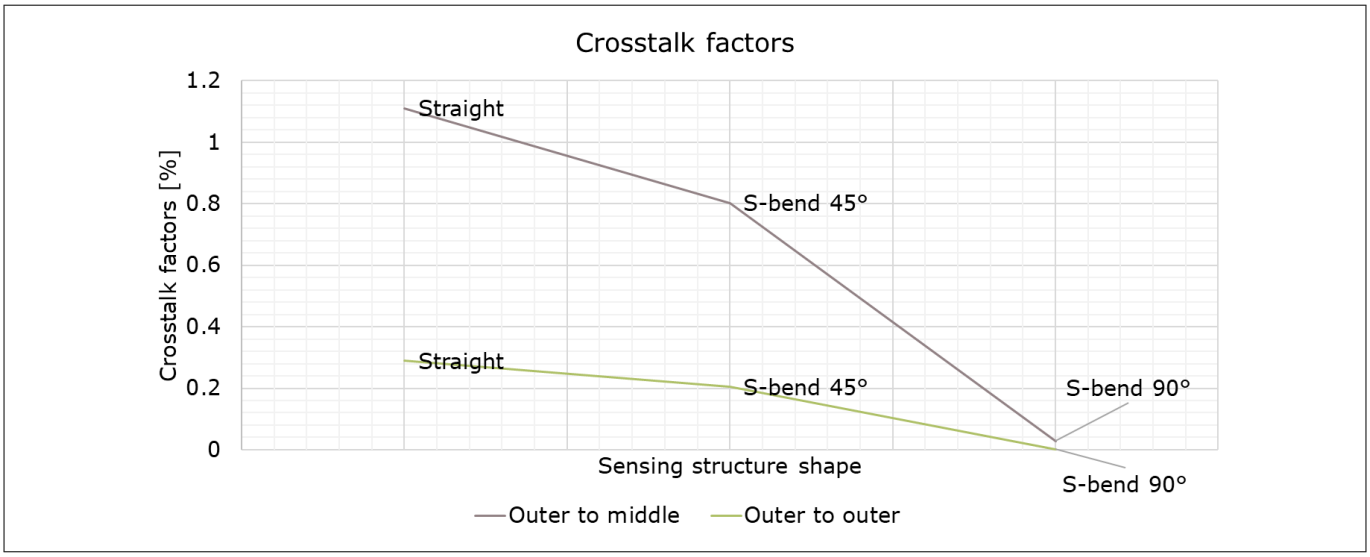

Figure 45 Crosstalk factors for Straight, 45° S-bend and 90° S-bend sensing structures

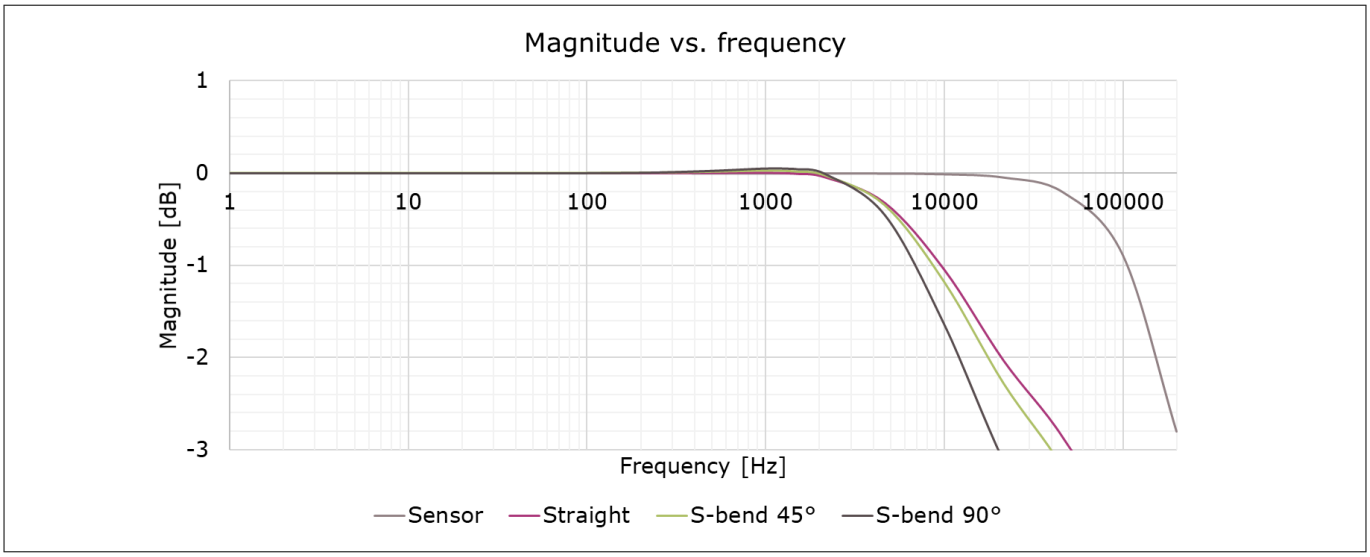

Figure 46 **Magnitude over frequency for Straight, 45° S-bend and 90° S-bend sensing structures**

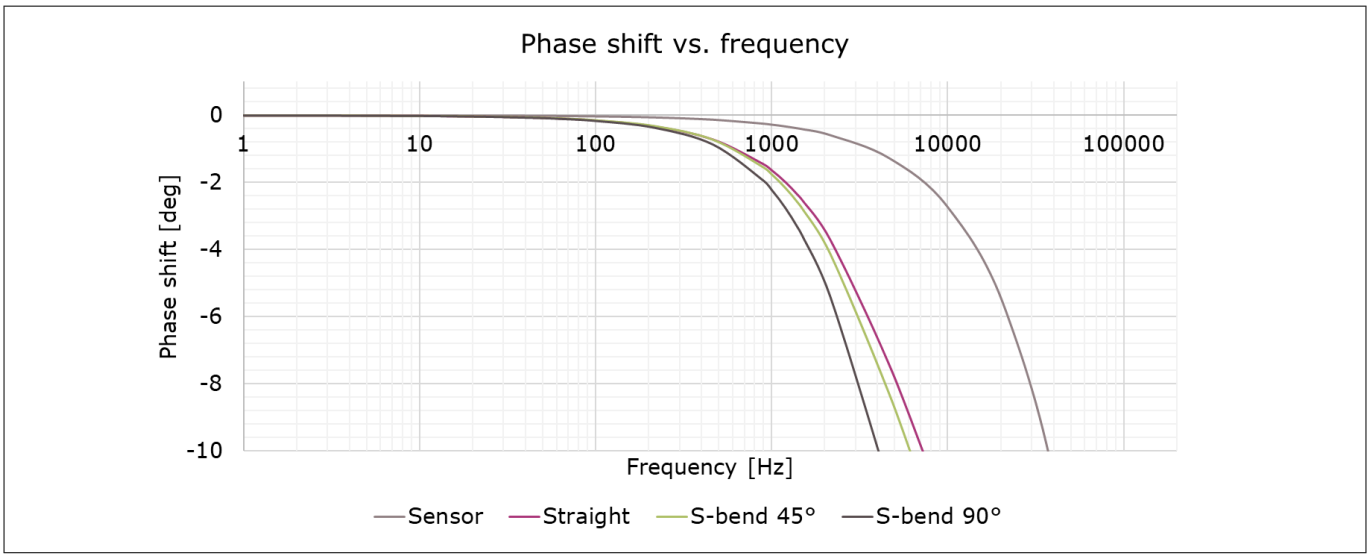

Figure 47 **Phase shift over frequency for Straight, 45° S-bend and 90° S-bend sensing structures**

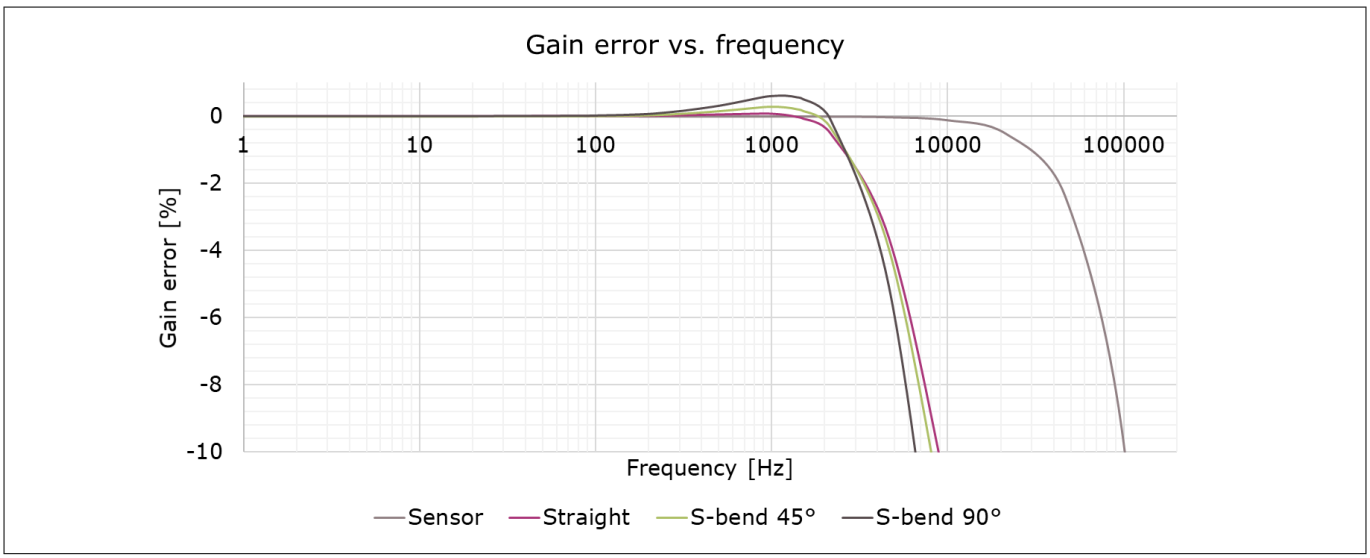

Figure 48 **Gain error over frequency for Straight, 45° S-bend and 90° S-bend sensing structures**

3.2 Vertical insertion on busbar support

Typically, busbars are used to carry the current in systems with current ratings above 500 A. It is possible to realize a sensing structure on a busbar by realizing slits at the sensing location, in order to increase the current density and hence the magnetic field on the sensing elements. The preferred sensor package is the PG-VSON-6 because it is leadless and compact, allowing easy mechanical integration and overmolding procedure. The vertical insertion on busbar support constitutes an alternative insertion method to the lateral insertion on busbar support. The sensor is soldered on a carrier PCB, typically overmolded, and the resulting sensing module is then inserted vertically in the busbar through a properly shaped slit. The overmolding material provides the voltage isolation between sensor and current rail.

3.2.1 Introduction

The busbar geometry is depicted in the following figures. The geometrical parameters have an effect on the performance factors: transfer factor, insertion resistance, frequency behavior, misalignment and crosstalk.

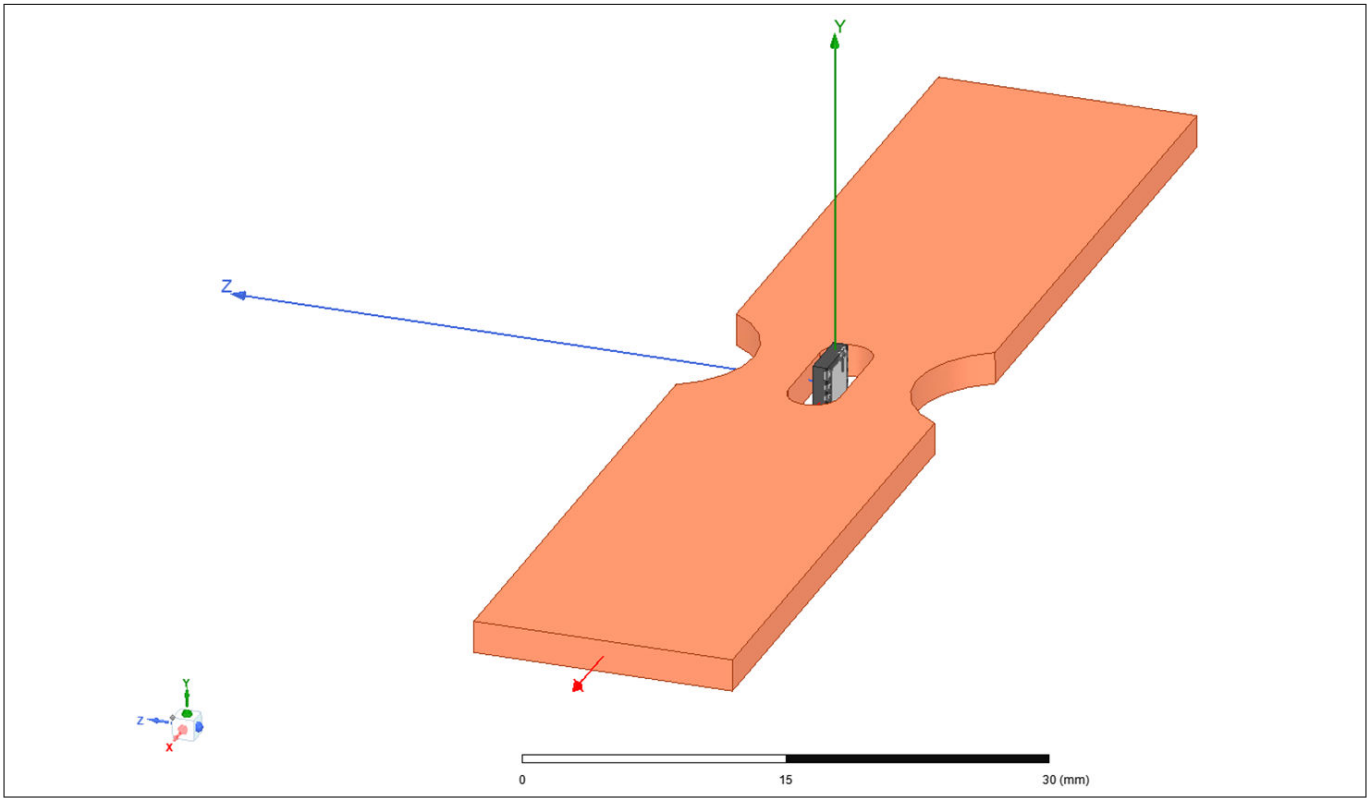

Figure 49 PG-VSON-6 package, Busbar support, vertical insertion, 3D view

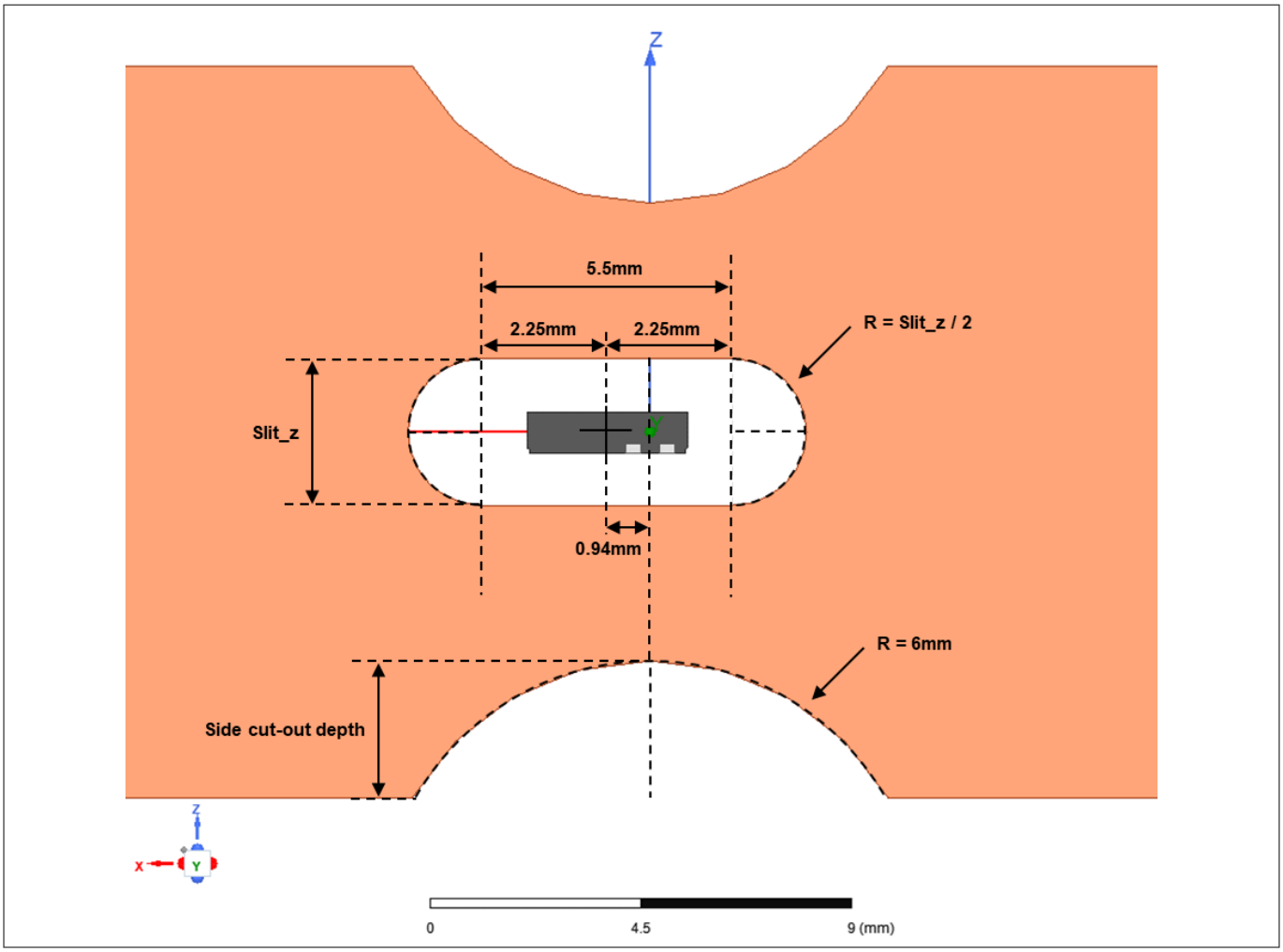

Figure 50 PG-VSON-6 package, Busbar support, vertical insertion, top view

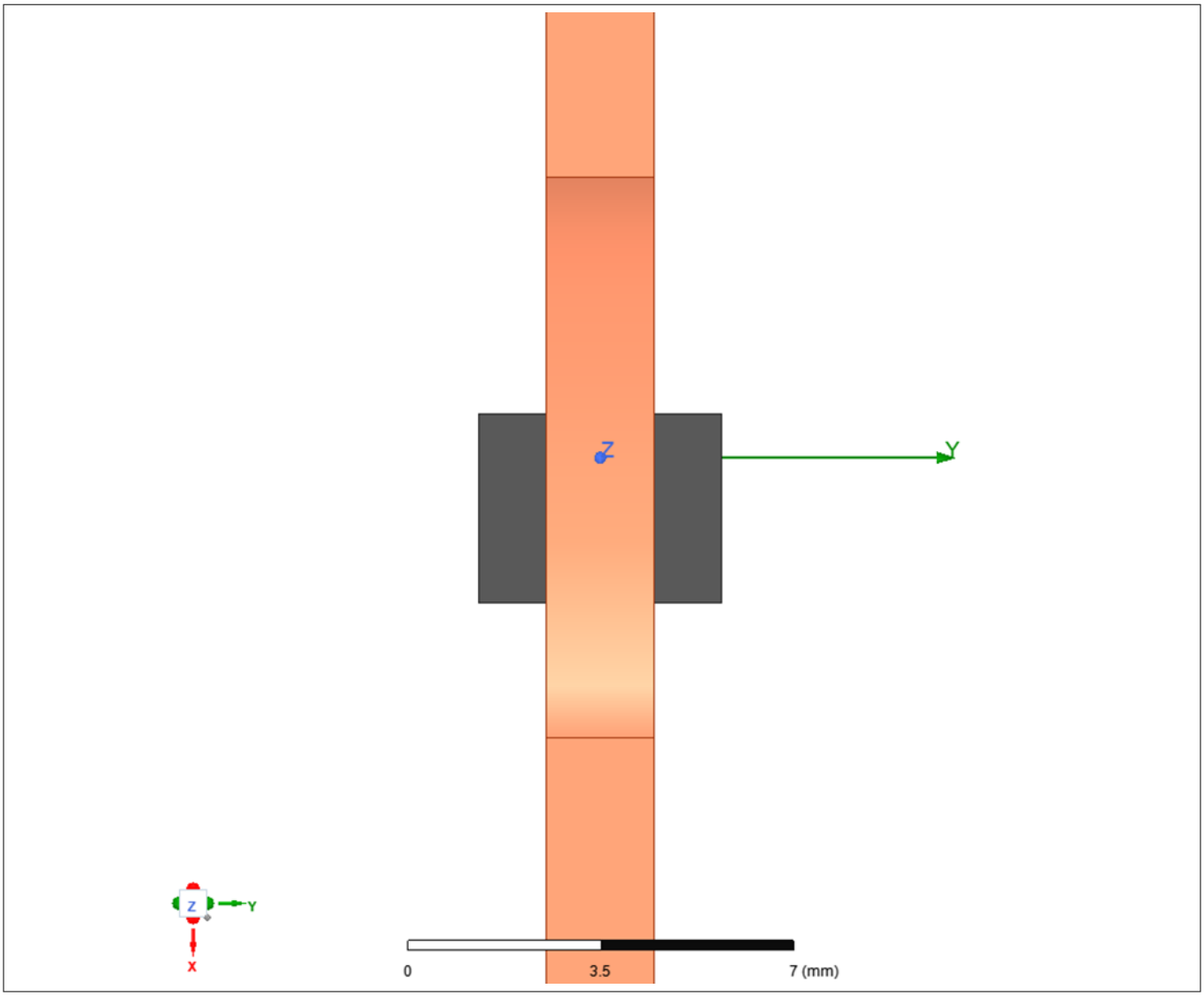

Figure 51 PG-VSON-6 package, Busbar support, vertical insertion, side view

3.2.2 Current rail transfer factor and insertion resistance

In first instance, the choice of the geometry will be the result of a trade-off between target transfer factor, which is directly linked to the target current full scale, and insertion resistance, which gives an indication of the additional power losses in the system due to the modifications done to the conductor. In the figures below the result of FEM simulations regarding current rail transfer factor and insertion resistance is shown. Different side cut-out depths and slit_z values have been swept in order to show what is the impact on the current rail transfer factor and on the insertion resistance. The analysis is done for different thicknesses of the busbar.

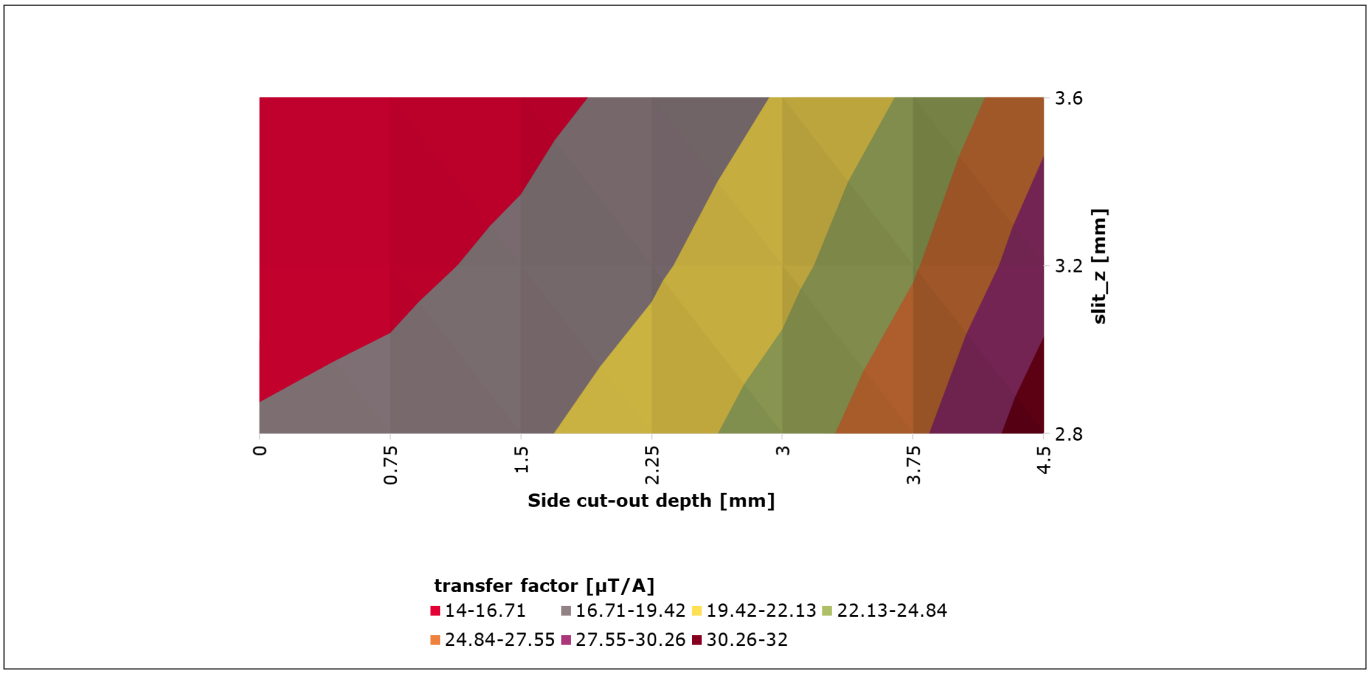

Figure 52 **Current rail transfer factor for a 1mm thick busbar. Sweep of side cut-out depth and slit_z values**

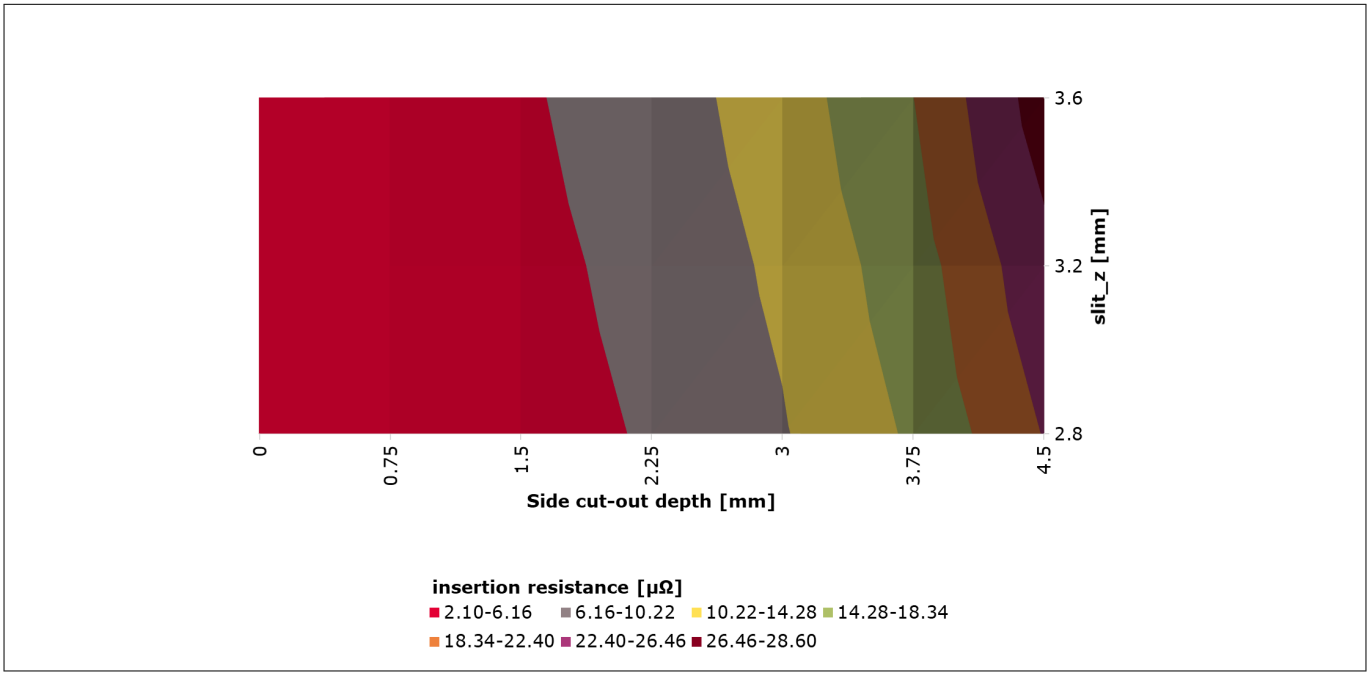

Figure 53 **Insertion resistance for a 1mm thick busbar. Sweep of side cut-out depth and slit_z values**

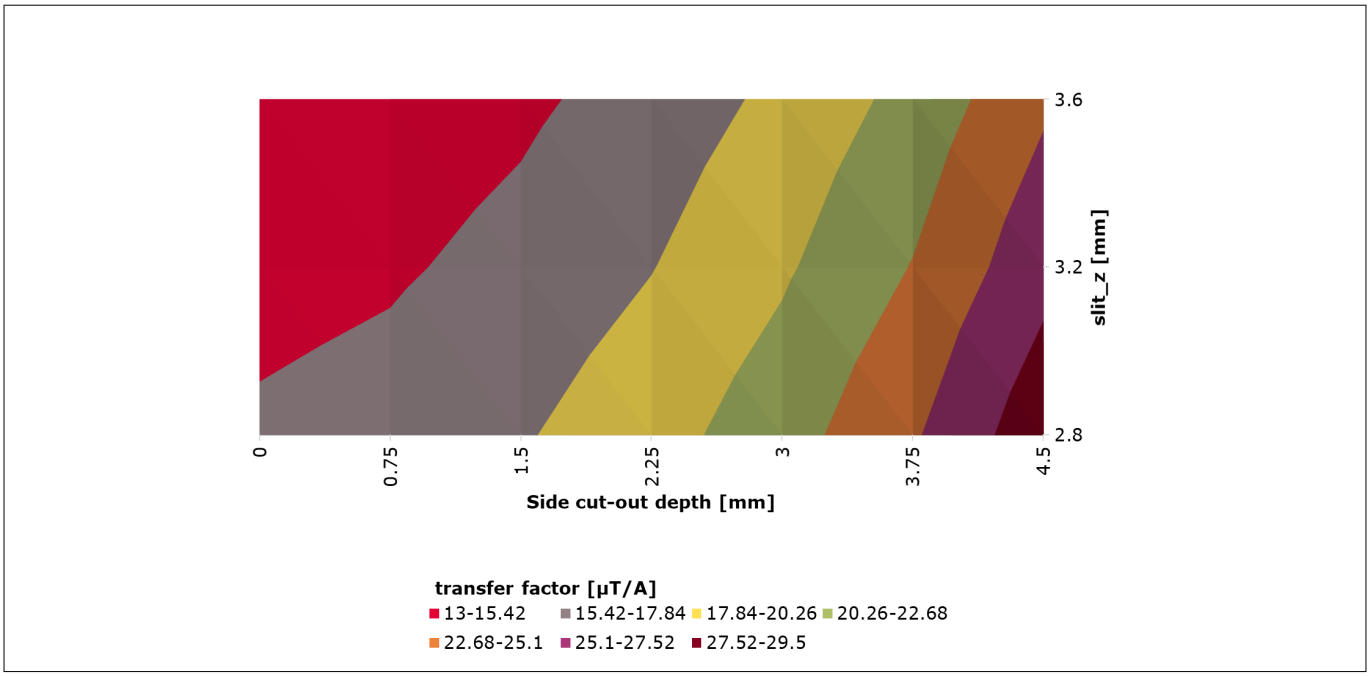

Figure 54 **Current rail transfer factor for a 2mm thick busbar. Sweep of side cut-out depth and slit_z values**

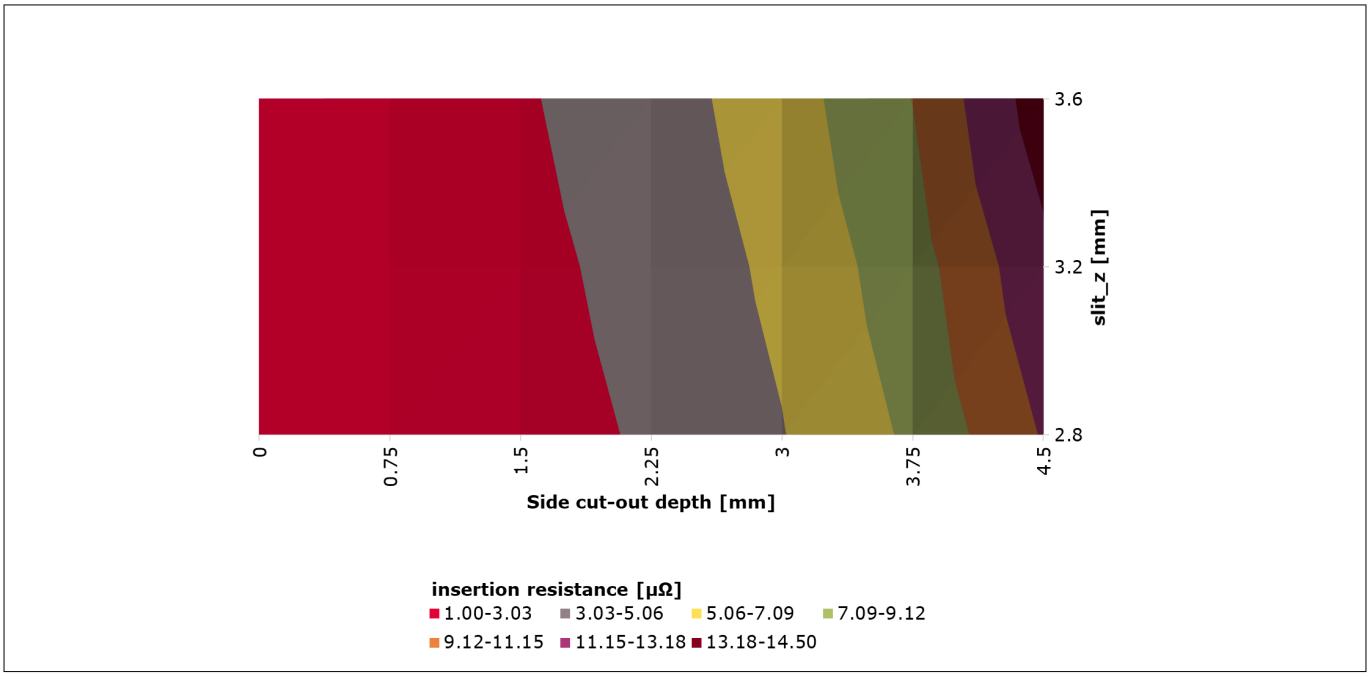

Figure 55 **Insertion resistance for a 2mm thick busbar. Sweep of side cut-out depth and slit_z values**

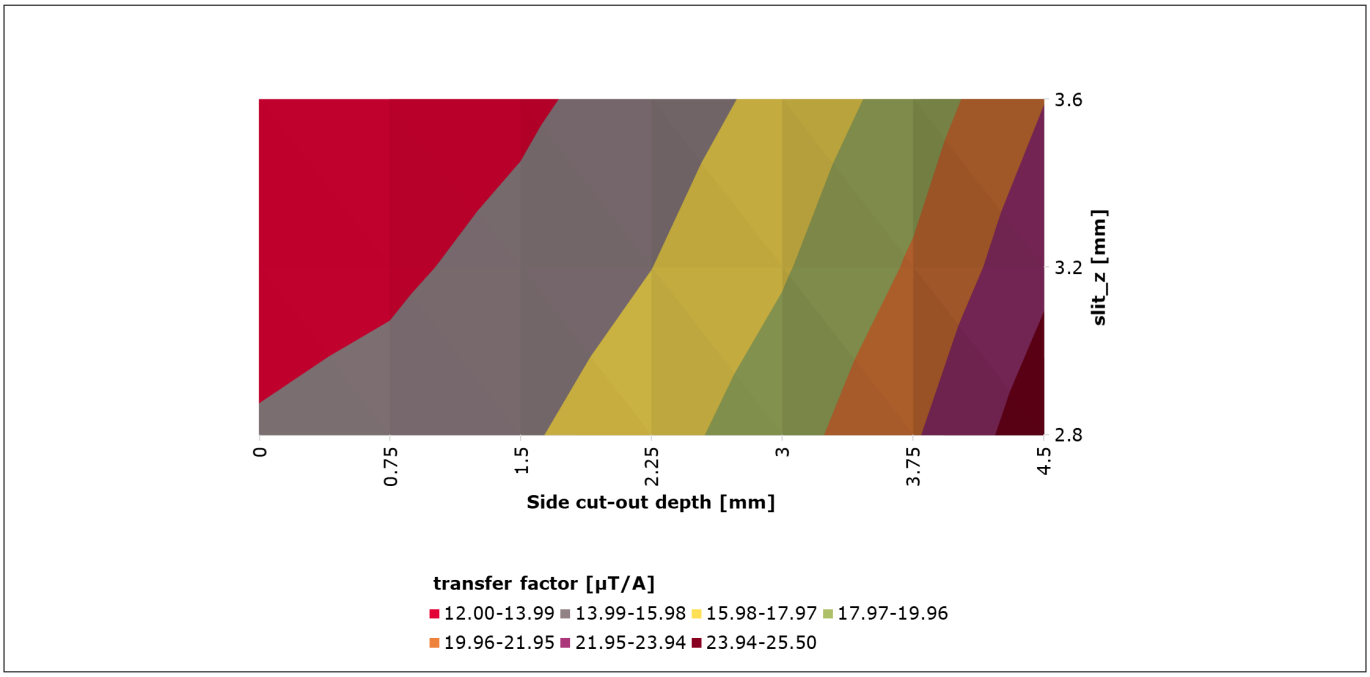

Figure 56 **Current rail transfer factor for a 3mm thick busbar. Sweep of side cut-out depth and slit_z values**

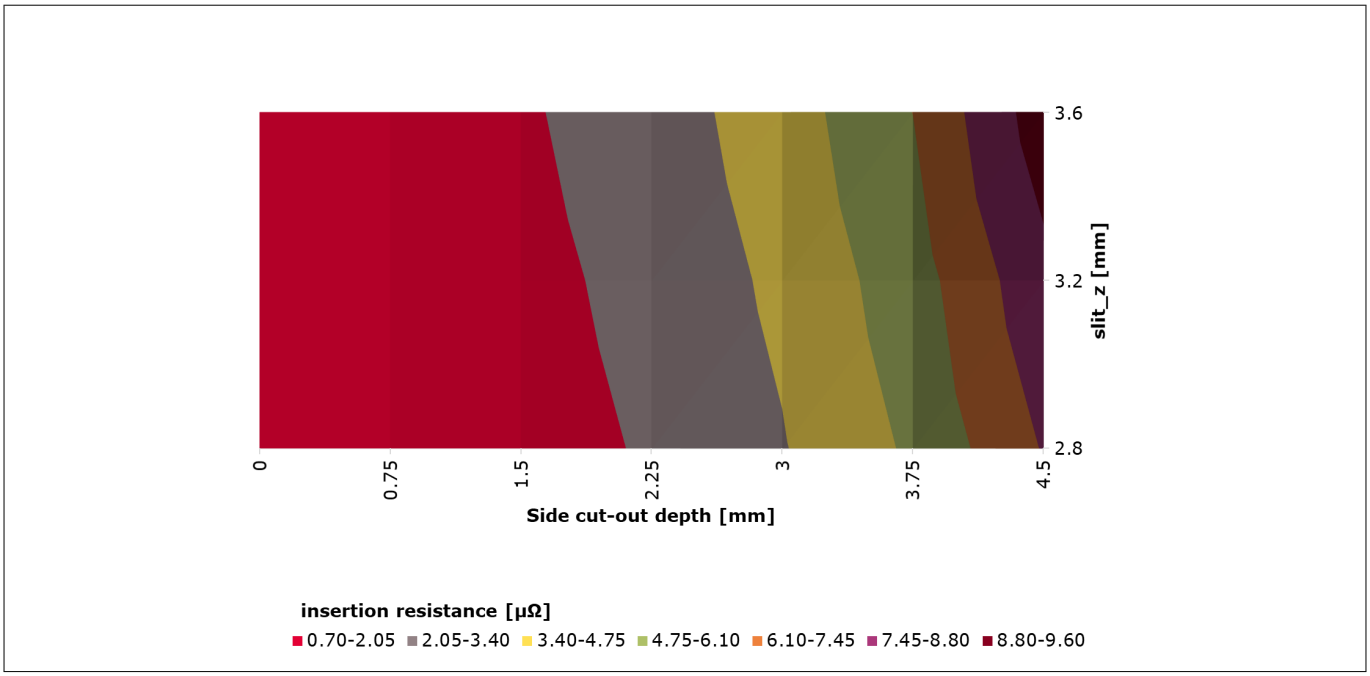

Figure 57 **Insertion resistance for a 3mm thick busbar. Sweep of side cut-out depth and slit_z values**

A bigger busbar thickness is clearly beneficial for the insertion resistance reduction since it creates a bigger cross section for the current flow, but it leads to lower transfer factors because of the lower current density. In the same way, a smaller side cut-out depth is beneficial for the insertion resistance reduction but leads to lower transfer factors.

Regarding the slit_z parameter, which indicates how wide the slit in the busbar is, it's usually better to keep it as small as possible, within the limits of the manufacturing rules and isolation requirements, which will depend on the overmolding process and overmolding material properties. In fact, a wider slit increases the insertion resistance without bringing a significant increase in the transfer factor, as it can be seen from the previously shown simulation data.

3.2.3 Bandwidth

Given the typical bandwidth of the current sensor, reported in the product datasheet [1], the bandwidth of the complete current measurement solution will be significantly influenced by the geometry of the sensing structure. The reason for this behavior is the change of the current density within the section of the conductor over frequency. Due to skin effect, the current is pushed toward the surface of the conductor, and induced eddy currents create an opposing field to the one generated by the current in the conductor that changes in amplitude depending on the frequency. The figure below shows how the current density is altered in the busbar structure over frequency. The impact on the frequency response will heavily depend on the geometry of the sensing structure. The typical magnitude [dB], phase shift [deg] and gain error [%] for different busbar thicknesses, side cut-out depths and slit_z values are shown in the figures below.

Reducing the busbar thickness helps in terms of bandwidth; the effect of both skin effect and eddy current effect is confined to a smaller thickness of conductor. A higher side cut-out depth and a bigger slit_z are beneficial in terms of bandwidth since the current is confined in a smaller, restricted area at the sensing location.

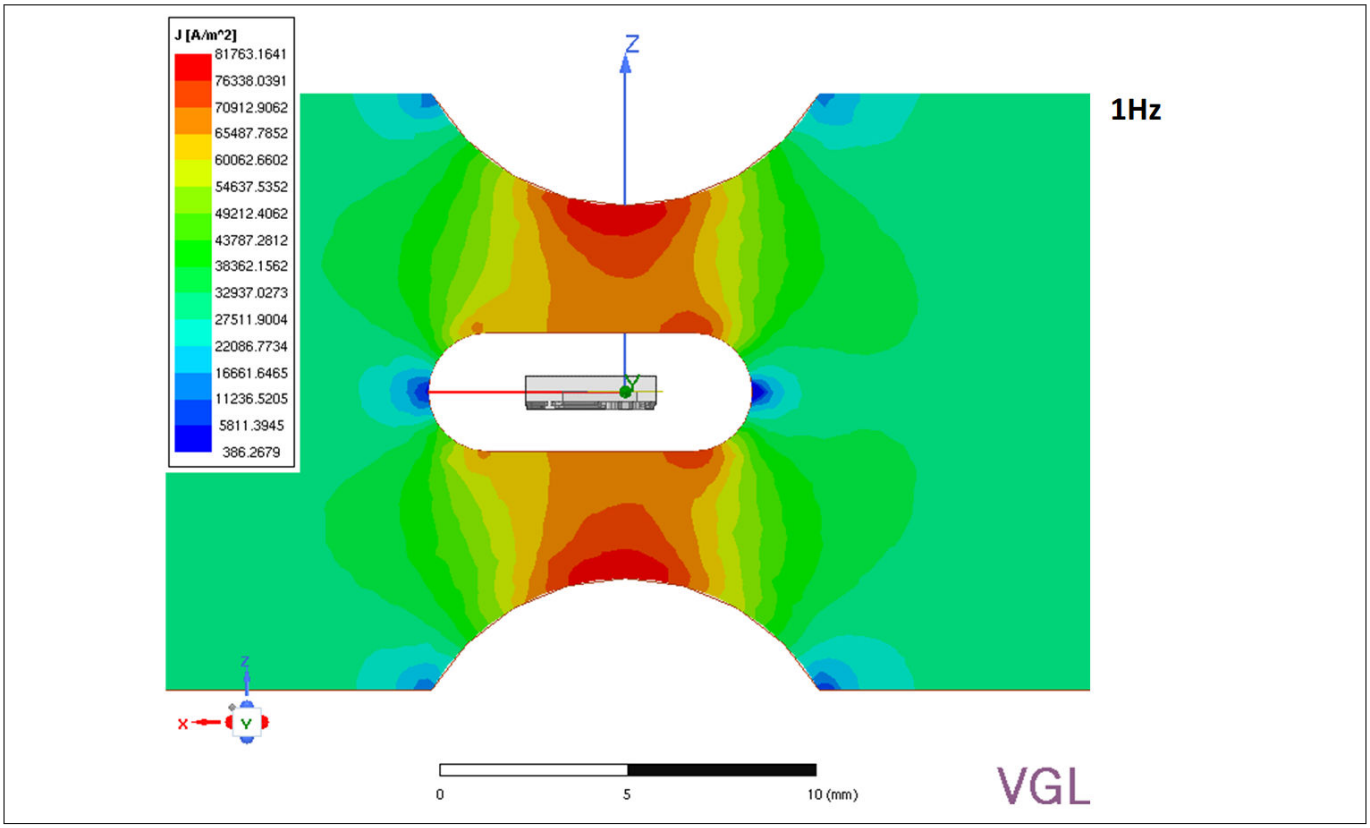

Figure 58 **Current density distribution on the surface of the sensing structure, on a 2 mm thick busbar. Side cut-out depth = 3 mm. Slit_z = 3.2 mm. Peak input current = 1 A, 1 Hz**

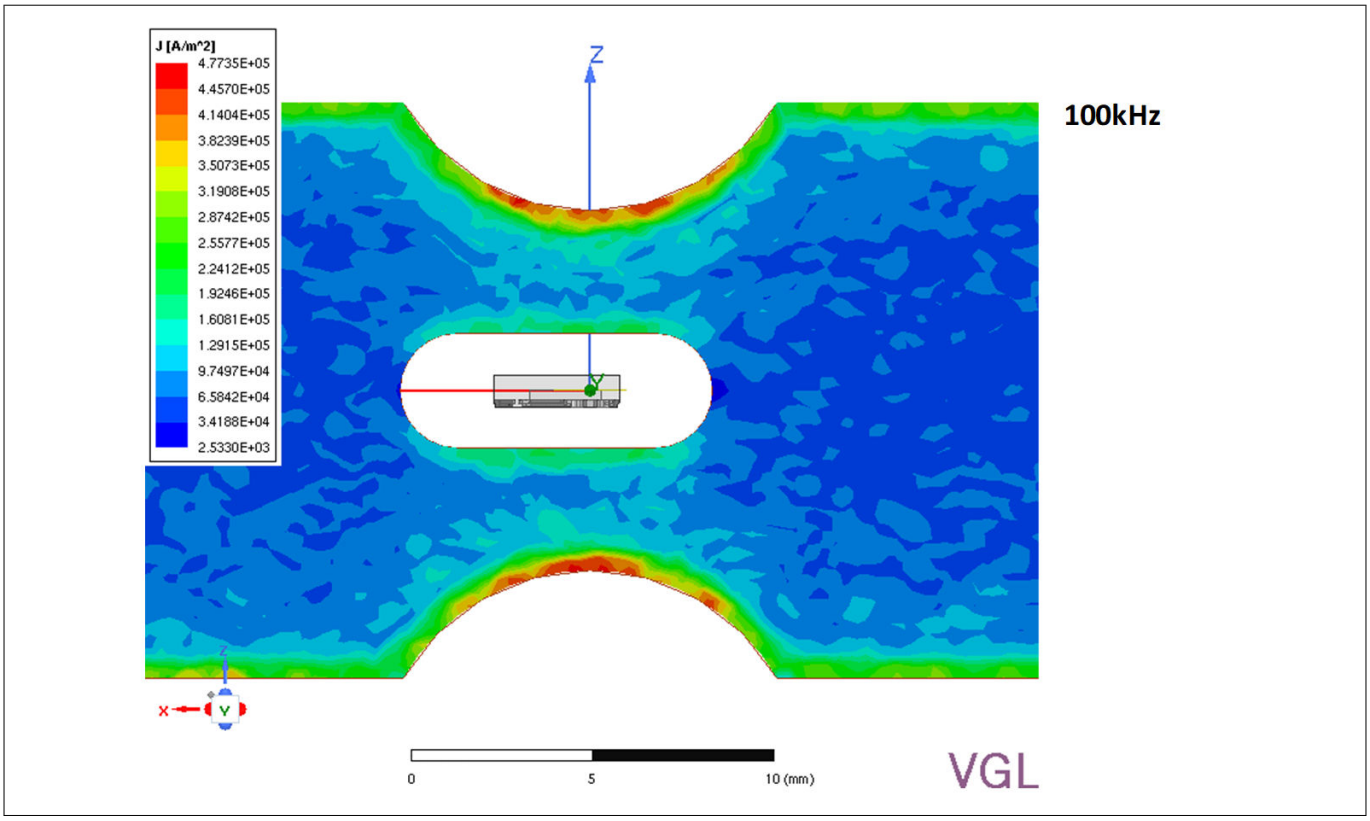

Figure 59 **Current density distribution on the surface of the sensing structure, on a 2 mm thick busbar. Side cut-out depth = 3 mm. Slit_z = 3.2 mm. Peak input current = 1 A, 100 kHz**

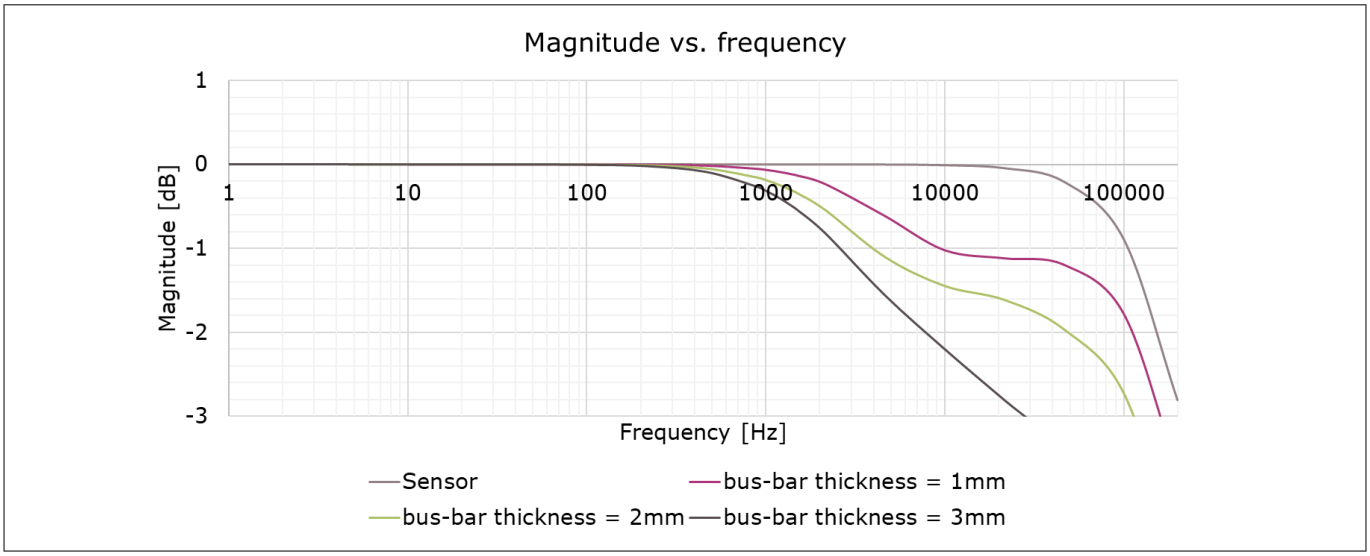

Figure 60 **Magnitude over frequency for different busbar thicknesses. Side cut-out depth = 3 mm. Slit_z = 3.2 mm**

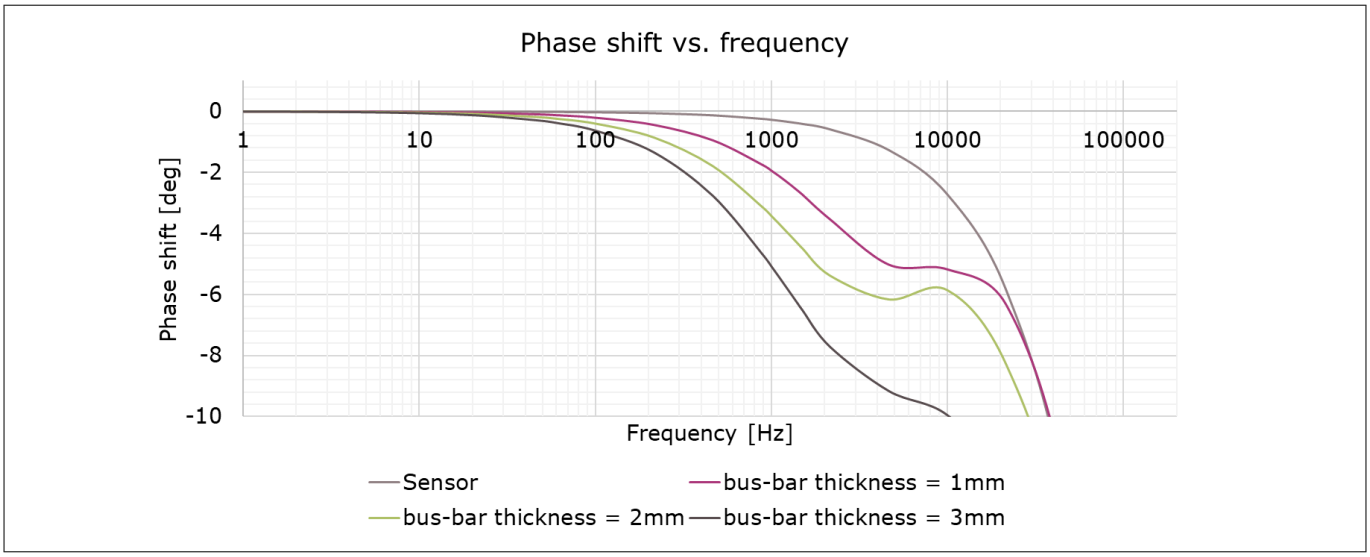

Figure 61 **Phase shift over frequency for different busbar thicknesses. Side cut-out depth = 3 mm. Slit_z = 3.2 mm**

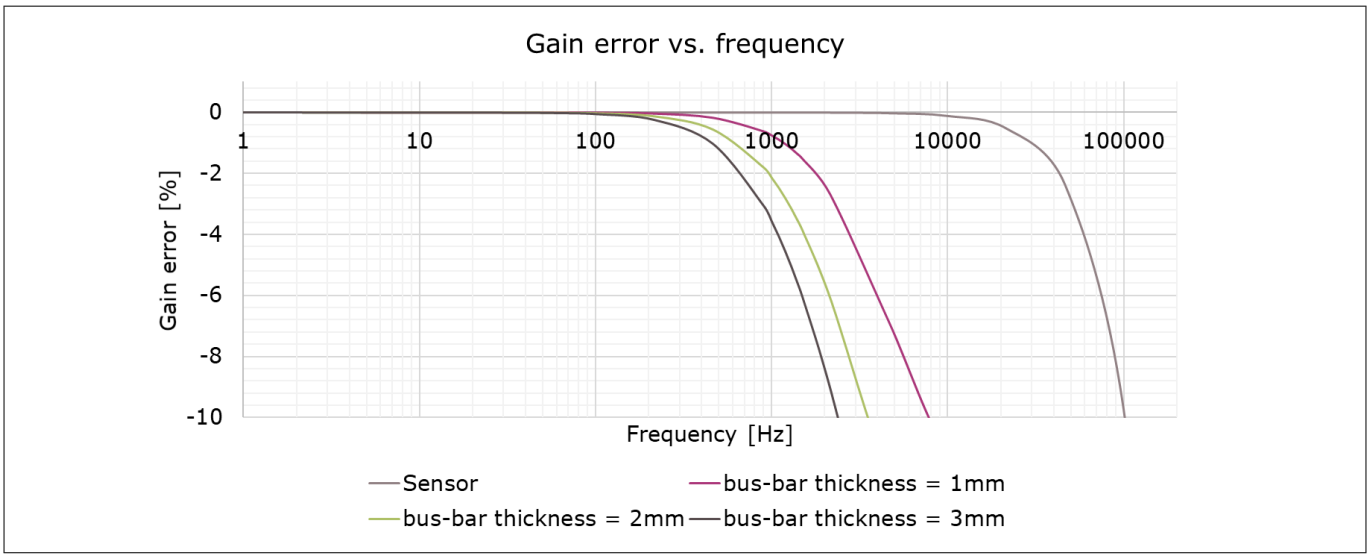

Figure 62 **Gain error over frequency for different busbar thicknesses. Side cut-out depth = 3 mm. Slit_z = 3.2 mm**

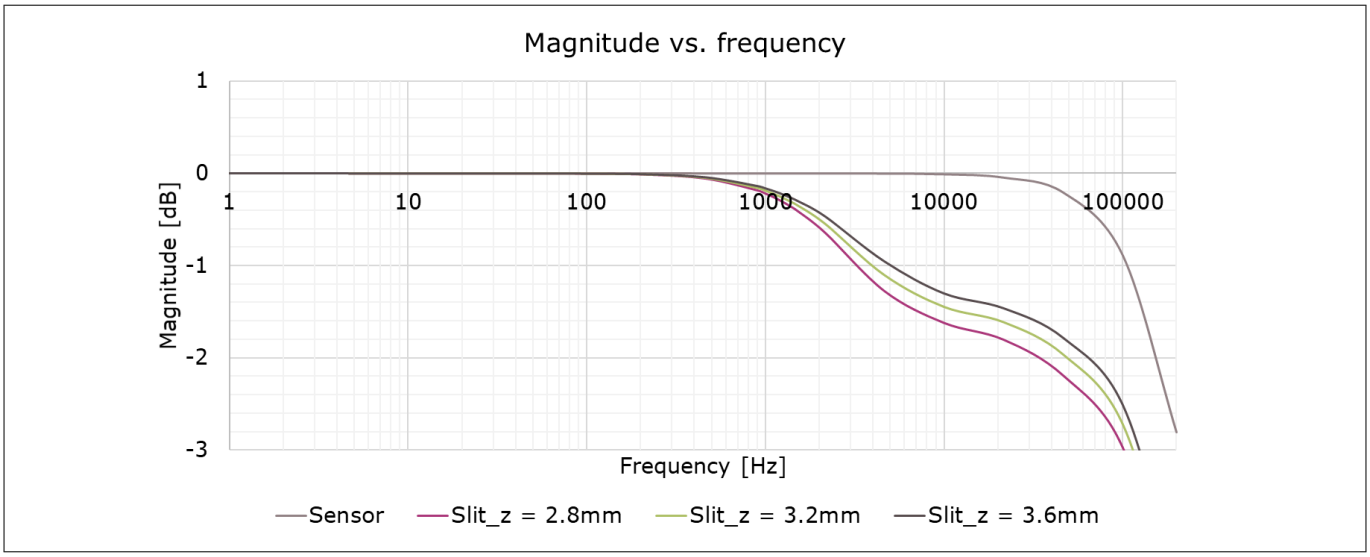

Figure 63 **Magnitude over frequency for a 2 mm thick busbar. Side cut-out depth = 3 mm. Sweep on slit_z value**

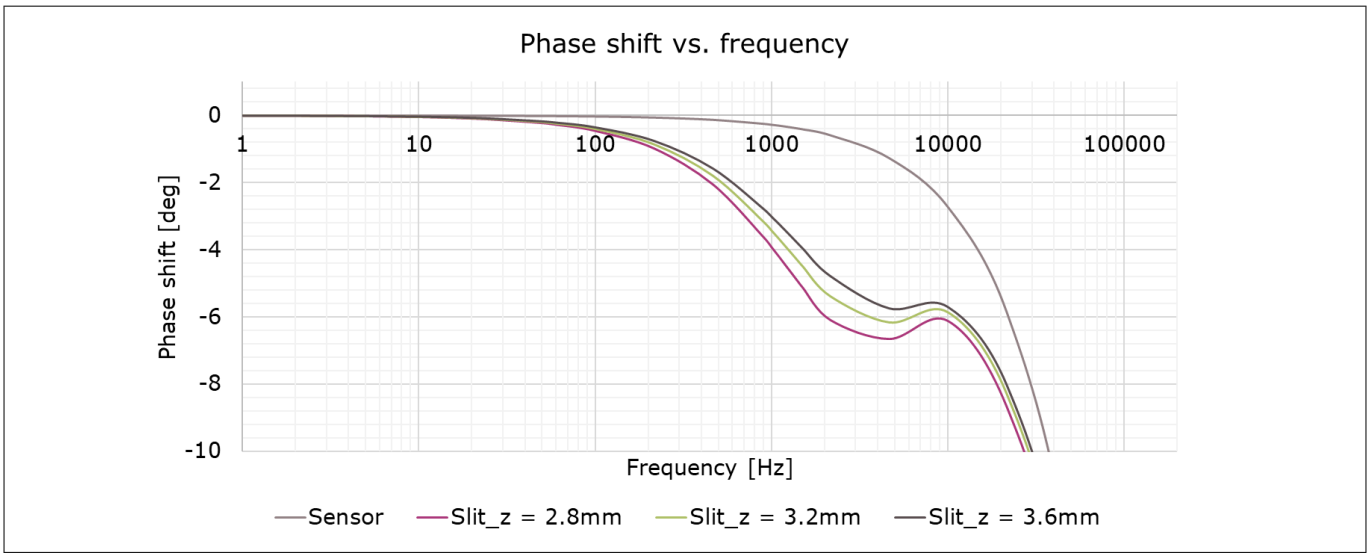

Figure 64 **Phase shift over frequency for a 2 mm thick busbar. Side cut-out depth = 3 mm. Sweep on slit_z value**

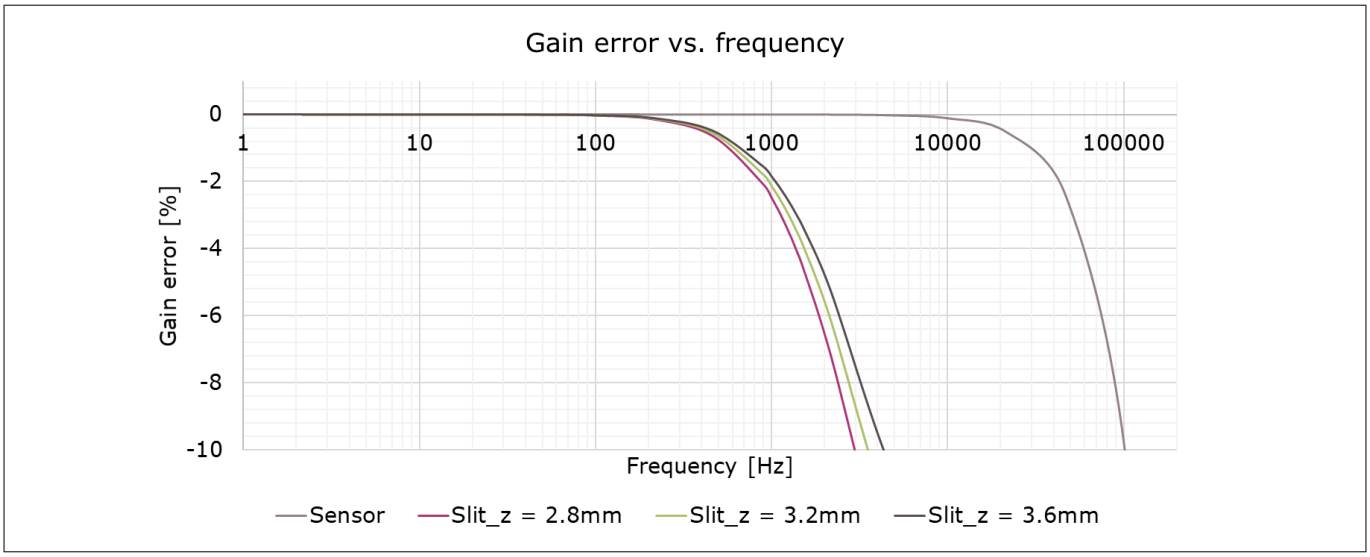

Figure 65 **Gain error over frequency for a 2 mm thick busbar. Side cut-out depth = 3 mm. Sweep on slit_z value**

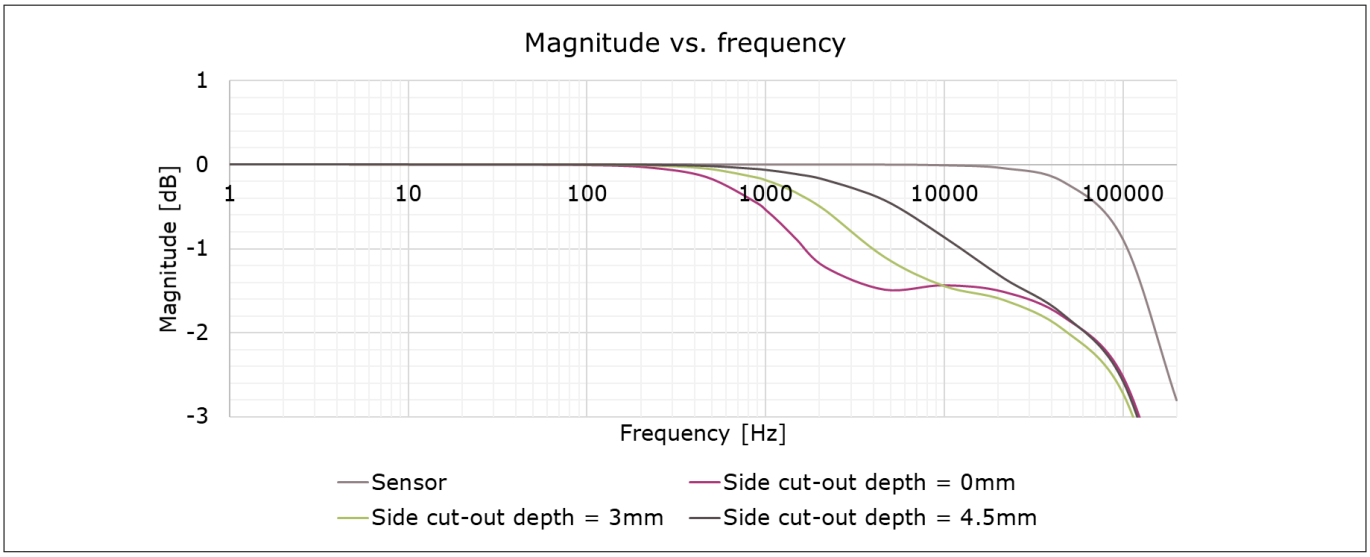

Figure 66 **Magnitude over frequency for a 2 mm thick busbar. Slit_z = 3.2 mm. Sweep on side cut-out depth value**

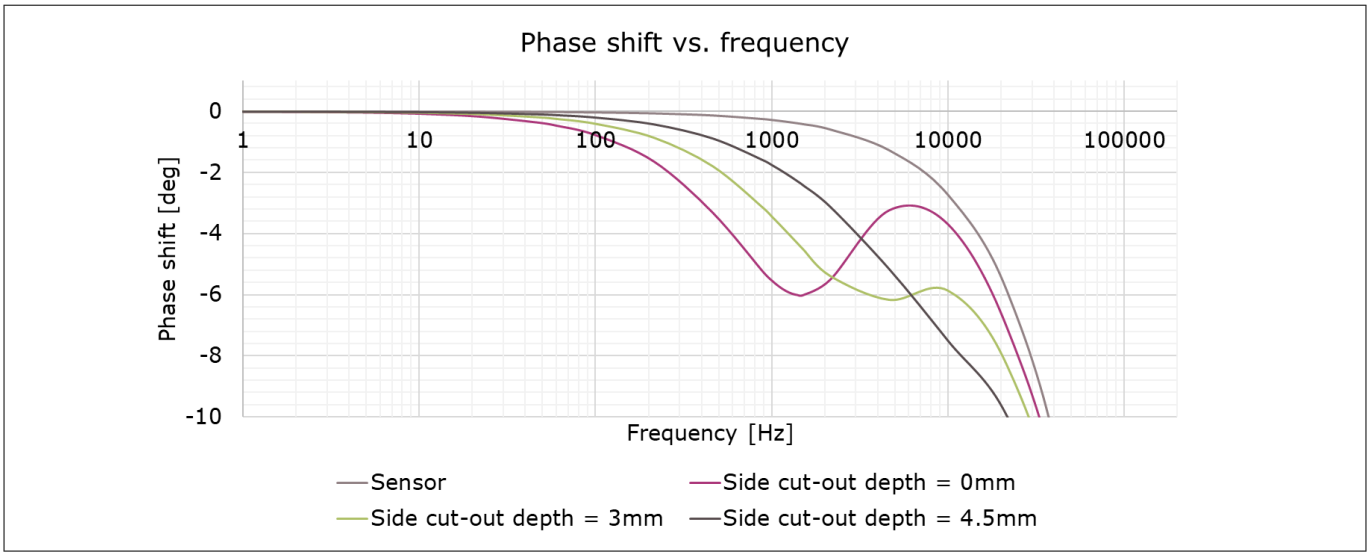

Figure 67 **Phase shift over frequency for a 2 mm thick busbar. Slit_z = 3.2 mm. Sweep on side cut-out depth value**

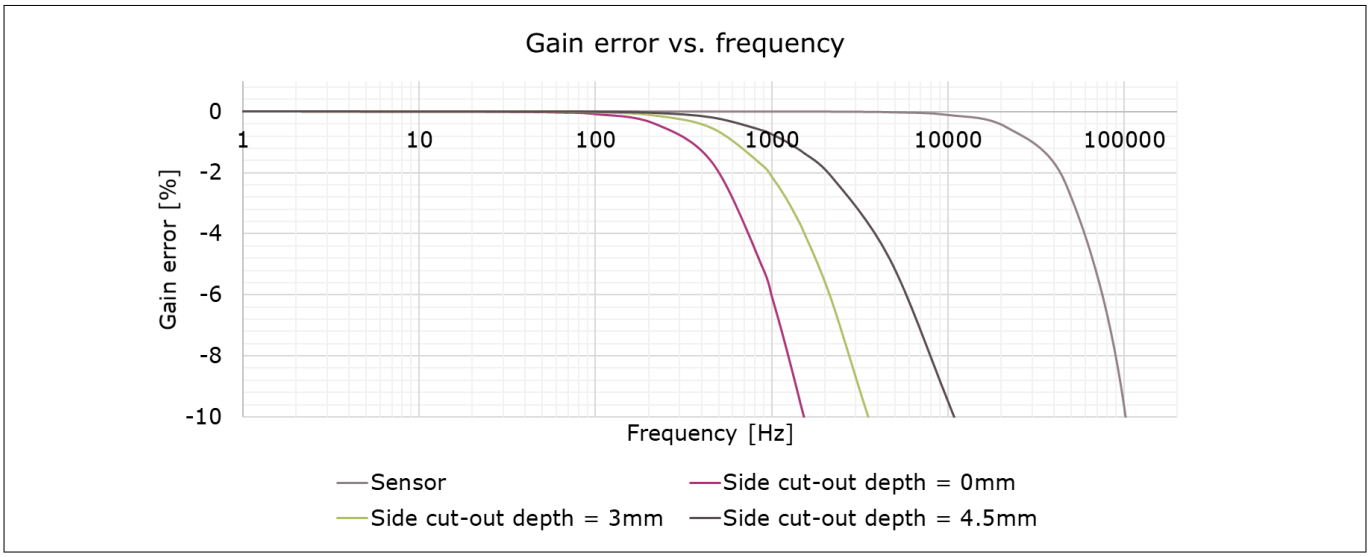

Figure 68 **Gain error over frequency for a 2 mm thick busbar. Slit_z = 3.2 mm. Sweep on side cut-out depth value**

3.2.4 Misalignment effects

If the sensor is not aligned with the current rail in its nominal position due to manufacturing tolerances, the transfer factor will differ from the nominal one. We refer to this error component as "transfer factor error". This error component will contribute to the total initial sensitivity error, and it is possible to compensate it within the calibration range specified in the product datasheet [1]. However, if the sensor gets displaced during system operation due to mechanical vibrations or thermal expansion effects, the transfer factor will experience a drift. Quantifying this error component is essential in order to verify that the in-system end of line calibration is feasible and that the transfer factor doesn't drift outside specifications during operation. In the figures below the results of transfer factor simulations in which the sensor is displaced in the three directions of space are shown, in case of different slit_z and side cut-out depth values. The analysis is done for a 2 mm thick busbar.

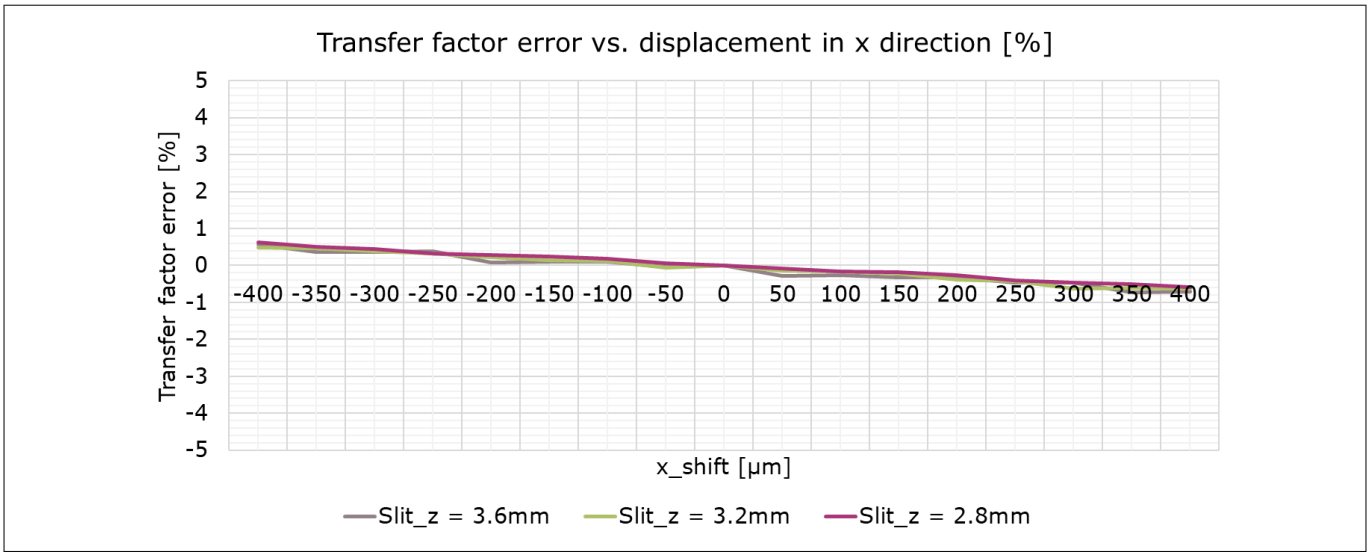

Figure 69 **Displacement in X direction. Current rail transfer factor error for a 2 mm thick busbar. Side cut-out depth = 3 mm. Sweep on slit_z value**

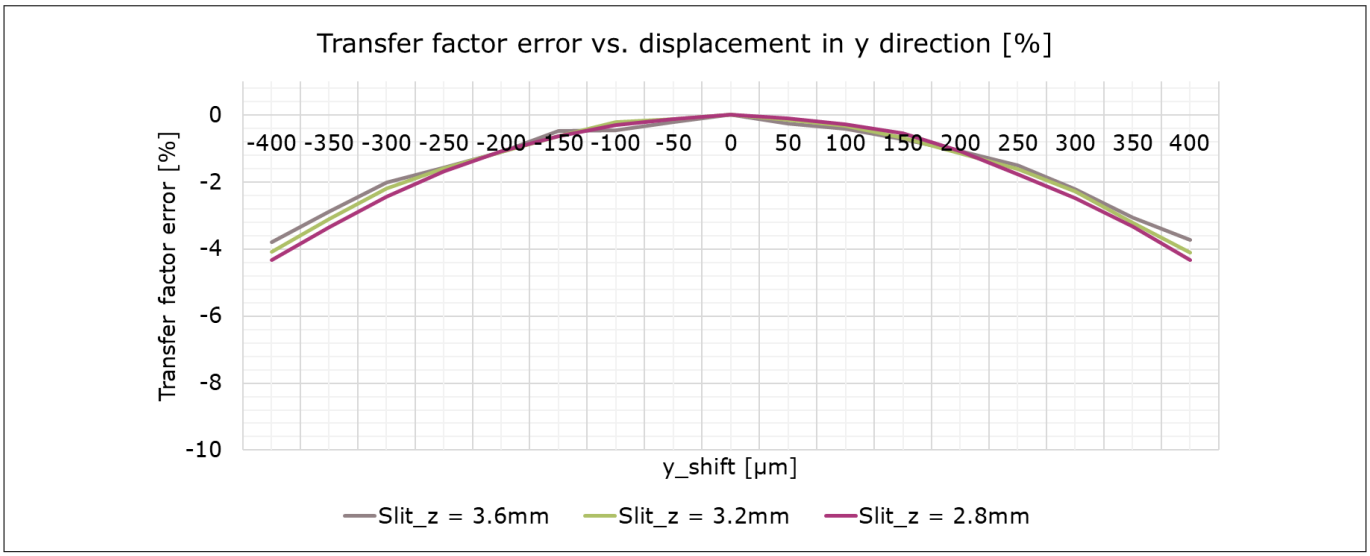

Figure 70 **Displacement in Y direction. Current rail transfer factor error for a 2 mm thick busbar. Side cut-out depth = 3 mm. Sweep on slit_z value**

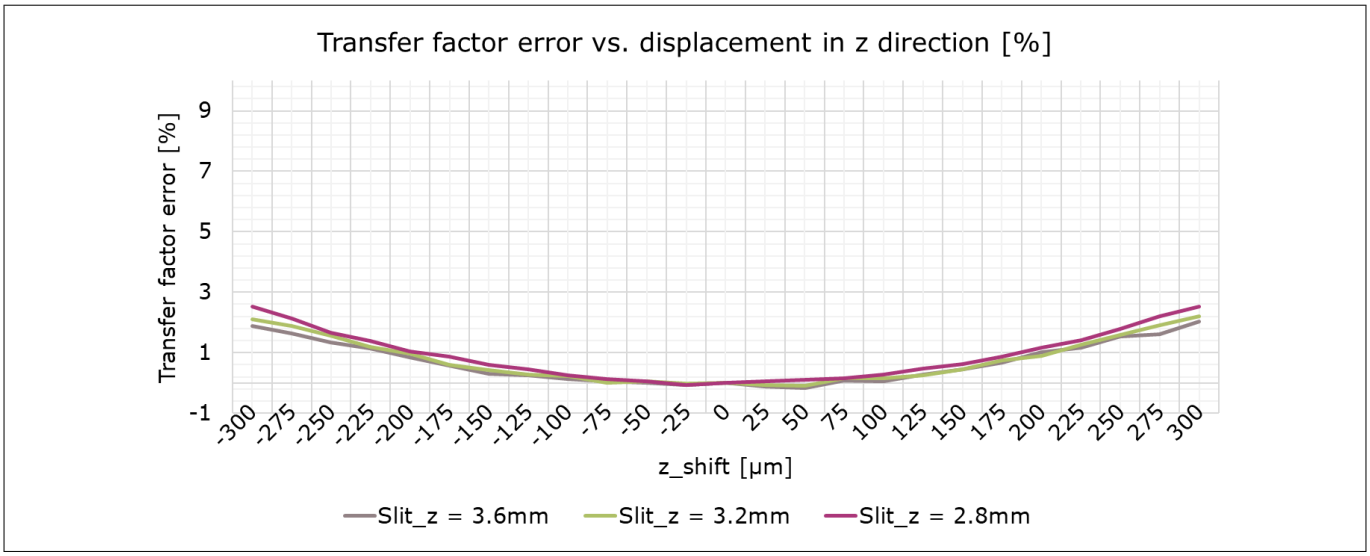

Figure 71 **Displacement in Z direction. Current rail transfer factor error for a 2 mm thick busbar. Side cut-out depth = 3 mm. Sweep on slit_z value**

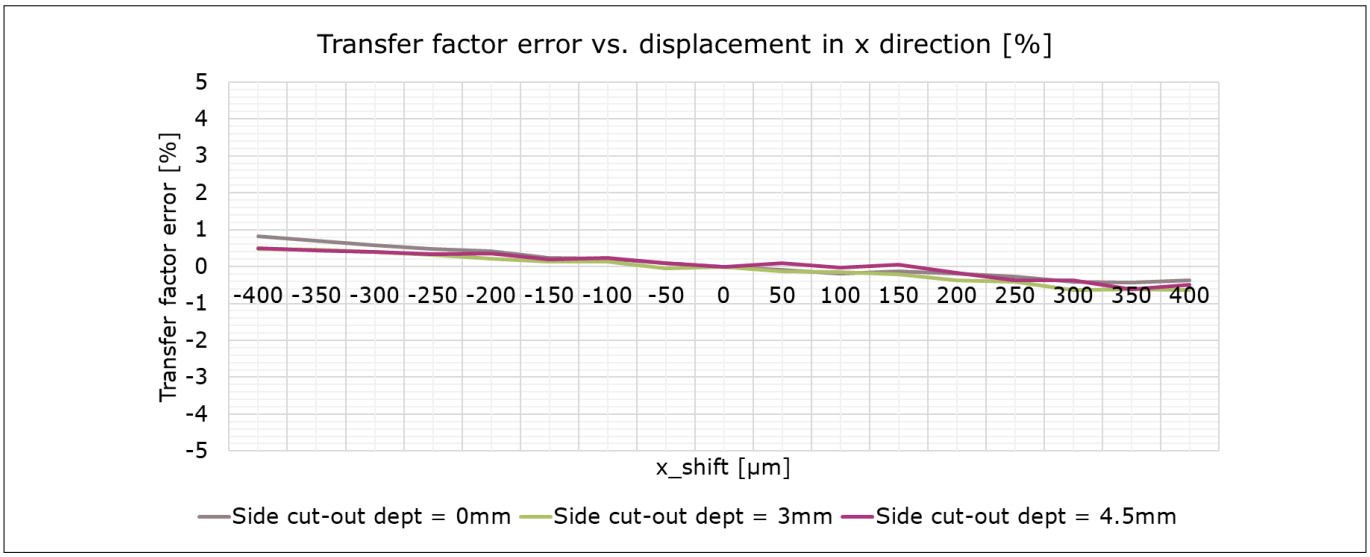

Figure 72 **Displacement in X direction. Current rail transfer factor error for a 2 mm thick busbar. Slit_z = 3.2 mm. Sweep on side cut-out depth value**

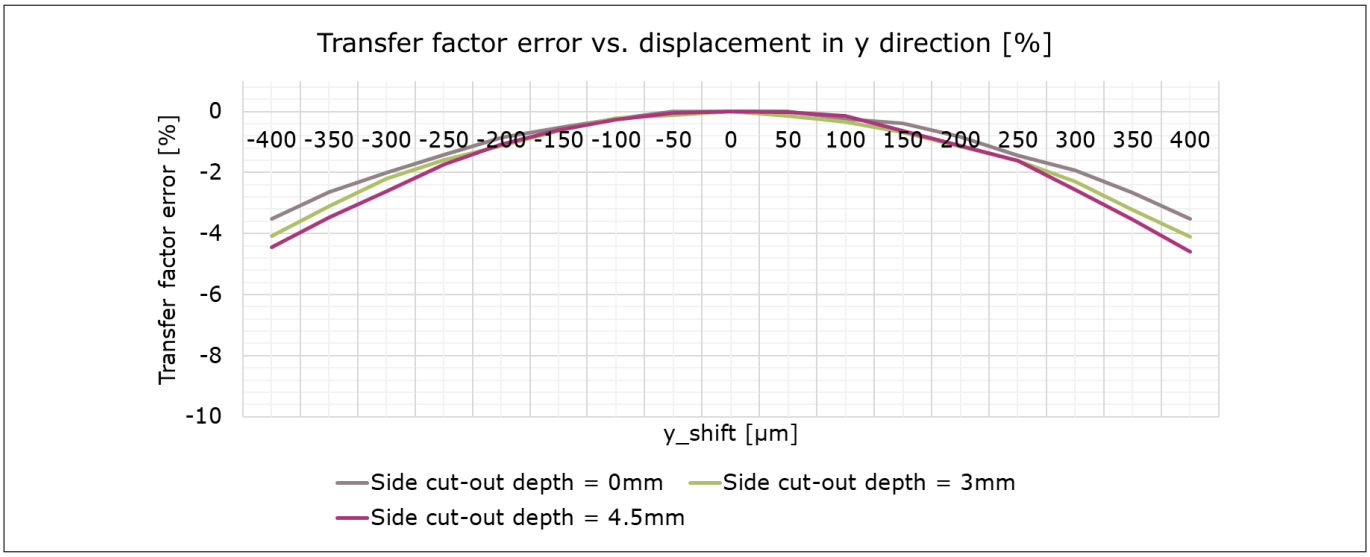

Figure 73 **Displacement in Y direction. Current rail transfer factor error for a 2 mm thick busbar. Slit_z = 3.2 mm. Sweep on side cut-out depth value**

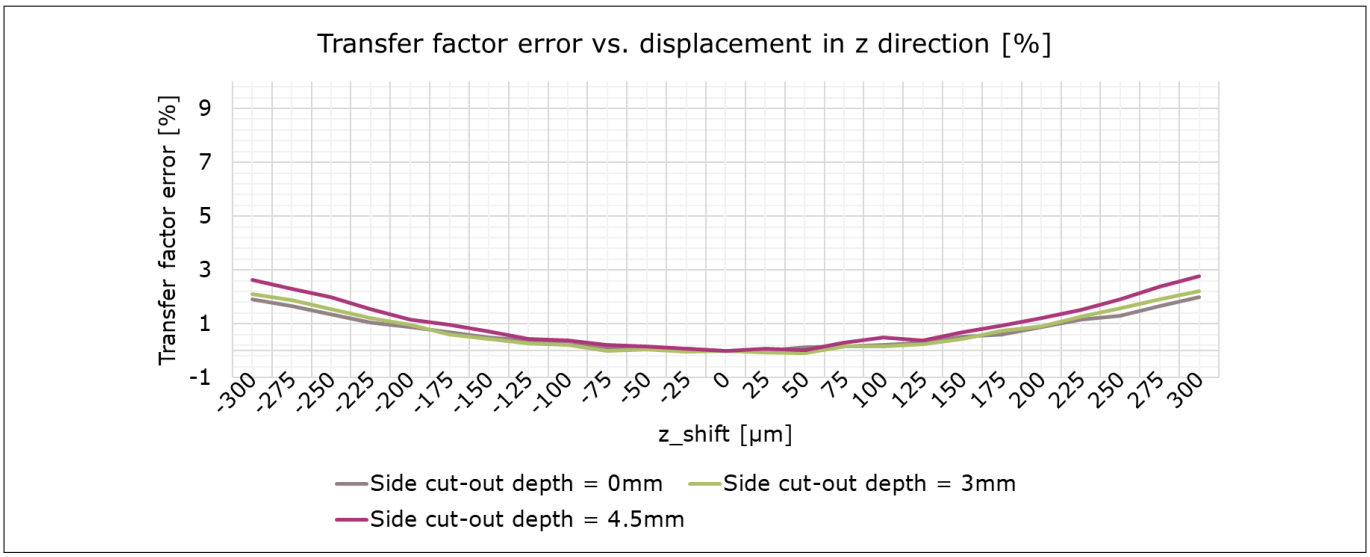

Figure 74 **Displacement in Z direction. Current rail transfer factor error for a 2 mm thick busbar. Slit_z = 3.2 mm. Sweep on side cut-out depth value**

The figures above show that misalignment errors lead to small transfer factor errors in case of vertical insertion sensing structure. The impact of different slit_z and side cut-out depth values is neglectable in the analyzed value ranges.

Misalignments have a minor impact on the frequency response as well. This impact is limited and usually neglectable if the sensing structure is symmetric with respect to the sensing elements location, as in the analyzed case. In the figures below the misalignment impact on the frequency response of the vertical insertion sensing structure is shown, for a worst-case misalignment of ± 0.4 mm in X and Y directions, -0.3 mm to +0.3 mm for Z direction.

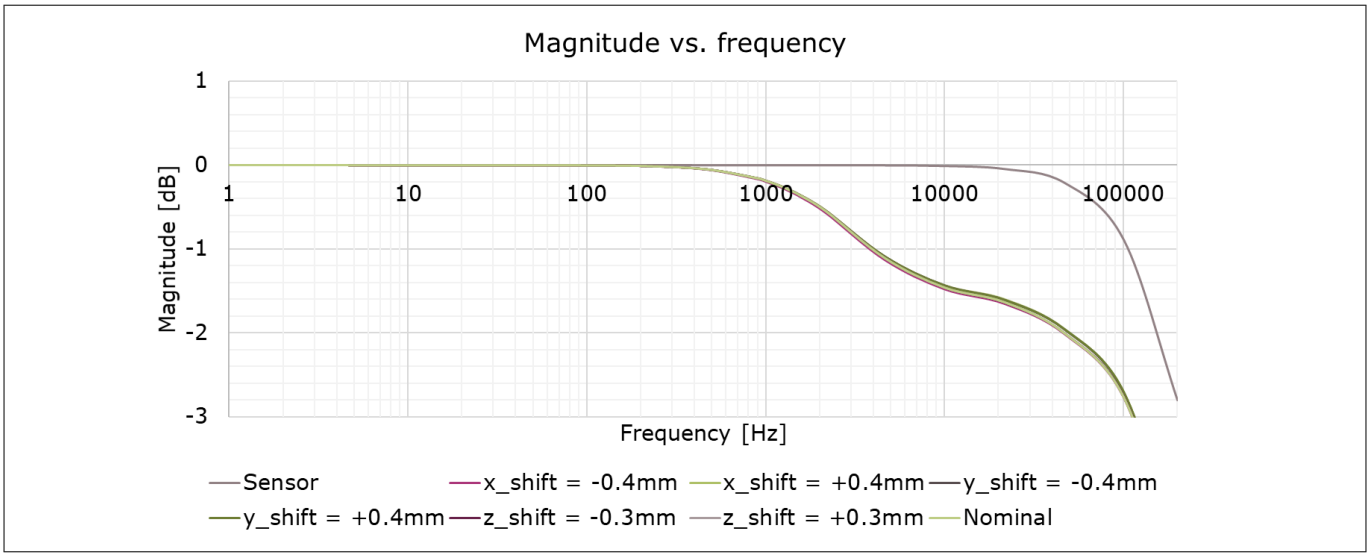

Figure 75 **Magnitude over frequency for a 2 mm thick busbar. Slit_z = 3.2 mm. Side cut-out depth = 3 mm. Sweep on x_shift, y_shift and z_shift values**

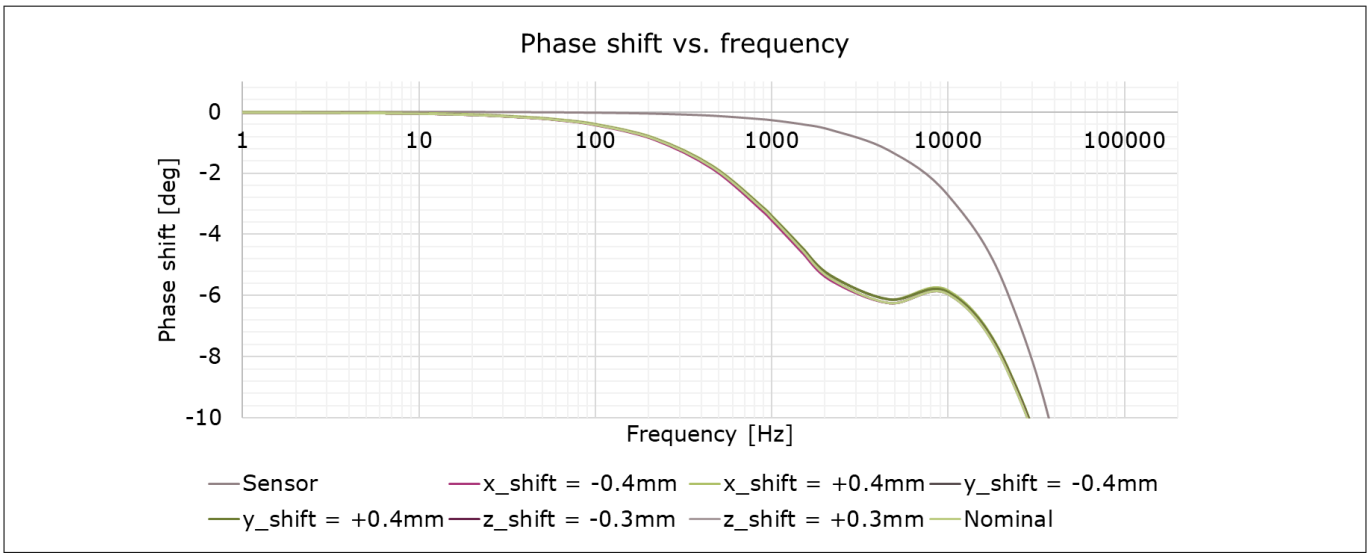

Figure 76 **Phase shift over frequency for a 2 mm thick busbar. Slit_z = 3.2 mm. Side cut-out depth = 3 mm. Sweep on x_shift, y_shift and z_shift values**

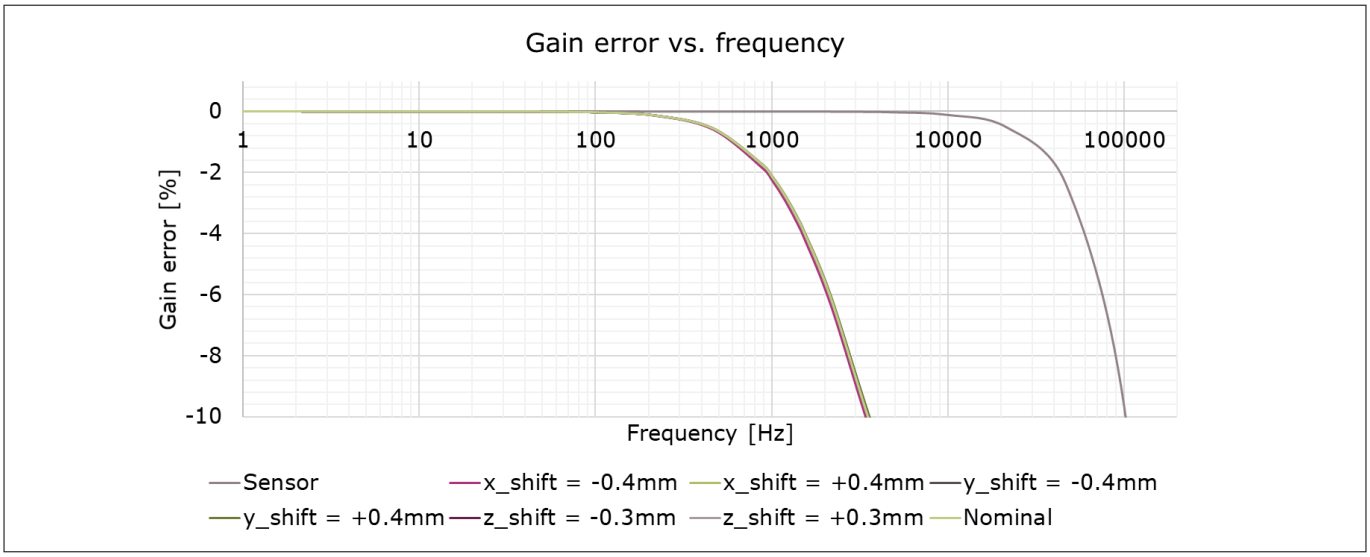

Figure 77 **Gain error over frequency for a 2 mm thick busbar. Slit_z = 3.2 mm. Side cut-out depth = 3 mm. Sweep on x_shift, y_shift and z_shift values**

3.2.5 Crosstalk

In case of multi-phase systems, the magnetic field generated by the current flowing in nearby phases can influence the current measurement. The percentage of signal that is measured on a phase and that flows in the nearby phase is here denominated as crosstalk factor.

The figure shows an example of three phase system constituted of three busbars with vertical insertion sensing structure. The middle-to-middle spacing in Z direction is 47 mm; this corresponds to the distance between the sensing structure centers belonging to adjacent phases. That results in a crosstalk factor of 0.6% between adjacent phases, 0.15% between right and left phases. It is important to mention that the crosstalk factor is stable over temperature and lifetime; it can be characterized for each system and the resulting error can be compensated. Further details about crosstalk compensation are available in the User manual [2].

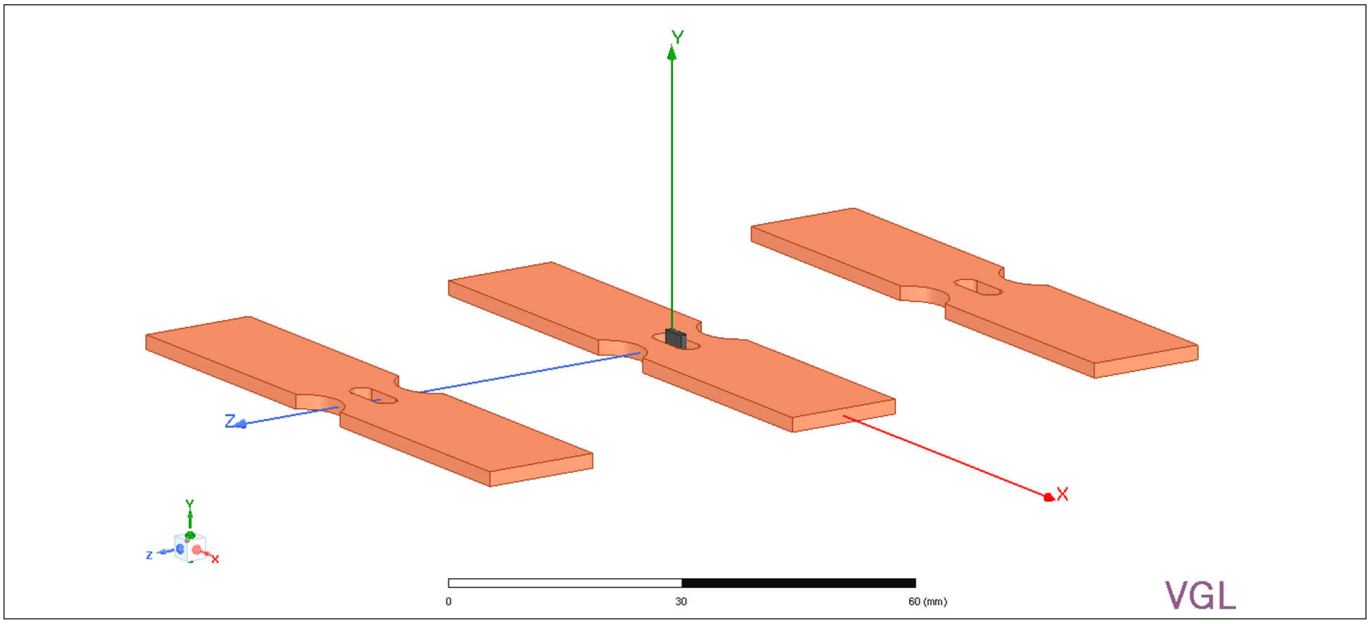

Figure 78 Three phases system made by three sensing structures, based on vertical insertion on busbar support. Slit_z = 3.2 mm. Side cut-out depth = 3 mm. Phase gap = 47 mm

4 PCB support

In case of PCB support, the sensor is soldered on the top or bottom layers of the PCB, and the sensing structure is realized on internal power layers in the PCB layer stack. The PCB dielectric material provides the needed voltage isolation between sensor and current rail. The preferred package type is the PG-TDSO-16 since the sensing elements are very close to the bottom of the package, allowing optimal sensing performance in case of PCB conductor.

Regarding the sensing structure shape, lateral insertion sensing structure can be realized, in both Straight and S-bend shapes. In this chapter, Straight insertion on PCB support is analyzed. The key differences between Straight and S-bend shapes are discussed in the previous chapter, in case of lateral insertion on busbar support (Chapter 3.1).

4.1 Straight shaped sensing structure

4.1.1 Introduction

The Straight slit shape is used, like in the busbar support case, as an example to demonstrate the effect of all geometrical parameters on the main performance factors: transfer factor, insertion resistance, frequency behavior, misalignment and crosstalk. The considerations done for this sensing structure can be extended to the case of an S-bend sensing structure.

The Straight slit sensing structure is optimal for systems in which the most important requirement is obtaining minimum power losses due to the insertion. It is in fact possible to obtain lower insertion resistance with respect to the S-bend case thanks to the fact that the current doesn't have to follow a "S shaped" path at sensor location, but rather flow always in the "Straight" direction. The PCB structure geometry and the analyzed layer stacks are shown in the figures below.

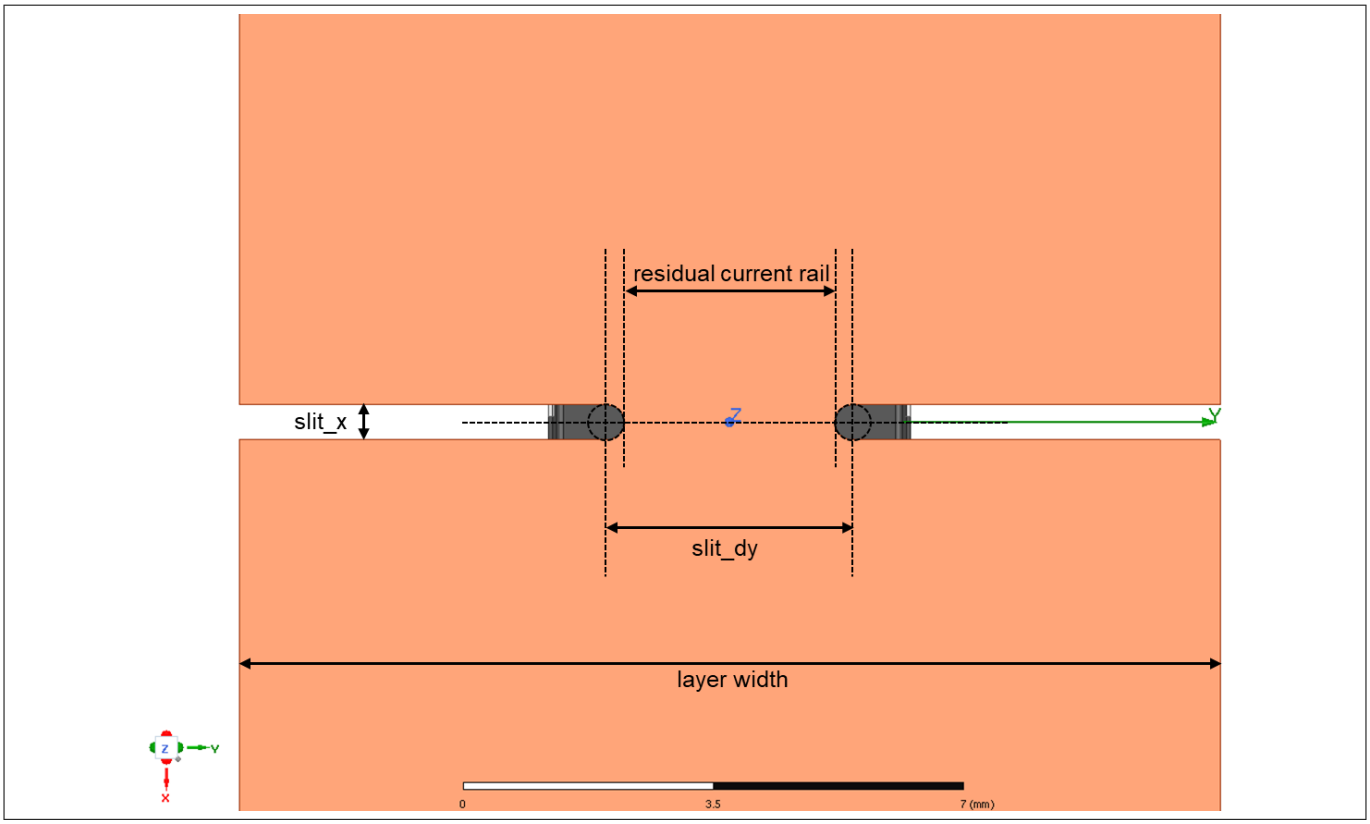

Figure 79 PG-TDSO-16 package, PCB support, lateral insertion, Straight slit sensing structure, top view

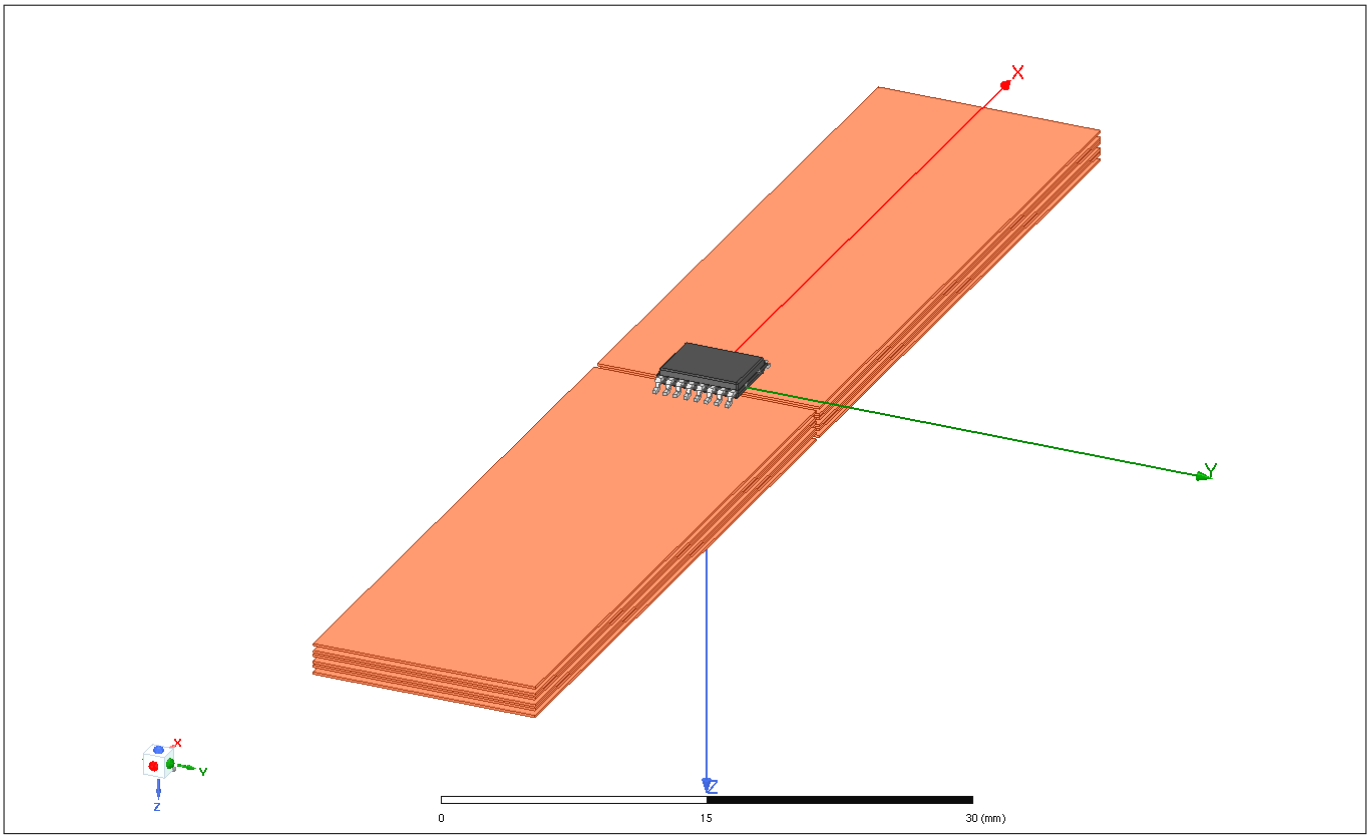

Figure 80 **PG-TDSO-16 package, PCB support, 6 conducting power layers, lateral insertion, Straight slit sensing structure, 3D view**

	Top Solder	0.02mm	Solder Resist
1	TOP	0.035mm	copper
	Dielectric 1	0.115mm	FR4
2	Power Layer 1	0.14mm	copper
	Core 1	0.3mm	FR4
3	Power Layer 2	0.14mm	copper
	Dielectric 2	0.115mm	FR4
4	BOTTOM	0.035mm	copper
	Bottom Solder	0.02mm	Solder Resist
	Bottom Overlay		

2 conducting power layers

Figure 81 **Layer stack example with two conducting power layers**

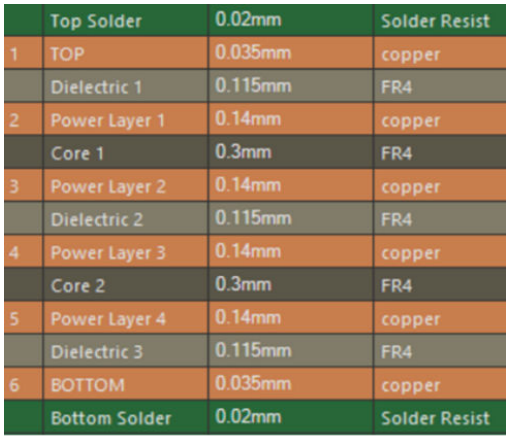

	Top Solder	0.02mm	Solder Resist
1	TOP	0.035mm	copper
	Dielectric 1	0.115mm	FR4
2	Power Layer 1	0.14mm	copper
	Core 1	0.3mm	FR4
3	Power Layer 2	0.14mm	copper
	Dielectric 2	0.115mm	FR4
4	Power Layer 3	0.14mm	copper
	Core 2	0.3mm	FR4
5	Power Layer 4	0.14mm	copper
	Dielectric 3	0.115mm	FR4
6	BOTTOM	0.035mm	copper
	Bottom Solder	0.02mm	Solder Resist

4 conducting power layers

Figure 82 Layer stack example with four conducting power layers

	Top Solder	0.02mm	Solder Resist
1	TOP	0.035mm	copper
	Dielectric 1	0.115mm	FR4
2	Power Layer 1	0.14mm	copper
	Core 1	0.3mm	FR4
3	Power Layer 2	0.14mm	copper
	Dielectric 2	0.115mm	FR4
4	Power Layer 3	0.14mm	copper
	Core 2	0.3mm	FR4
5	Power Layer 4	0.14mm	copper
	Dielectric 3	0.115mm	FR4
6	Power Layer 5	0.14mm	copper
	Core 3	0.3mm	FR4
7	Power Layer 6	0.14mm	copper
	Dielectric 4	0.115mm	FR4
8	BOTTOM	0.035mm	copper
	Bottom Solder	0.02mm	Solder Resist

6 conducting power layers

Figure 83 Layer stack example with six conducting power layers

4.1.2 Current rail transfer factor and insertion resistance

In first instance, the choice of the geometry will be the result of a trade-off between target transfer factor, which is directly linked to the target current full scale, and insertion resistance, which gives an indication of the additional power losses in the system due to the modifications done to the conductor. In the figures below the result of FEM simulations regarding current rail transfer factor and insertion resistance is shown. Different residual current rail and slit_x values have been swept in order to show what is the impact on the current rail transfer factor and on the insertion resistance. The analysis is done for different number of PCB power layers.

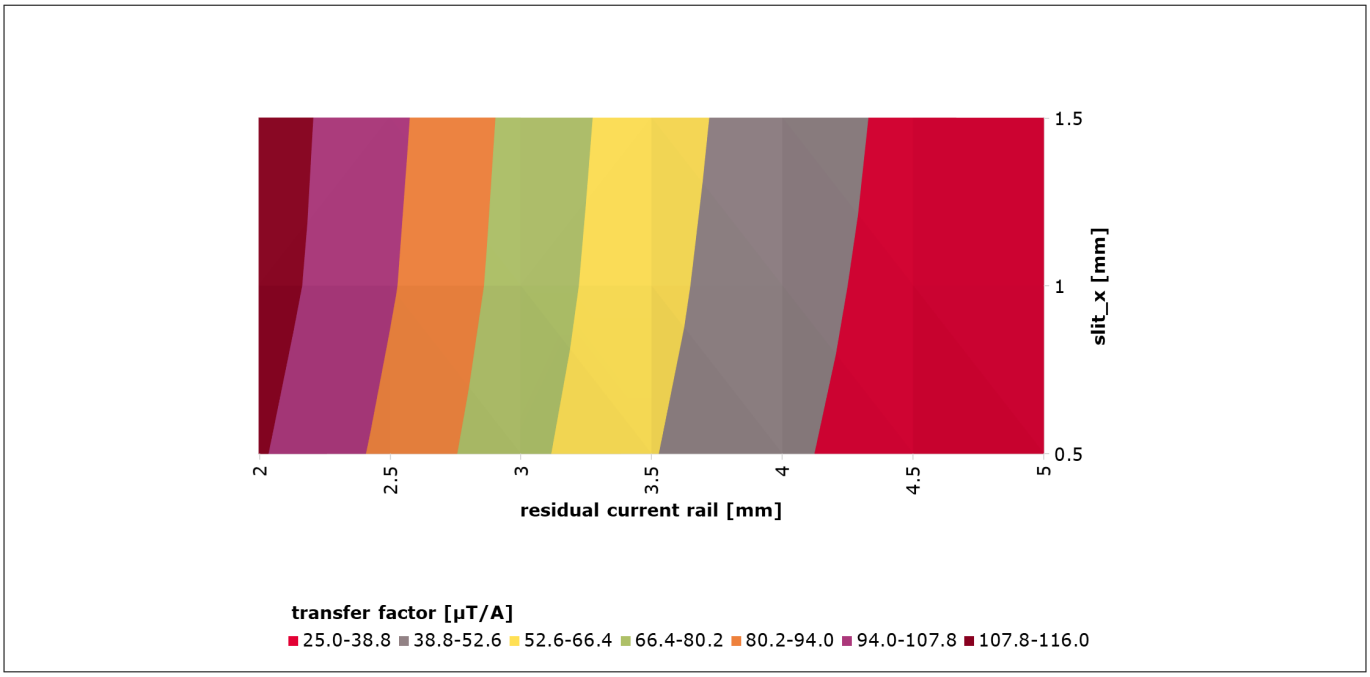

Figure 84 **Current rail transfer factor for a 2 power layer PCB. Sweep of residual current rail and slit_x values**

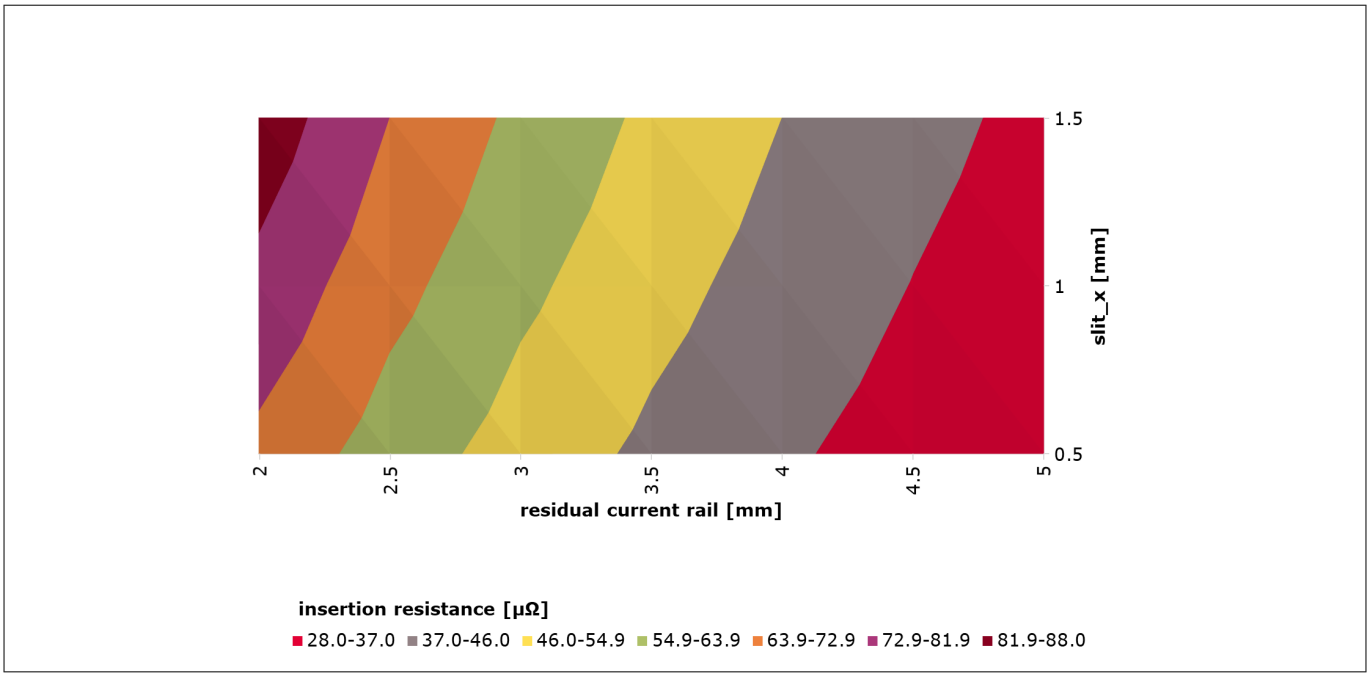

Figure 85 **Insertion resistance for a 2 power layer PCB. Sweep of residual current rail and slit_x values**

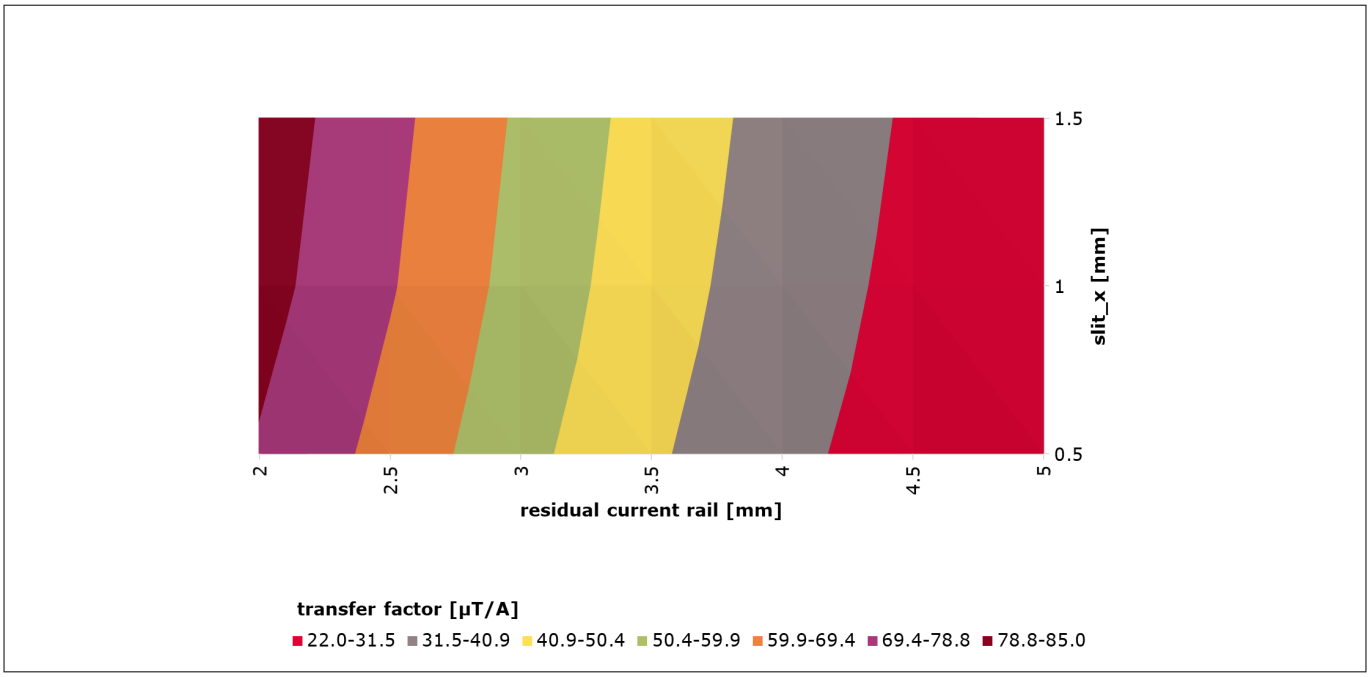

Figure 86 **Current rail transfer factor for a 4 power layer PCB. Sweep of residual current rail and slit_x values**

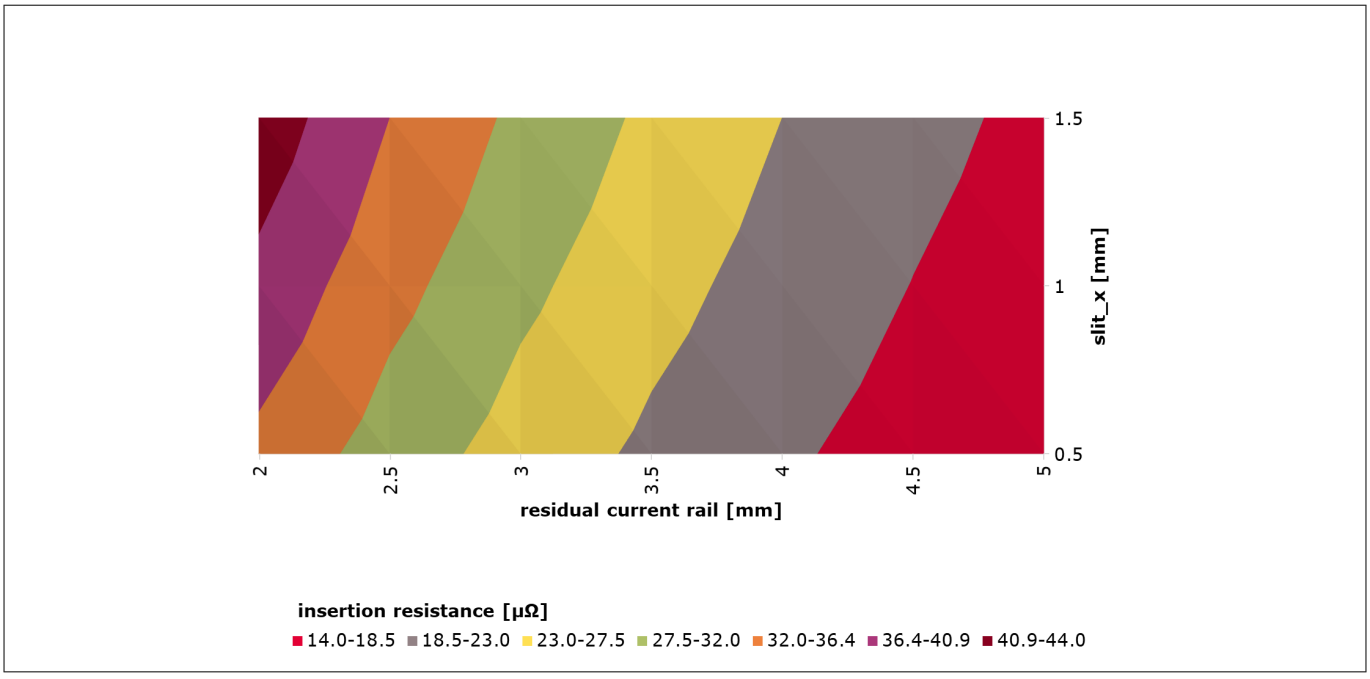

Figure 87 **Insertion resistance for a 4 power layer PCB. Sweep of residual current rail and slit_x values**

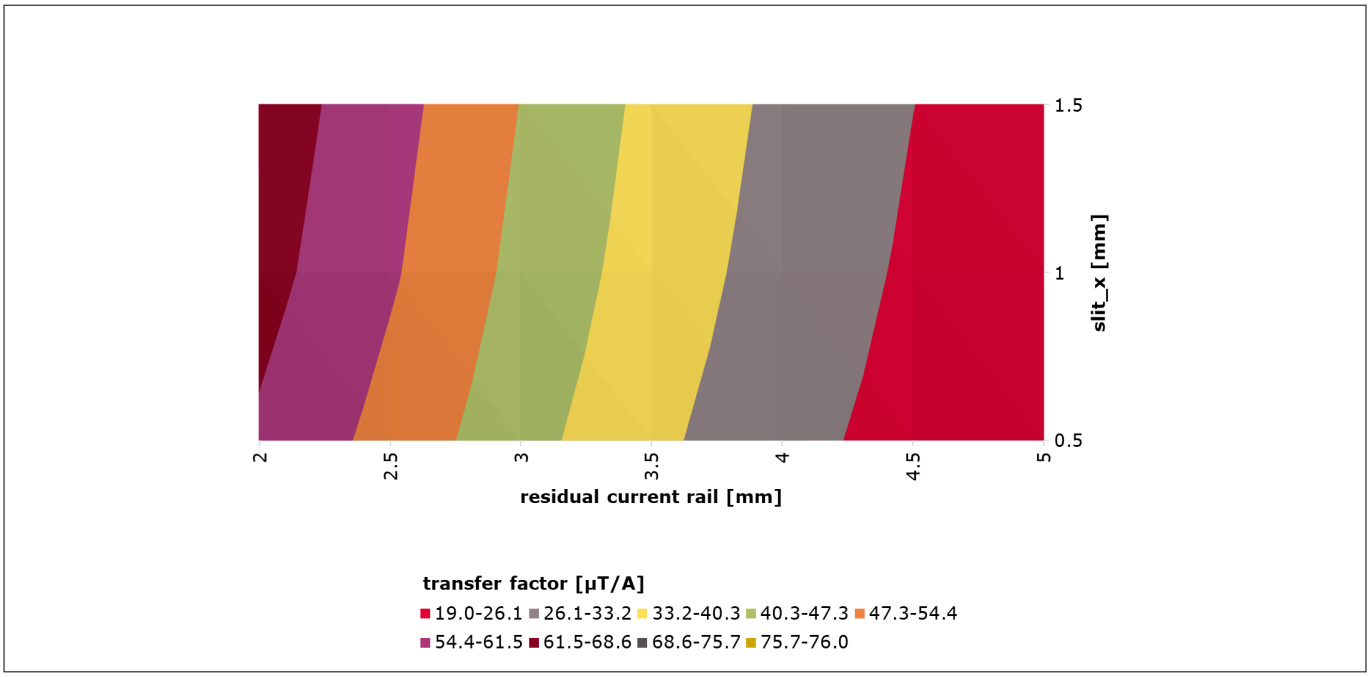

Figure 88 **Current rail transfer factor for a 6 power layer PCB. Sweep of residual current rail and slit_x values**

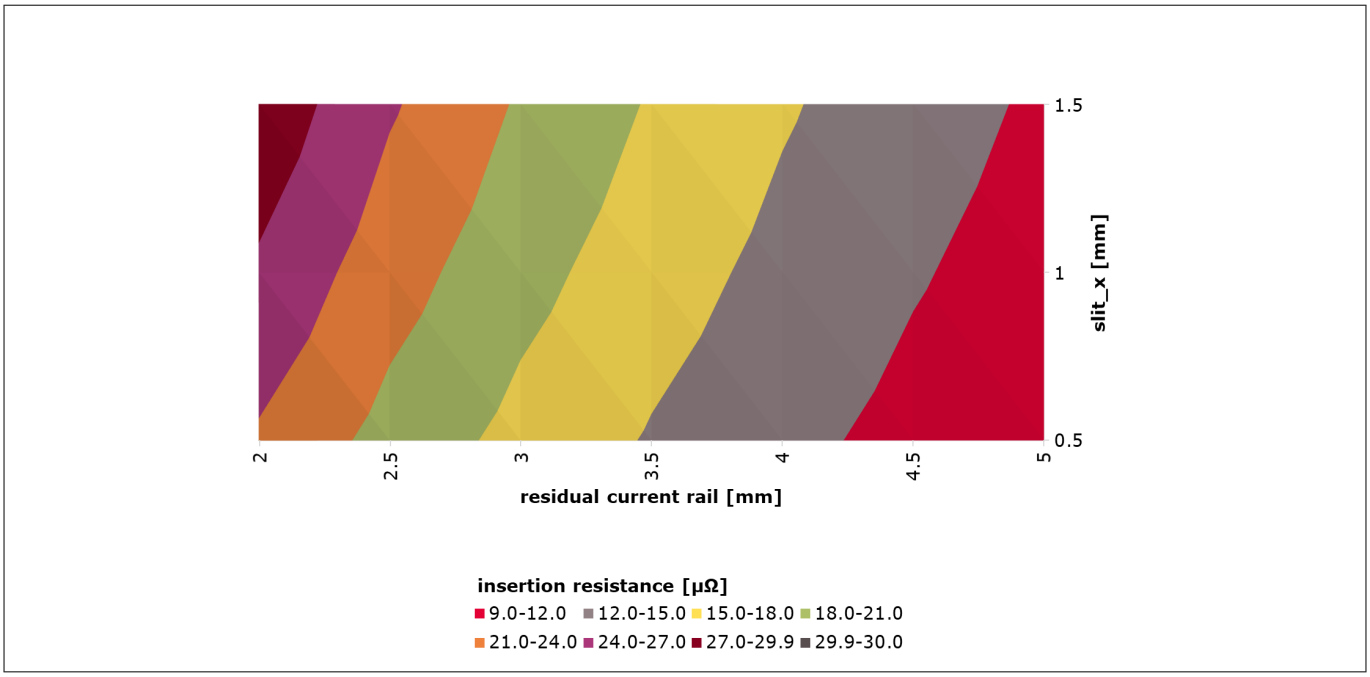

Figure 89 **Insertion resistance for a 6 power layer PCB. Sweep of residual current rail and slit_x values**

A high number of power layers is clearly beneficial for the insertion resistance reduction since it creates a bigger cross section for the current flow, but it leads to lower transfer factors because of the lower current density. In the same way, a wider residual current rail is beneficial for the insertion resistance reduction but leads to lower transfer factors.

Regarding the slit_x parameter, which indicates how wide the slit in the PCB layer is, it's usually better to keep it as small as possible, within the limits of the manufacturing rules. In fact, a wider slit increases the insertion resistance without bringing a significant increase in the transfer factor, as it can be seen from the previously shown simulation data. However, small slit_x and residual current rail values result in increased sensitivity to misalignment errors.

4.1.3 Bandwidth

Given the typical bandwidth of the current sensor, reported in the product datasheet [1], the bandwidth of the complete current measurement solution will be significantly influenced by the geometry of the sensing structure. The reason for this behavior is the change of the current density within the section of the conductor over frequency. Due to skin effect, the current is pushed toward the surface of the conductor, and induced eddy currents create an opposing field to the one generated by the current in the conductor that changes in amplitude depending on the frequency. The figure below shows how the current density is altered in the PCB structure over frequency. The impact on the frequency response will heavily depend on the geometry of the sensing structure. The typical magnitude [dB], phase shift [deg] and gain error [%] for a different number of power layers, residual current rail lengths and slit_x values are shown in the figures below.

Reducing the number of power layers helps in terms of bandwidth; the effect of both skin effect and eddy current effect is confined to a lower number of layers. A smaller residual current rail and a bigger slit_x are beneficial in terms of bandwidth since the current is confined in a smaller, restricted area at the sensing location.

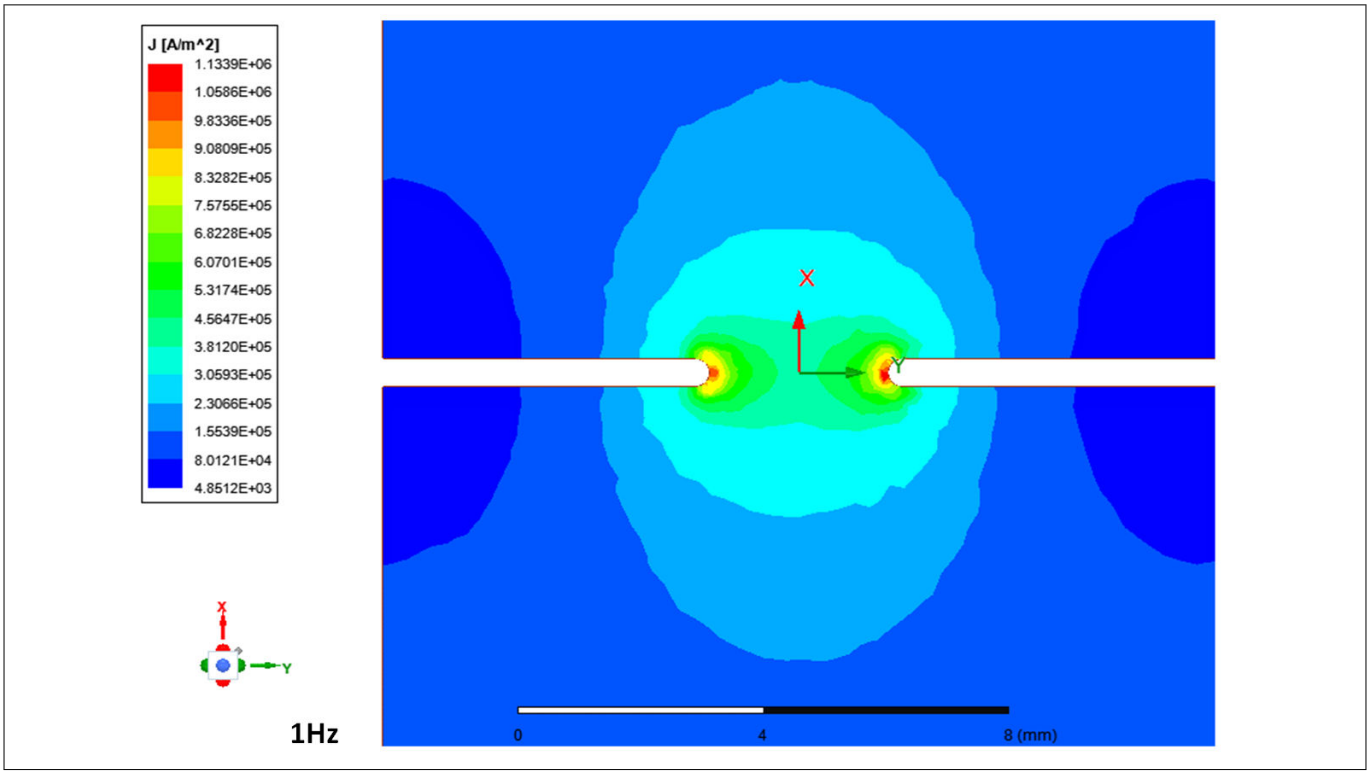

Figure 90 **Current density distribution on the surface of the sensing structure, on a 4 power layers PCB. Residual current rail = 3 mm. Slit_x = 0.5 mm. Peak input current = 1 A, 1 Hz**

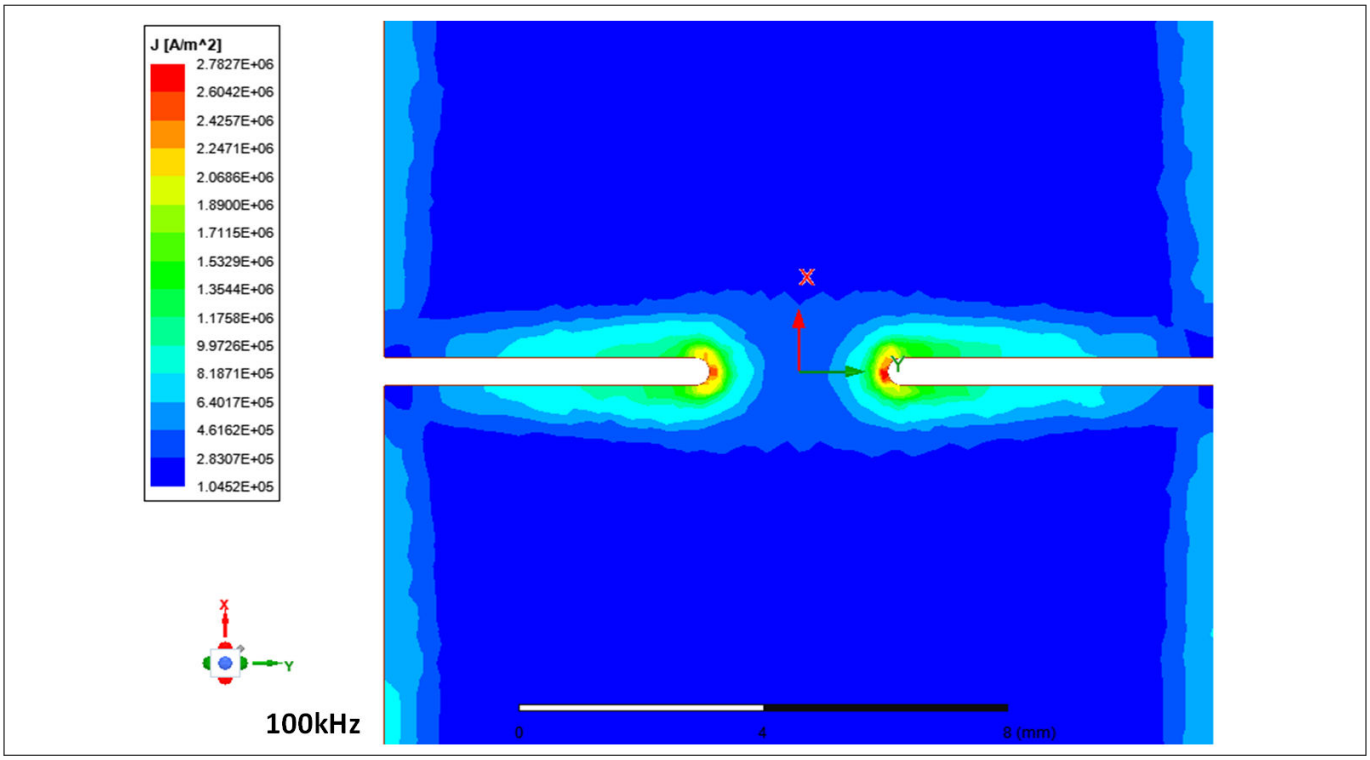

Figure 91 **Current density distribution on the surface of the sensing structure, on a 4 power layers PCB. Residual current rail = 3 mm. Slit_x = 0.5 mm. Peak input current = 1 A, 100 kHz**

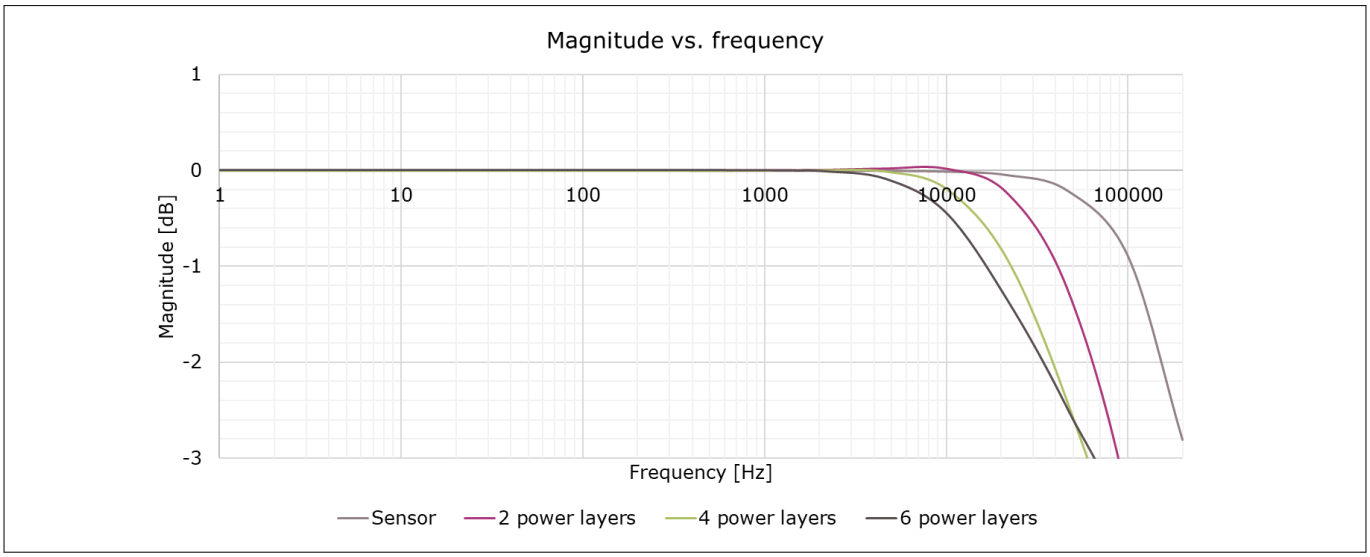

Figure 92 **Magnitude over frequency for a different number of power layers. Residual current rail = 3 mm. Slit_x = 2 mm**

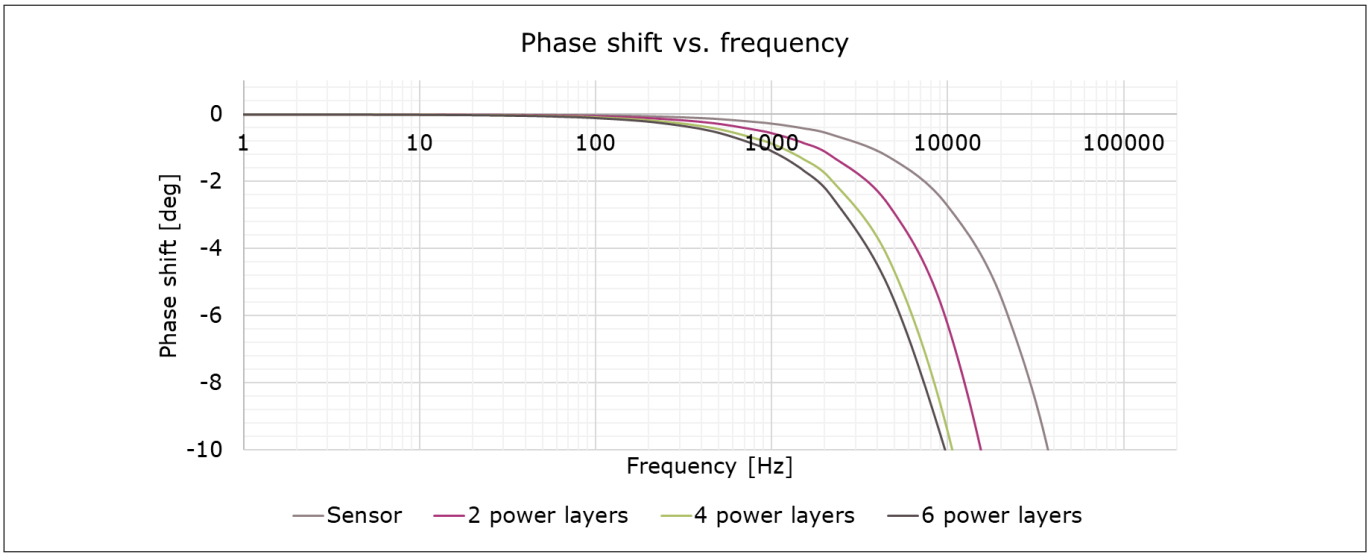

Figure 93 **Phase shift over frequency for a different number of power layers. Residual current rail = 3 mm. Slit_x = 2 mm**

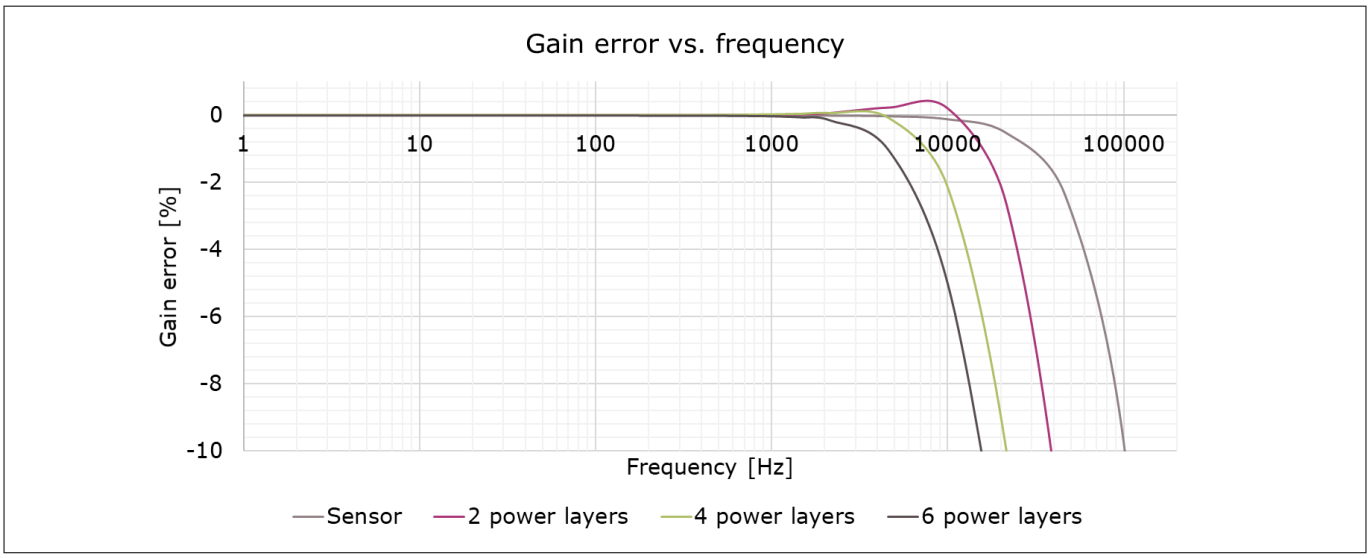

Figure 94 **Gain error over frequency for a different number of power layers. Residual current rail = 3 mm. Slit_x = 2 mm**

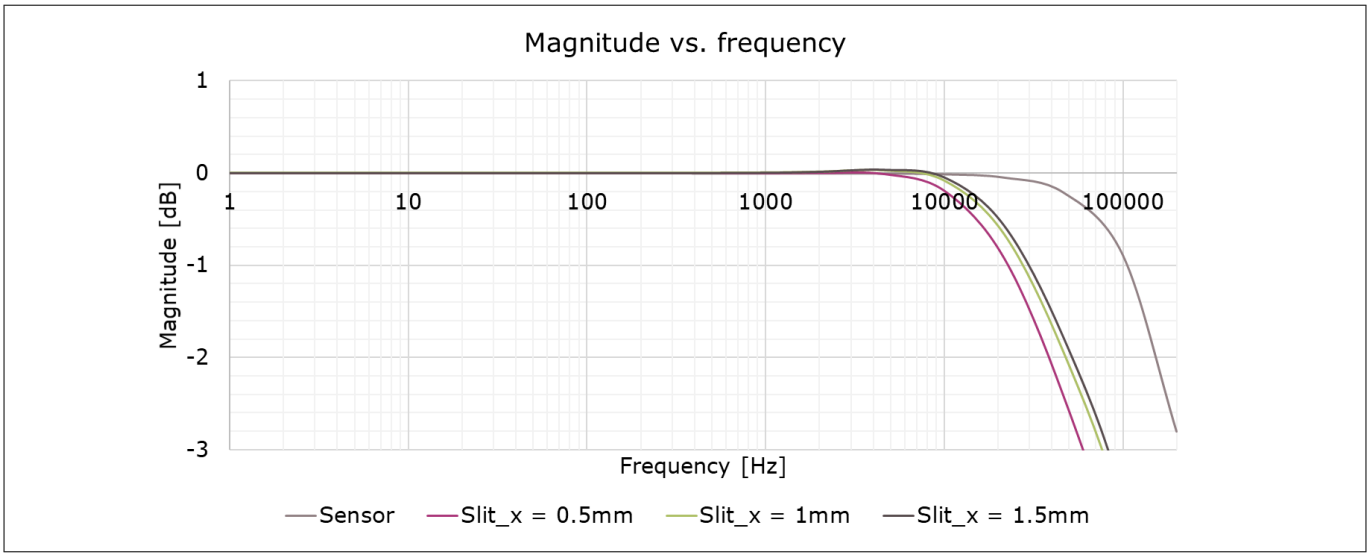

Figure 95 **Magnitude over frequency for a 4 power layers PCB. Residual current rail = 3 mm. Sweep on slit_x value**

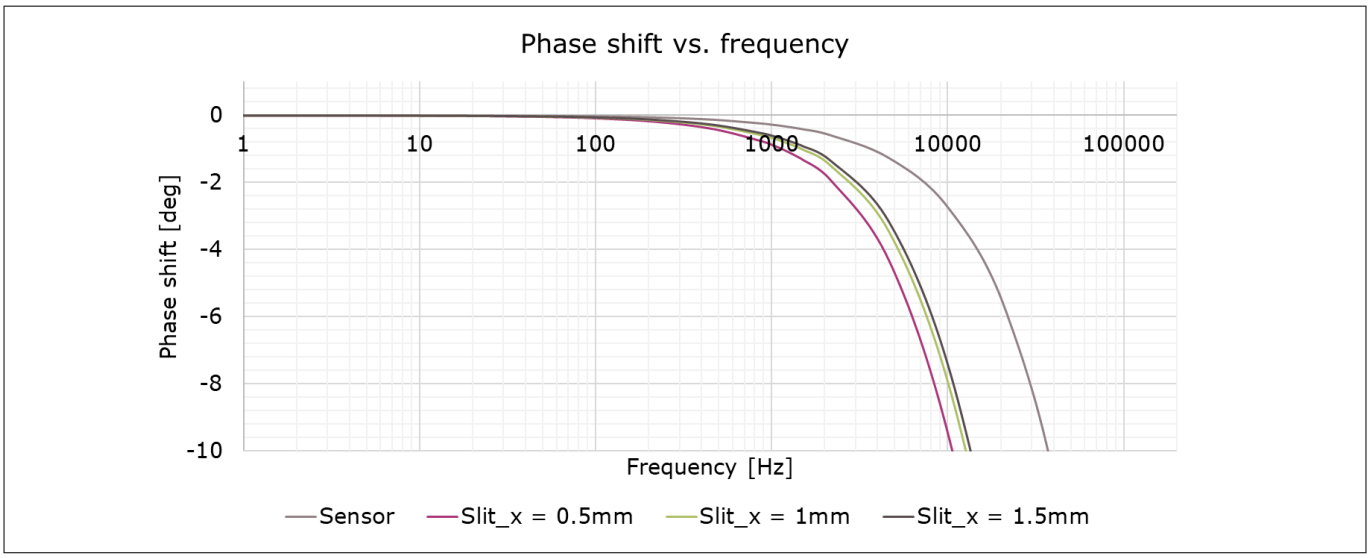

Figure 96 **Phase shift over frequency for a 4 power layers PCB. Residual current rail = 3 mm. Sweep on slit_x value**

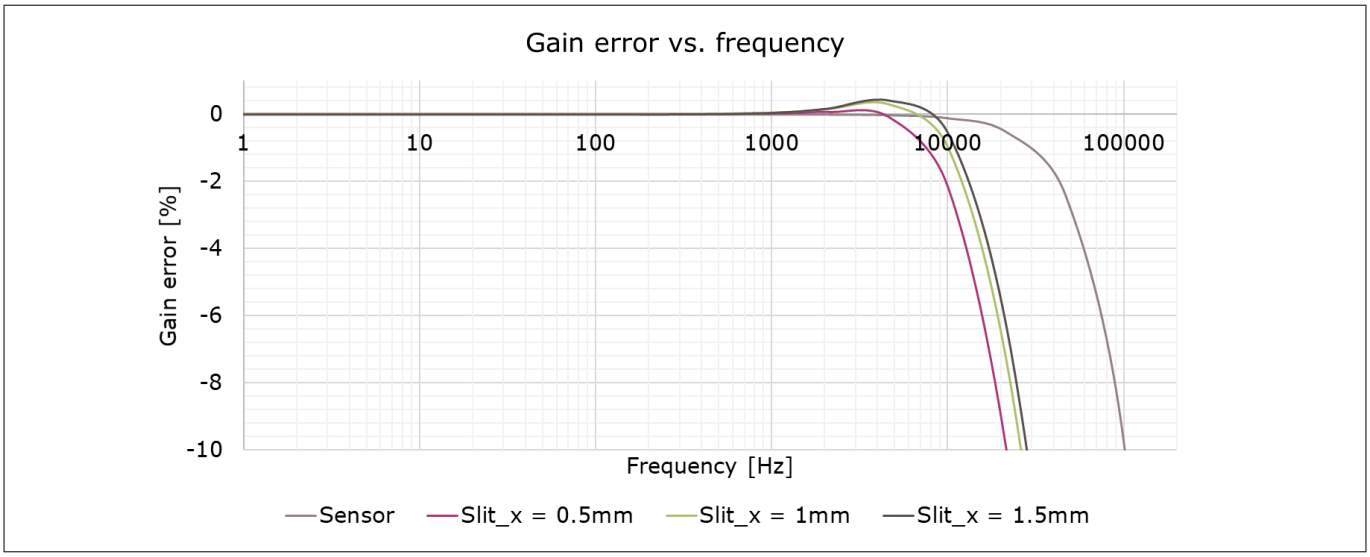

Figure 97 **Gain error over frequency for a 4 power layers PCB. Residual current rail = 3 mm. Sweep on slit_x value**

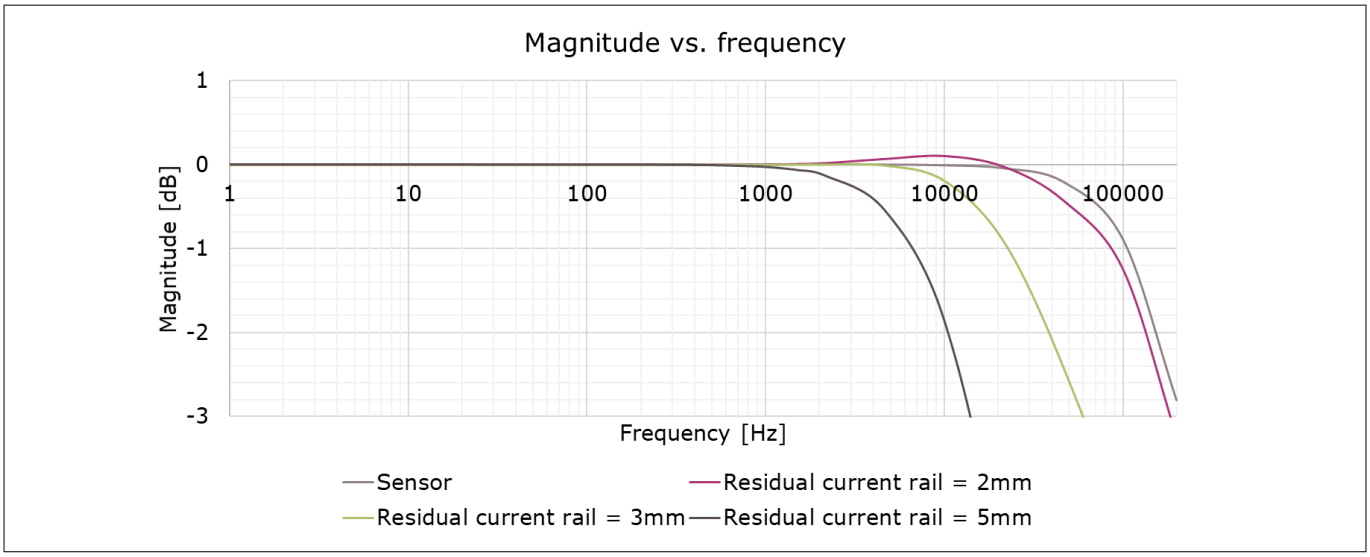

Figure 98 **Magnitude over frequency for a 4 power layers PCB. Slit_x = 0.5 mm. Sweep on residual current rail value**

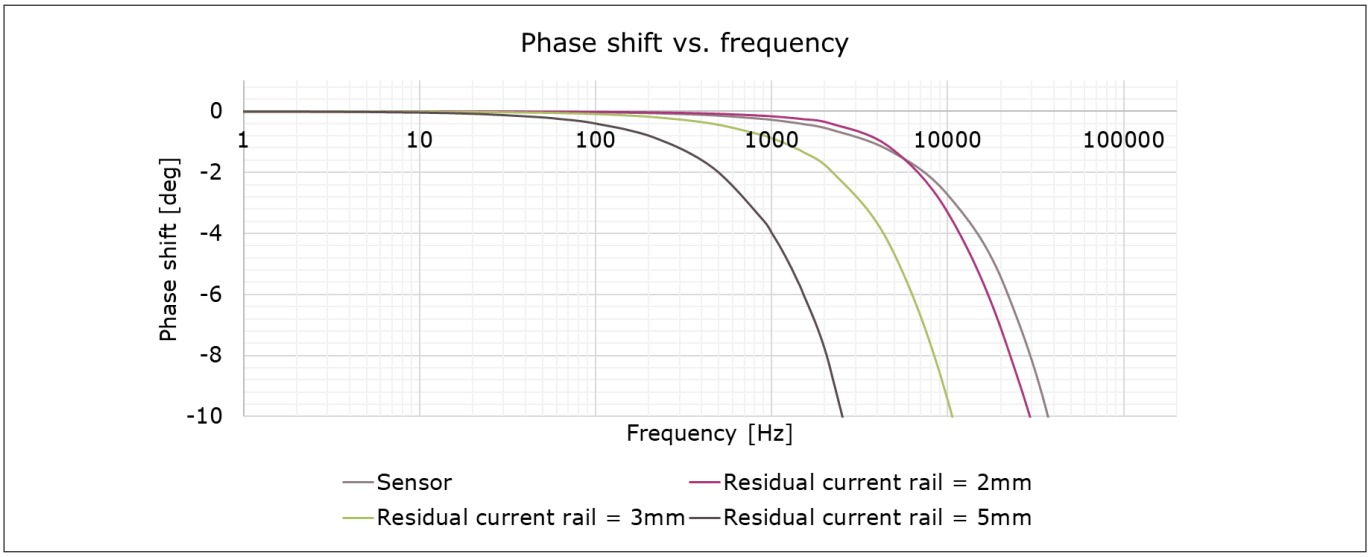

Figure 99 **Phase shift over frequency for a 4 power layers PCB. Slit_x = 0.5 mm. Sweep on residual current rail value**

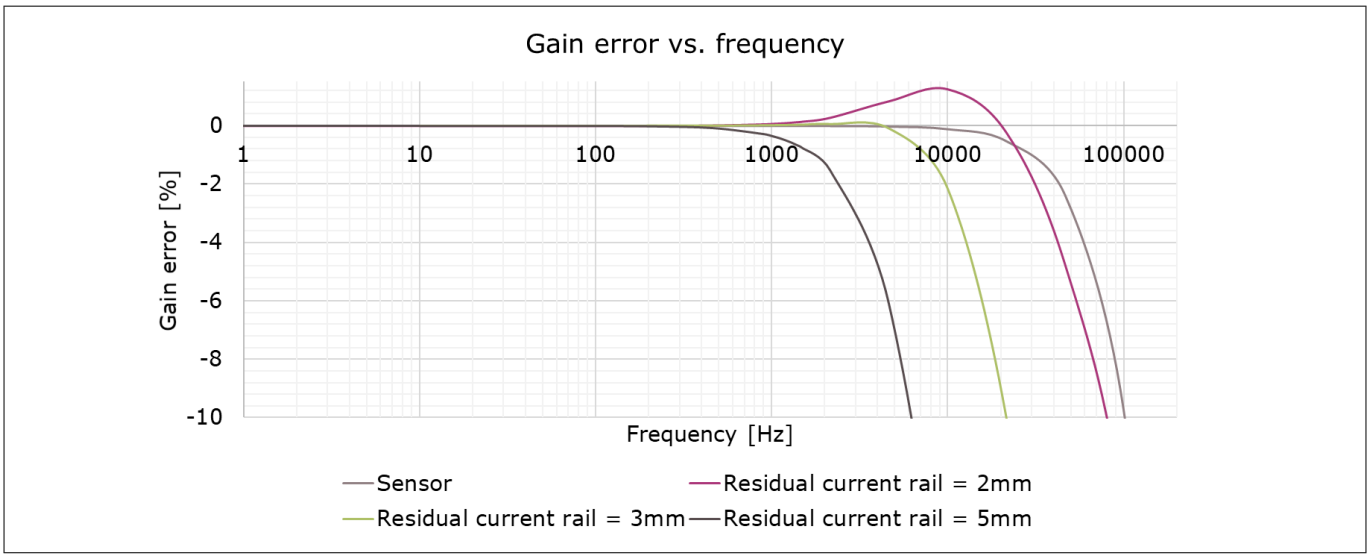

Figure 100 **Gain error over frequency for a 4 power layers PCB. Slit_x = 0.5 mm. Sweep on residual current rail value**

4.1.4 Misalignment effects

If the sensor is not aligned with the current rail in its nominal position due to manufacturing tolerances, the transfer factor will differ from the nominal one. We refer to this error component as "transfer factor error". This error component will contribute to the total initial sensitivity error, and it is possible to compensate it within the calibration range specified in the product datasheet [1]. However, if the sensor gets displaced during system operation due to mechanical vibrations or thermal expansion effects, the transfer factor will experience a drift. Quantifying this error component is essential in order to verify that the in-system end of line calibration is feasible and that the transfer factor doesn't drift outside specifications during operation. In the figures below the results of transfer factor simulations in which the sensor is displaced in the three directions of space are shown, in case of different slit_x and residual current rail values. The analysis is done on the 4 power layers PCB structure example.

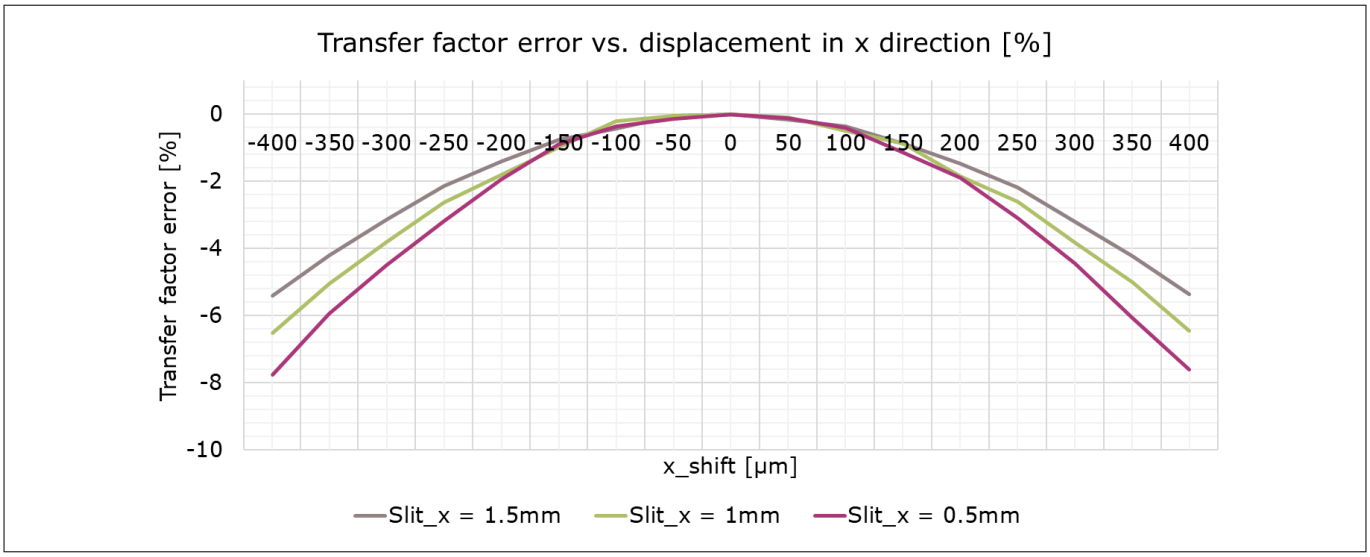

Figure 101 **Displacement in X direction. Current rail transfer factor error for a 4 power layers PCB. Residual current rail = 3 mm. Sweep on slit_x value**

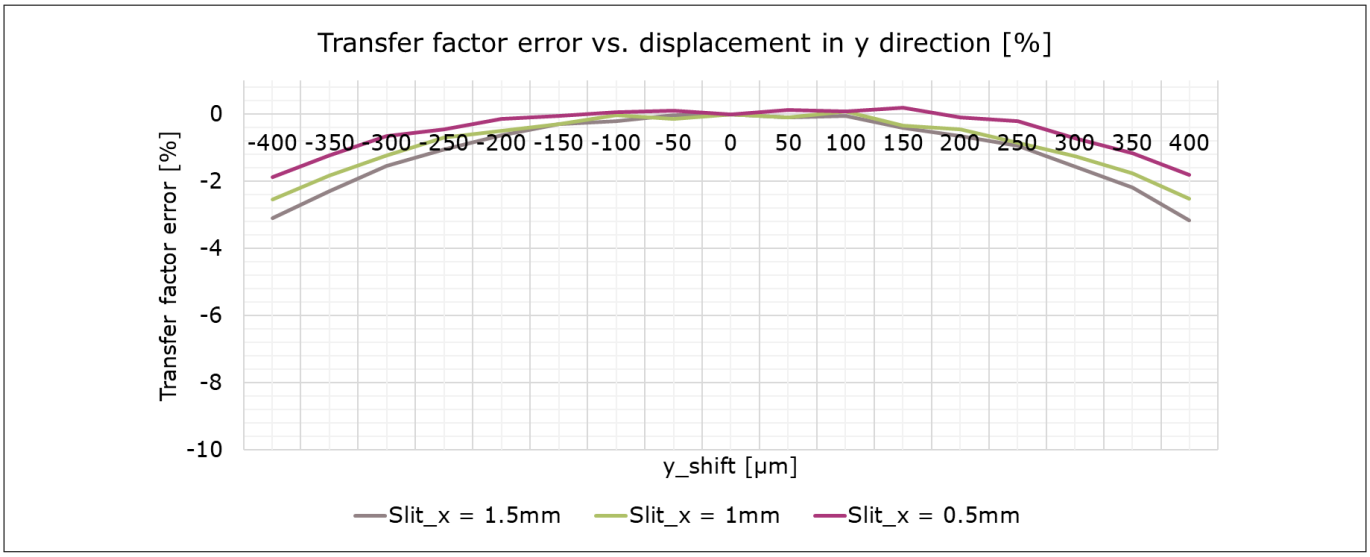

Figure 102 **Displacement in Y direction. Current rail transfer factor error for a 4 power layers PCB. Residual current rail = 3 mm. Sweep on slit_x value**

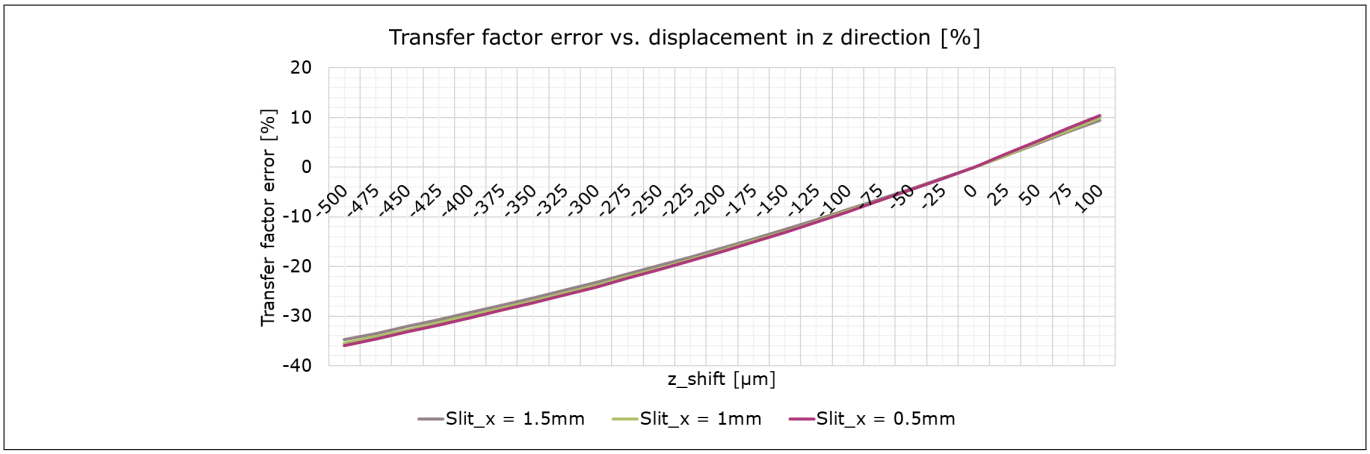

Figure 103 **Displacement in Z direction. Current rail transfer factor error for a 4 power layers PCB. Residual current rail = 3 mm. Sweep on slit_x value**

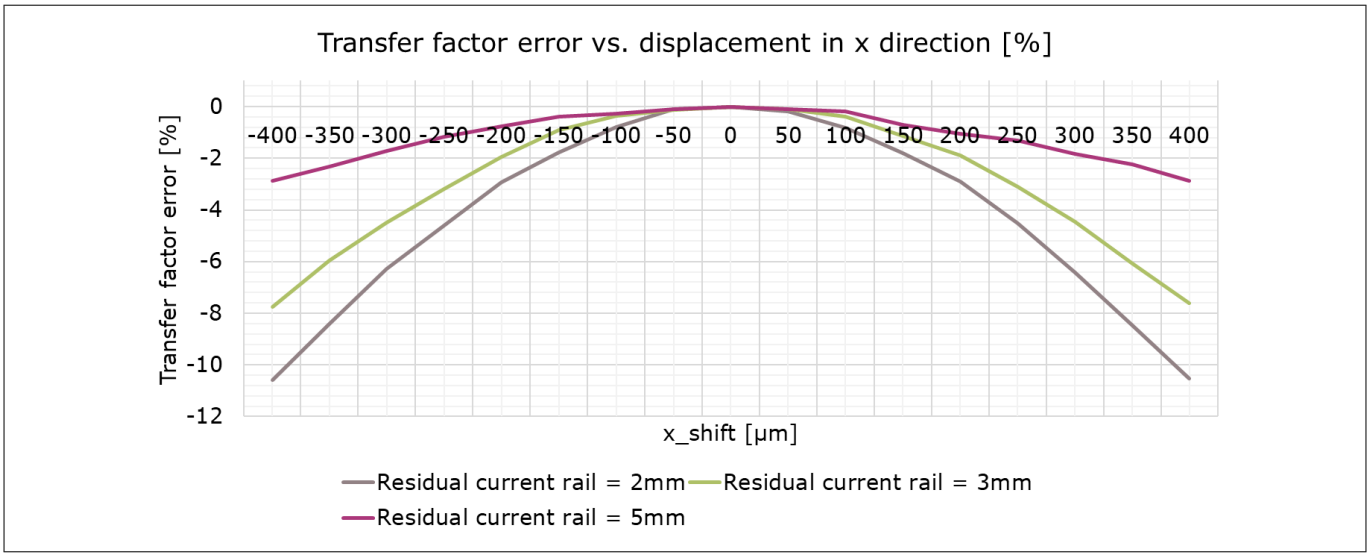

Figure 104 **Displacement in X direction. Current rail transfer factor error for 4 power layers PCB. Slit_x = 0.5 mm. Sweep on residual current rail value**

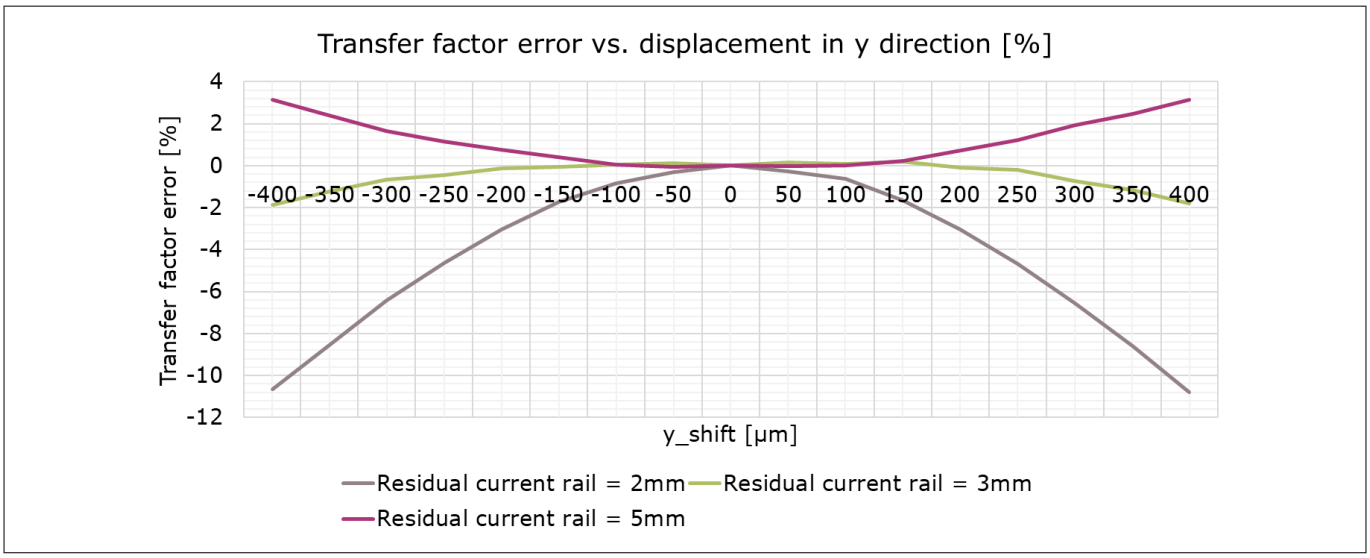

Figure 105 **Displacement in Y direction. Current rail transfer factor error for 4 power layers PCB. Slit_x = 0.5 mm. Sweep on residual current rail value**

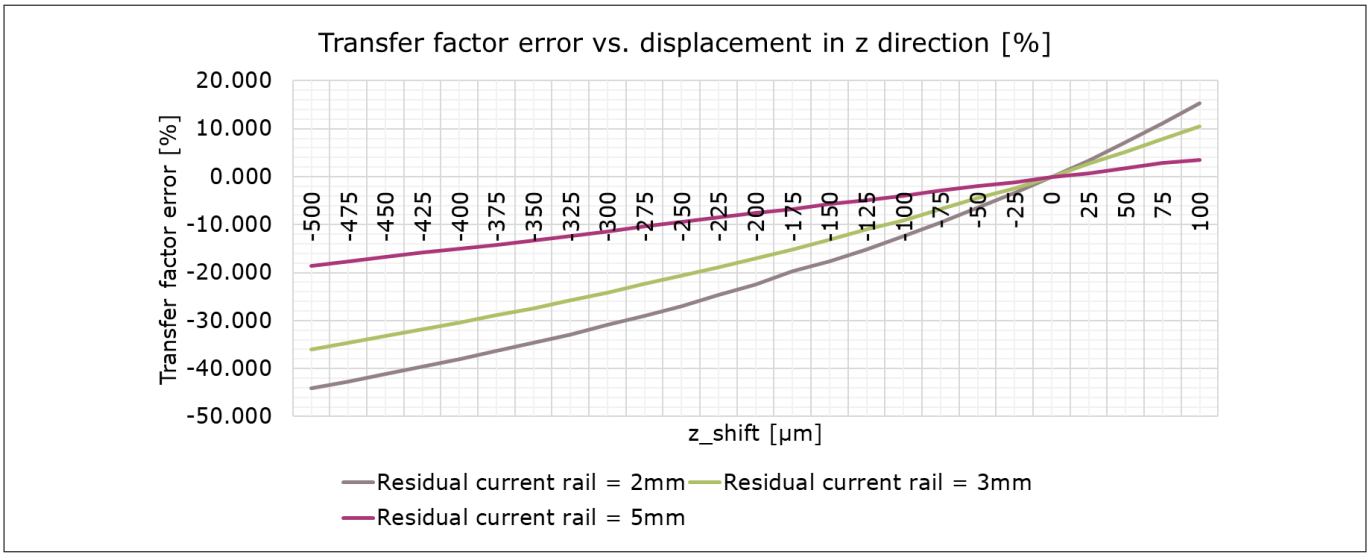

Figure 106 **Displacement in Z direction. Current rail transfer factor error for 4 power layers PCB. Slit_x = 0.5 mm. Sweep on residual current rail value**

In case misalignment has a critical impact, a wider slit_x value can help with obtaining less sensitivity to misalignments in X direction. A wider residual current rail can in turn reduce the sensitivity to misalignments in Y direction. However, both measures will lead to a reduction of the nominal transfer factor, as shown in the previous paragraphs.

Misalignments have a minor impact on the frequency response as well. This impact is limited and usually neglectable if the sensing structure is symmetric with respect to the sensing elements location. Magnitude and phase shift are affected; in the figures below the misalignment impact on the frequency response on the PCB structure example is shown, for a worst-case misalignment of ± 0.4 mm in X and Y directions, -0.4 mm to +0.1 mm for Z direction.

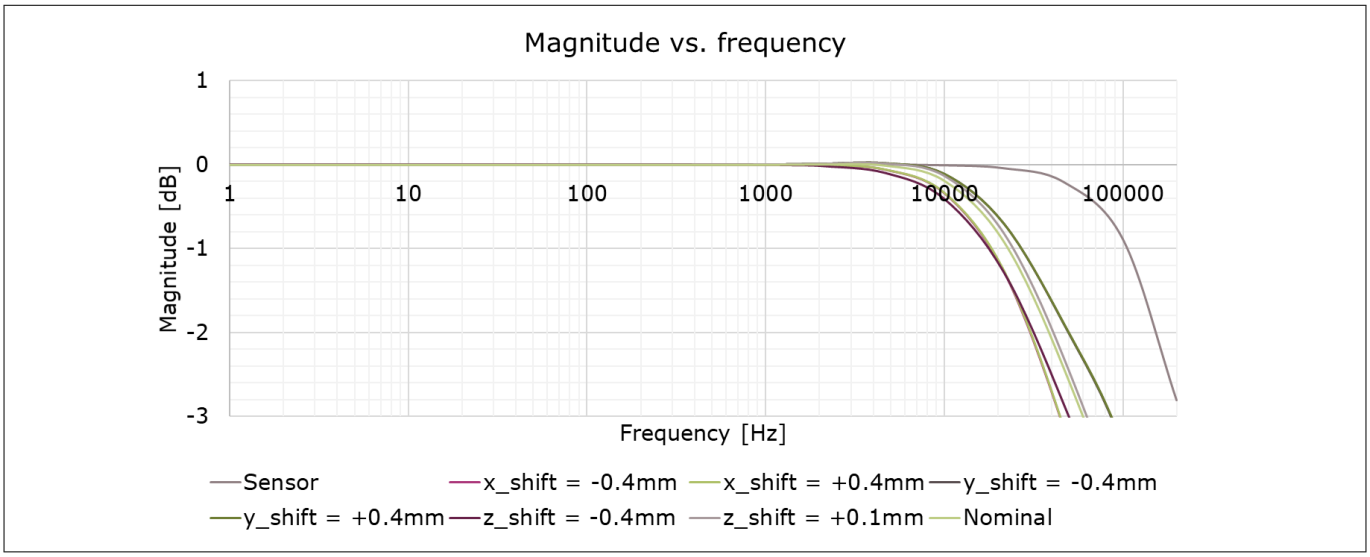

Figure 107 **Magnitude over frequency for a 4 power layers PCB. Slit_x = 2 mm. Residual current rail = 3 mm. Sweep on x_shift, y_shift and z_shift values**

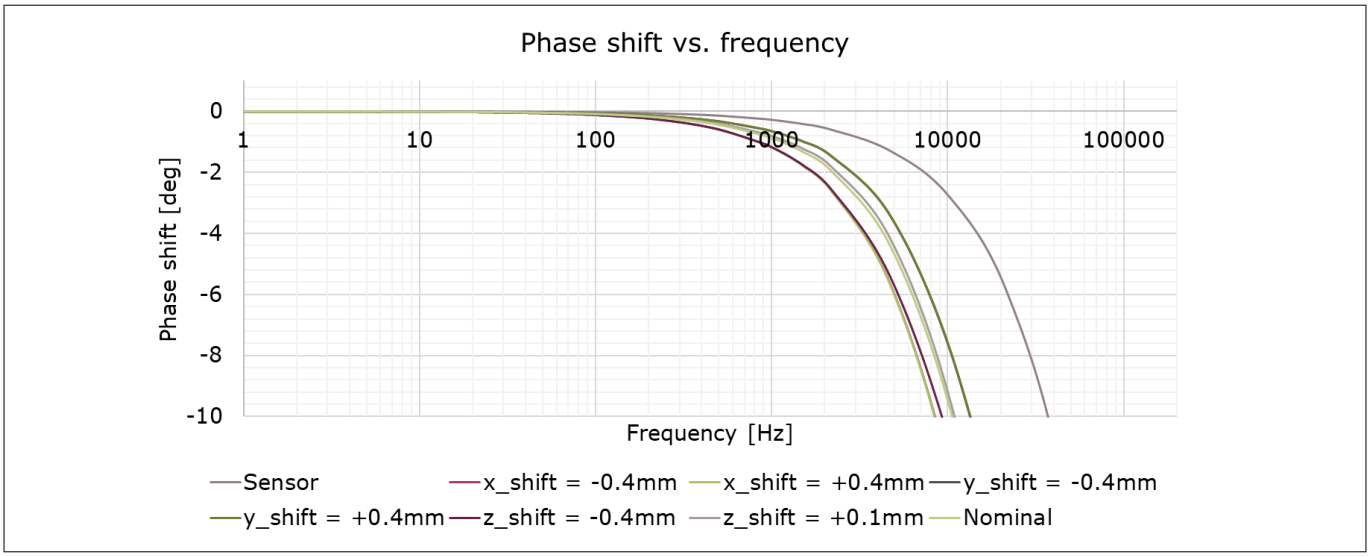

Figure 108 **Phase shift over frequency for a 4 power layers PCB. Slit_x = 2 mm. Residual current rail = 3 mm. Sweep on x_shift, y_shift and z_shift values**

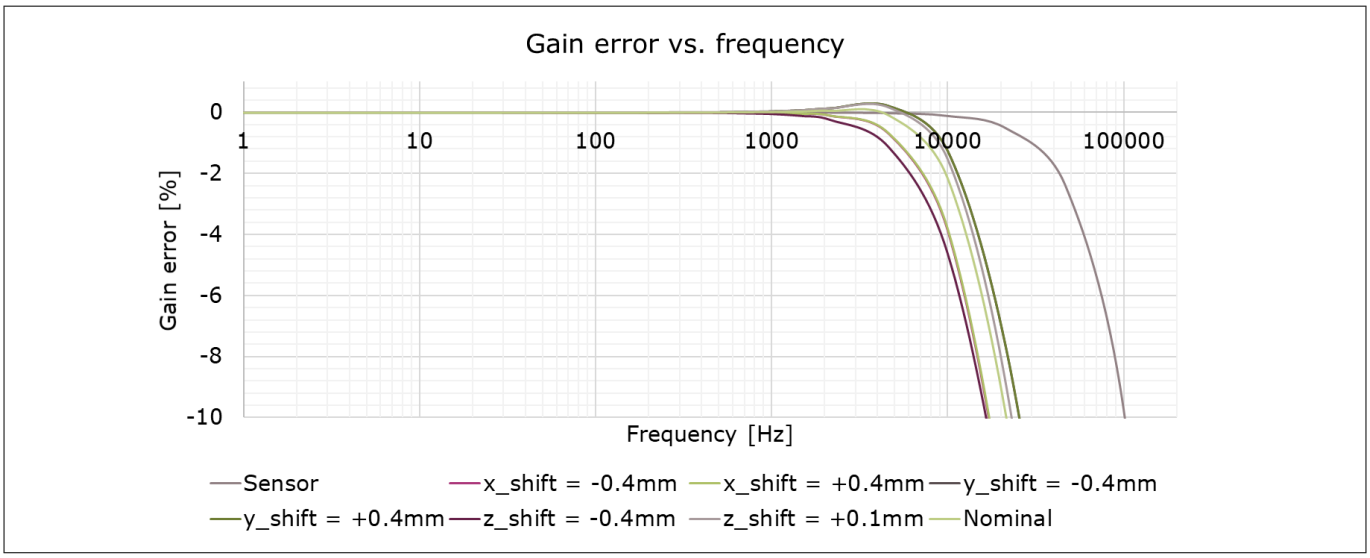

Figure 109 **Gain error over frequency for a 4 power layers PCB. Slit_x = 2 mm. Residual current rail = 3 mm. Sweep on x_shift, y_shift and z_shift values**

4.1.5 Crosstalk

In case of multi-phase systems, the magnetic field generated by the current flowing in nearby phases can influence the current measurement. The percentage of signal that is measured on a phase and that flows in the nearby phase is here denominated as crosstalk factor.

The figure shows an example of three phase system constituted of three of the PCB structure examples. The middle-to-middle spacing in Y direction is 24mm; this corresponds to the distance between the sensing structure centers belonging to adjacent phases. That results in a crosstalk factor of 0.8% between adjacent phases, 0.2% between right and left phases. In case the phases are very close to each other, like in the outer to middle case, the crosstalk factor is 0.8%. This value can be reduced through a different sensor orientation and it is important to mention that the crosstalk factor is stable over temperature and lifetime; it can be characterized for each system and the resulting error can be compensated. Further details about crosstalk compensation are available in the User manual [2].

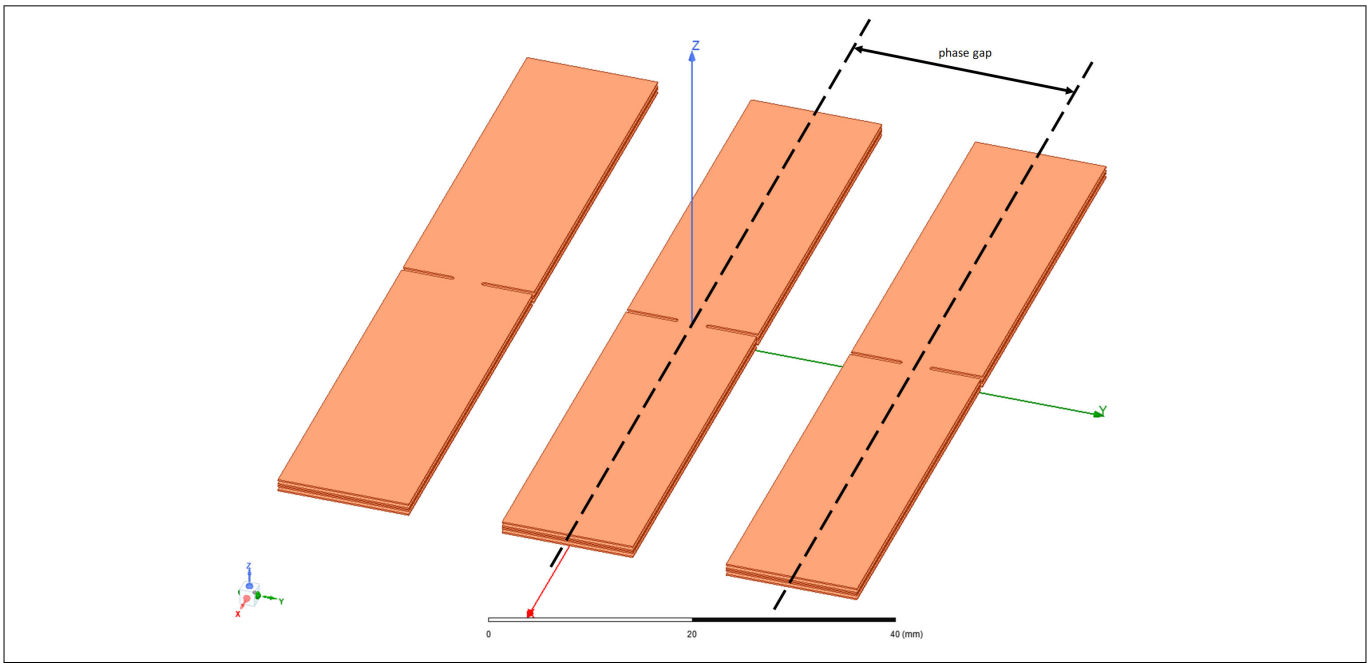

Figure 110 Three phases system made by three sensing structures, based on a 4 power layers PCB. Slit_x = 0.5 mm. Residual current rail = 3 mm. Phase gap = 24 mm

4.2 S-bend shaped sensing structure

This crosstalk factor between phases in a multi phase system can be reduced through a different sensor orientation with respect to the Straight orientation. Please refer to Chapter 3.1.2 in order to understand how to reduce the crosstalk factor at the expense of either transfer factor or insertion resistance using a S-bend shaped sensing structure.

5 Glossary

Notation	Description
EEPROM	Electrically Erasable Programmable Read-Only Memory.
PCB	Printed Circuit Board.
TF	Transfer Factor.
DC	Direct Current.
FEM	Finite Element Method.

6 References

[1] Infineon-TLE4972-AE35S5-DS-vxx_xx-EN.pdf; Infineon-TLE4972-AE35D5-DS-vxx_xx-EN.pdf
[2] Infineon-TLE4972-User_manual-vxx_xx-EN

7 Revision History

Document revision	Date of release	Description of changes
01.01	19.05.2022	• Added vertical insertion use case; • Editorial changes.
01.00	18.03.2022	Initial release.

Trademarks

All referenced product or service names and trademarks are the property of their respective owners.

Edition 2022-05-19

Published by

Infineon Technologies AG

81726 Munich, Germany

Do you have a question about any aspect of this document?

Email: erratum@infineon.com

Document reference
IFX-yzn1652786702721

Important notice

The information contained in this application note is given as a hint for the implementation of the product only and shall in no event be regarded as a description or warranty of a certain functionality, condition or quality of the product. Before implementation of the product, the recipient of this application note must verify any function and other technical information given herein in the real application. Infineon Technologies hereby disclaims any and all warranties and liabilities of any kind (including without limitation warranties of non-infringement of intellectual property rights of any third party) with respect to any and all information given in this application note.

The data contained in this document is exclusively intended for technically trained staff. It is the responsibility of customer's technical departments to evaluate the suitability of the product for the intended application and the completeness of the product information given in this document with respect to such application.

Warnings

Due to technical requirements products may contain dangerous substances. For information on the types in question please contact your nearest Infineon Technologies office.

Except as otherwise explicitly approved by Infineon Technologies in a written document signed by authorized representatives of Infineon Technologies, Infineon Technologies' products may not be used in any applications where a failure of the product or any consequences of the use thereof can reasonably be expected to result in personal injury.